Università degli Studi di Trieste
sede amministrativa del dottorato di ricerca

Scuola di Dottorato di Ingegneria dell'Informazione
xxiv ciclo

FRACTAL ANALYSIS OF THE EEG AND CLINICAL APPLICATIONS

(SSD ING-INF/06 Bioingegneria Elettronica ed Informatica)

Dottoranda
Monica CUSENZA

Direttore della Scuola
Chiar.mo Prof. Walter UKOVICH
Università degli Studi di Trieste

Supervisore
Chiar.mo Prof. Agostino ACCARDO
Università degli Studi di Trieste

Anno Accademico 2010/2011

Monica Cusenza: *Fractal analysis of the EEG and clinical applications*, 2012, February.

E-MAIL:
monica.cusenza@gmail.com

"Mountains are not cones, clouds are not spheres,
trees are not cylinders, neither does lightning
travel in a straight line."

- Benoît B. Mandelbrot
"The fractal geometry of nature" (1982)

"The mind as a whole is self-similar
no matter whether it refers to the large or the small."

- Anaxagoras
"Fragment No. 12" (456 BC)

"In examining disease, we gain wisdom about
anatomy and physiology and biology.
In examining the person with disease,
we gain wisdom about life."

- Oliver Sacks
"The man who mistook his wife for a hat
and other clinical tales" (1985)

ABSTRACT

Most of the knowledge about physiological systems has been learned using linear system theory. The randomness of many biomedical signals has been traditionally ascribed to a noise-like behavior. An alternative explanation for the irregular behavior observed in systems which do not seem to be inherently stochastic is provided by one of the most striking mathematical developments of the past few decades, i.e., chaos theory. Chaos theory suggests that random-like behavior can arise in some deterministic nonlinear systems with just a few degrees of freedom. One of the most evocative aspects of deterministic chaos is the concept of fractal geometry. Fractal structure, characterized by self-similarity and noninteger dimension, is displayed in chaotic systems by a subset of the phase space known as strange attractor. However, fractal properties are observed also in the unpredictable time evolution and in the $\frac{1}{f^{\beta}}$ power-law of many biomedical signals. The research activities carried out by the Author during the PhD program are concerned with the analysis of the fractal-like behavior of the EEG. The focus was set on those methods which evaluate the fractal geometry of the EEG in the time domain, in the hope of providing physicians and researchers with new valuable tools of low computational cost for the EEG analysis. The performances of three widely used techniques for the direct estimation of the fractal dimension of the EEG were compared and the accuracy of the fBm scaling relationship, often used to obtain indirect estimates from the slope of the spectral density, was assessed. Direct estimation with Higuchi's algorithm turned out to be the most suitable methodology, producing correct estimates of the fractal dimension of the electroencephalogram also on short traces, provided that minimum sampling rate required to avoid aliasing is used. Based on this result, Higuchi's fractal dimension was used to address three clinical issues which could involve abnormal complexity of neuronal brain activity: 1) the monitoring of carotid endarterectomy for the prevention of intraoperative stroke, 2) the assessment of the depth of anesthesia to monitor unconsciousness during surgery and 3) the analysis of the macro-structural organization of the EEG in autism with respect to mental retardation. The results of the clinical studies suggest that, although linear spectral analysis still represents a valuable tool for the investigation of the EEG, time domain fractal analysis provides additional information on brain functioning which traditional analysis cannot achieve, making use of techniques of low computational cost.

SOMMARIO

La maggior parte delle conoscenze acquisite sui sistemi fisiologici si deve alla teoria dei sistemi lineari. Il comportamento pseudo stocastico di molti segnali biomedici è stato tradizionalmente attribuito al concetto di rumore. Un'interpretazione alternativa del comportamento irregolare rilevato in sistemi che non sembrano essere intrinsecamente stocastici è fornita da uno dei più sorprendenti sviluppi matematici degli ultimi decenni: la teoria del caos. Tale teoria suggerisce che una certa componente casuale può sorgere in alcuni sistemi deterministici non lineari con pochi gradi di libertà. Uno degli aspetti più suggestivi del caos deterministico è il concetto di geometria frattale. Strutture frattali, caratterizzate da auto-somiglianza e dimensione non intera, sono rilevate nei sistemi caotici in un sottoinsieme dello spazio delle fasi noto con il nome di attrattore strano. Tuttavia, caratteristiche frattali possono manifestarsi anche nella non prevedibile evoluzione temporale e nella legge di potenza $\frac{1}{f^{\beta}}$ tipiche di molti segnali biomedici. Le attività di ricerca svolte dall'Autore nel corso del dottorato hanno riguardato l'analisi del comportamento frattale dell'EEG. L'attenzione è stata rivolta a quei metodi che affrontano lo studio della geometria frattale dell'EEG nel dominio del tempo, nella speranza di fornire a medici e ricercatori nuovi strumenti utili all'analisi del segnale EEG e caratterizzati da bassa complessità computazionale. Sono state messe a confronto le prestazioni di tre tecniche largamente utilizzate per la stima diretta della dimensione frattale dell'EEG e si è valutata l'accuratezza della relazione di scaling del modello fBm, spesso utilizzata per ottenere stime indirette a partire dalla pendenza della densità spettrale di potenza. Il metodo più adatto alla stima della dimensione frattale dell'elettroencefalogramma è risultato essere l'algoritmo di Higuchi, che produce stime accurate anche su segmenti di breve durata a patto che il segnale sia campionato alla minima frequenza di campionamento necessaria ad evitare il fenomeno dell'aliasing. Sulla base di questo risultato, la dimensione frattale di Higuchi è stata utilizzata per esaminare tre questioni cliniche che potrebbero coinvolgere una variazione della complessità dell'attività neuronale: 1) il monitoraggio dell'endoarterectomia carotidea per la prevenzione dell'ictus intraoperatorio, 2) la valutazione della profondità dell'anestesia per monitorare il livello di incoscienza durante l'intervento chirurgico e 3) l'analisi dell'organizzazione macro-strutturale del EEG nell'autismo rispetto alla condizione di ritardo mentale. I risultati degli studi clinici suggeriscono che, sebbene l'analisi spettrale rappresenti ancora uno strumento prezioso per l'indagine dell'EEG, l'analisi frattale nel dominio del tempo fornisce informazioni aggiuntive sul funzionamento del cervello che l'analisi tradizionale non è in grado di rilevare, con il vantaggio di impiegare tecniche a basso costo computazionale.

ACKNOWLEDGMENTS

First and foremost, I would like to express my gratitude to the University of Trieste for the PhD studentship grant, and to my supervisor, Prof. Agostino Accardo, without whom this work would not have been possible.

I am grateful to Fabrizio Monti, MD, of the Neurophysiopathology Sub Division of the Clinical Neurology Ward at the AOTS Hospital of Trieste for sharing his medical knowledge with me.

I acknowledge all of the specialists of the Anesthesiology and Reanimation Clinic at the IRCCS "Burlo Garofolo" Scientific Institute of Trieste for their helpfulness.

I owe special gratitude to my former colleague Andrea Orsini for the pleasant and fruitful collaboration.

I gratefully acknowledge Sergio Zanini, MD, PhD, and Paolo Brambilla, MD, PhD, of the Developmental Psychopathology Unit at the IRCCS "Eugenio Medea" Scientific Institute of Udine for the constructive discussions and the helpful suggestions.

I would also like to thank my colleagues and friends, Francesco and Mariangela, for the good moments we have shared during these years.

I am grateful to my friends for bearing with me through the last few months and for the invaluable encouragement provided during this work. A special thanks goes to my best friend, Stefano, whose confidence in me has often been stronger than my own.

Finally, I wish to thank my parents, Leonardo and Gabriella, for supporting and loving me, and my brother, Giuseppe, who has passed on to me his passion for learning. To them I dedicate this thesis.

CONTENTS

1 INTRODUCTION

Background

Electroencephalography is the recording of brain electrical activity. It is a non invasive, simple and relatively cheap technique which provides a measure of neuronal functioning with high temporal resolution. When appropriately processed, the EEG is a valuable tool for the diagnosis and prognosis of many neurological disorders as well as for the monitoring of cerebral functions. It allows the identification of abnormal patterns, the localization of brain sources and the detection of event related potentials. The analysis of the electroencephalogram is also useful to understand how the electrical patterns modify between different brain activities, during the transition from wakefulness to sleep or with age. These are the reasons why great effort has been devoted to the development of suitable signal processing techniques to analyze EEG.

Since the EEG signal, as many biomedical time series, is apparently random in time, it has been traditionally ascribed to stationary stochastic processes and thus analyzed with linear techniques. The autocorrelation of EEG samples, as well as the power carried by the different waves, have been widely used as quantitative measures of brain electrical activity. A more recent perspective to address the irregular behavior of the EEG stems from chaos theory. According to chaos theory randomness can also be displayed by deterministic nonlinear dynamical systems with just a few degrees of freedom. Chaotic systems, though deterministic, are highly unpredictable due to their sensitive dependence on initial conditions. However, the rules governing the dynamics of such systems are, actually, simple. Chaos theory provides new techniques for the analysis of many physiological systems and suggests the existence of simple mathematical models for their description. The most characteristic measures of a chaotic system are the largest Lyapunov exponent, which quantifies the rate of the exponential divergence of nearby trajectories in the phase space, and the correlation dimension, representing the unusual geometry of the so-called strange attractor. Both measures generally require the reconstruction of the attractor in the phase space from the available observation in time, procedure that may be computationally expensive. An alternative way to approach the study of complex systems is offered by fractal geometry. The main features of fractal objects, namely self-similarity and noninteger dimension, can be displayed also by a time series directly in the time domain. In this perspective, the fractal-like behavior of the EEG and its unusual power spectrum can be characterized by parameters like the fractal dimension, the power-law exponent and the Hurst index. A fruitful connection between the aforementioned

measures is provided by fractional Brownian motion (fBm), a simple mathematical model for the description of the EEG.

Aims of the thesis

This thesis explores the time domain approach for the study of the chaotic behavior of brain electrical activity based on the analysis of the fractal-like features of the EEG signal. The aims of the thesis are: 1) to determine the most accurate methodology for the fractal analysis of the EEG in the time domain and 2) to assess the ability of EEG fractal analysis to provide additional information to that achieved by traditional spectral analysis.

Thesis outline

The thesis is divided into two parts, reflecting the twofold nature of Author's research activity.

The first part provides the theoretical notions and the analysis tools necessary to understand the Author's approach to the clinical issues presented in the second part. After a brief overview of the basics about electroencephalography (Chapter 2), the fundamental concepts of nonlinear dynamical systems theory are described in Chapter 3, with particular focus on the notions of deterministic chaos, sensitivity to initial conditions and strange attractor. The tools for the analysis of irregular time series in the phase space, based on chaotic systems theory, are then provided. Chapter 4 presents an alternative perspective for the study of complex systems producing irregular time series based on the notion of fractal geometry. The concepts of self-similarity and fractal dimension are then introduced and adapted for the characterization of fractal objects in time. The characteristics of fractional Brownian motion, the most useful mathematical model for the fractal processes in nature, including the EEG, are then discussed. At the end of this chapter, Author's approach to the analysis of the EEG is described. The next two chapters contain two theoretical studies conducted by the Author in order to define the most accurate methodology for the study of the fractal-like behavior of the EEG in the time domain. In Chapter 5 the Author presents a comparison of three widely used algorithms for the estimation of the fractal dimension of time series directly in the time domain. The most reliable algorithm in terms of accuracy and sensitivity to estimation parameters, namely the sampling frequency and the time window length, is identified and will be used for all further investigations. In Chapter 6 the Author discusses the accuracy of the fBm model, evaluating how much the EEG scaling relationship between the fractal dimension and the power-law exponent deviates from the theoretical one, valid for fBm, widely used in literature for the indirect estimation of EEG fractal dimension.

The second part of the thesis contains three applications of time domain fractal analysis of the EEG to clinical issues which presumably involve abnormal complexity of neuronal activity. Chapter 7 presents a study on the monitoring of carotid endarterectomy (CEA) conducted in close collaboration with the Neurophysiopathology Sub Division of the Clinical Neurology Ward at the AOTS Hospital of Trieste. CEA is a common surgical procedure for the prevention of stroke in patient with high-grade carotid stenosis. The standard procedure implies a reduction of cerebral blood flow, in the hemisphere associated with

the carotid clamping, which may lead to intraoperative ischemia. Although some objective measures have been proposed to quantify the risk of intraoperative stroke, the commonest practice is still the visual assessment of the EEG, subject to the experience of the neurophysiologist and prone to human error. Aim of the study was the development of a reliable decision support system based on EEG parameterization. Chapter 8 presents a preliminary study on the monitoring of anesthesia in operating room carried out in cooperation with the IRCCS "Burlo Garofolo" Scientific Institute of Trieste. During surgery, an anesthesiologist is responsible for administering the hypnotic agent to prevent both over dosing side effects and intraoperative awareness. As a consequence of intraoperative awareness, the patient may recall all of the details of the surgical procedure and develop some form of anxiety disorder. Despite the fact that several commercial monitors, based on complex algorithms, are already available to monitor unconsciousness, intraoperative awareness is still a major clinical problem. Aim of the study was the identification of an effective and easy-to-calculate index for the quantification of unconsciousness during general anesthesia. The last study, presented in Chapter 9, was carried out in close collaboration with the Developmental Psychopathology Unit at the IRCCS "Eugenio Medea" Scientific Institute of Udine. Subject of the research was the macro-structural organization of neuronal activity in autism both in the awake state and during sleep. The investigation was aimed at the identification of one or more parameters capable of discriminating autism from mental retardation, on the basis of brain electrical activity, for early diagnosis and intervention purposes. In the three aforementioned studies the fractal dimension was compared with traditional spectral measures as well as with a time domain nonlinear index, i.e., the zero-crossings. General conclusions are provided in Chapter 10, while Appendix A gives a brief description of the algorithm for the zero-crossings count.

Software

All the algorithms used for data analysis were implemented by the Author in the MATLAB environment (The MathWorks, Inc.).

Part I

Fractal analysis of the EEG

2 ELECTROENCEPHALOGRAPHY

CONTENTS

The rationale for the application of advanced digital signal processing techniques to the electrical signals measured from the brain of human subjects lies in the assumption that the electroencephalogram reflects neuronal functioning and is, therefore, an indicator of the status of the whole body. In this chapter, after a brief history of electroencephalography, the physiological concepts underlying the generation of the EEG signal are introduced. An overview of the rhythms that characterize the EEG is then presented. The problems of recording and conditioning of the raw signal are finally addressed. The concepts presented in the present chapter are adapted from Sanei and Chambers [2007].

2.1 HISTORY

The first recording of brain electrical activity was performed in 1875 by English scientist Richard Canton using a galvanometer connected to the scalp of a human subject through two electrodes. At that time, the term "electroencephalogram" (EEG) was coined to denote the writing of brain electrical activity recorded from the head. However, the first report of the EEG on photographic paper in 1929 is due to German psychiatrist Hans Berger, who is known among electroencephalographers as the discoverer of the human EEG. During the 1930s the interest in the recording of the EEG raised up. In 1932 the Rockefeller foundation produced the first differential amplifier for EEG and the importance of multichannel recordings was right after recognized. Research activity focused on the EEG started in the USA around 1934 with the studies on the alpha rhythm, epileptic seizure and brain activity during sleep, and lead to the foundation of the American EEG Society in 1947. Analysis of EEG signals was introduced right after the early recordings, when Berger himself applied Fourier transformation to the recorded traces. Throughout the years, the power of the EEG as a source of information about the brain became more and more evident and brought to the development of clinical and experimental studies for detection,

diagnosis, treatment and prognosis of several neurological abnormalities, as well as for the characterization of many physiological states.

2.2 ORIGIN OF THE EEG

The Central Nervous System (CNS) consists of the brain and its natural extension, the spinal cord. The brain is largely made up by nerve cells (or *neurons*) and glia cells.

Neurons

Neurons are electrically excitable cells that receive, process and transmit information by electro-chemical signaling. A typical neuron consists of a cell body (signal processor) with branching dendrites (signal receivers) and an axon (signal transmitter) often sheathed in myelin (Fig. 1). The information transmitted by an axon, the so-called *action potential*, is transmitted to the following neuron across a specialized junction called synapse. Neurons are electrically excitable cells characterized by a resting membrane potential of approximately -70 mV. This voltage is determined by the intra- and extracellular concentrations of Na^+, K^+, Cl^- and Ca^{2+} ions, which are maintained by means of metabolically driven ion pumps combined with chemically-gated ion channels embedded in the membrane. Changes in the ionic concentrations on the two sides of the membrane, induced by chemical activity at the preceding synapse, can modify the function of the voltage-gated ion channels. The opening and closing of these channels induce deviations from the resting potential. A *depolarization* occurs when the interior potential becomes less negative while a *hyperpolarization* occurs when the voltage inside the membrane becomes more negative. If the depolarization is large enough to drive the interior voltage above a threshold of about -55 mV, an action potential (a spike up to approximately +30 mV) is triggered and travels down the axon. If the axon ends in an excitatory synapse, an excitatory postsynaptic potential occurs in the following neuron (depolarization). If the axon ends in an inhibitory synapse, an inhibitory postsynaptic potential will occur in the following neuron (hyperpolarization).

Membrane potential

Action potential

EEG

An EEG signal is the measurement of the microscopic synaptic currents mainly produced within the dendrites of special neurons called *pyramidal neurons*. Pyramidal neurons, located in the cerebral cortex, in the hippocampus and in the amigdala, are characterized by highly branched axons and dendrites. The large number of synaptic connections allows the pyramidal neuron to receive (transmit) signals from (to) many different neurons. When neighboring pyramidal neurons are activated synchronously, the sum of the microscopic synaptic currents generates a magnetic field and a secondary electrical field. Since the signal is attenuated by head tissues and corrupted by noise generated within the brain, only large populations of active pyramidal neurons can generate enough potential to be recordable using scalp electrodes.

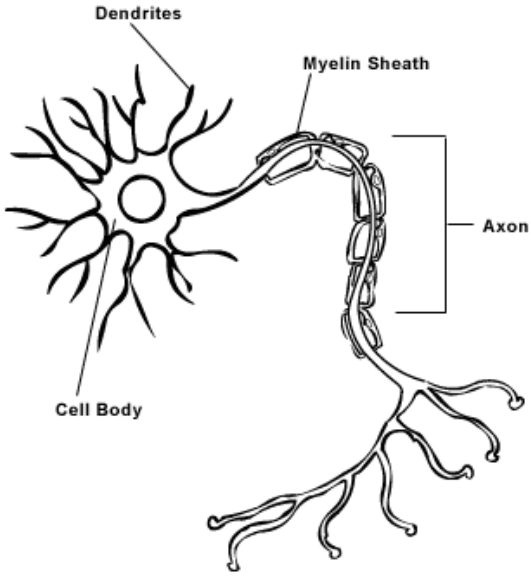

Figure 1: Structure of a typical neuron.

2.3 EEG RHYTHMS

Five major brain rhythms are recognized in the EEG: delta, theta, alpha, beta and gamma, each characterized by a specific frequency range. The characteristics of the waves change not only with pathology or age, but also according to the physiological state (wakefulness or sleep, for example). The delta rhythm, in the range 0.5-4 Hz, is primarily associated with deep sleep. Delta activity occurs also in case of coma and other disorders of consciousness, as well as during anesthesia. Theta activity, with frequencies between 4 and 8 Hz, appears as consciousness slips toward drowsiness or during deep meditation. Theta waves occur mainly during infancy and childhood and are abnormal in the awake adults. Alpha activity, in the range 8-13 Hz, commonly appears as a sinusoidal signal. It is characteristic of eyes-closed awake state (relaxed awareness) and is mainly present in the occipital lobes. The beta waves are associated with active thinking and problem solving and are usually found in adults within the range 13-30 Hz. Gamma activity refers to waves with frequencies above 30 Hz and seems to be related to consciousness. The frequency ranges of the five EEG rhythms are summarized in Tab. 1.

2.4 RECORDING OF THE EEG

A typical multichannel EEG recording is performed with scalp electrodes, commonly Ag/AgCl disks less than 3 mm in diameter, with long flexible leads that can be plugged into an amplifier. In order

Table 1: Frequency ranges of EEG characteristic rhythms.

Rhythm	Frequency range [Hz]
delta (δ)	0.5-4
theta (θ)	4-8
alpha (α)	8-13
beta (β)	13-30
gamma (γ)	>30

to avoid distortion, the electrode impedance is generally kept below 5 kΩ. Electrodes are applied to the scalp of the subject according to the so-called *10-20 system*. The 10-20 system is a method for the electrode positioning recommended by the International Federation of Societies for Electroencephalography and Clinical Neurophysiology [Jasper, 1958]. Proposed to ensure standardized reproducibility, the positioning method is based on constant distances from specific anatomic landmarks. The location of the electrodes on the front-back line of the skull is based on dividing the distance between the *nasion* (N) and the *inion* (I) over the vertex in the midline. The positioning on the left-right line of the skull is similarly based on dividing the distance between the ears over the vertex in the midline. Each location is characterized by a letter, to identify the underlying brain region (Fig. 2a), and a number, to identify the brain hemisphere. The letter "F", "T", "C", "P" and "O", denotes the frontal, temporal, central, parietal and occipital brain regions, respectively. Odd numbers identify electrodes placed in the left hemisphere, whereas even number refer to those on the right hemisphere. Locations along the midline are denoted by letter "z". To understand how channels are located in the 10-20 system, consider the example of Fig. 2b. The first location, Fp1, is positioned at 10% of the NI distance from N, the second one, F3, is located at 20% of the NI distance from Fp1 (corresponding to 30% from N) and so on in steps of 20% until location O1 which is positioned at 20% of the NI distance from the preceding one, P3, and at 10% of the NI distance from I. The 10-20 system is a conventional electrode setting meant for 21 channels. However, further locations were added to meet the use of a larger number of electrodes. For multichannel recordings, electrode caps are often used.

10-20 system

Electrodes montage

EEG signal can be recorded according to different modalities. In the *differential montage*, each derivation represents the difference of two adjacent electrodes. To record Fp1-F3, for example, the inputs of the differential amplifier are Fp1 and F3. In the *referential montage*, each derivation represents the difference between a certain electrode and a designed reference. One or two reference electrodes are commonly used. The most used physical references are vertex (Cz), linked-ears and tip of the nose. Also reference-free recording techniques, which actually use a common average reference, can be used. In order to avoid topographic distortion, the reference should be chosen as neutral as possible.

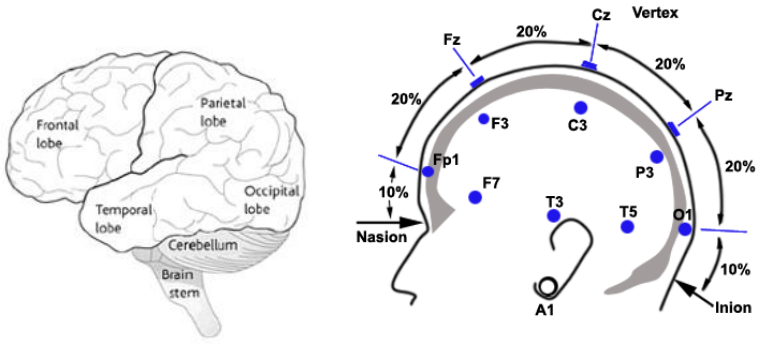

(a) Brain lobes **(b)** 10-20 system

Figure 2: International 10-20 system of electrode placement.

EEG conditioning

The EEG recorded from the scalp has amplitudes of about 10-100 μV and can contain frequencies up to 200-300 Hz. Raw EEG may be corrupted by many physiological and non-physiological artifacts. The main physiological artifacts derive from electrical activity of the heart (ECG), eyes movements and blinks, muscle activity and sweating. Power-line interference, impedance fluctuations and electrical noise from electronic components are the most frequent non-physiological noise sources. In order to retain the effective information, reject artifacts and prevent aliasing, EEG signals have to be filtered prior to being analyzed. A highpass filter, with cutoff frequency below 0.5 Hz, is generally used in order to remove low frequency baseline drift. A low pass filter must be used to reject high frequency noise and to prevent aliasing. The low pass cutoff frequency is set according to the application. The neuronal information of routine EEG is generally limited to approximately 50-70 Hz. Notch filters may be required in order to reject the power-line frequency (50 or 60 Hz according to the country). All filters must be designed in order to avoid the introduction of undesired distortions. The sampling frequency, that must be chosen according to the Nyquist-Shannon sampling theorem, commonly ranges from 100 to approximately 1000 Hz. Sometimes, when a higher spectral resolution is required for the representation of the signal in the frequency domain, sampling frequencies of up to 2 kHz may be used.

3 DYNAMICAL SYSTEMS AND CHAOS THEORY

CONTENTS

Since the early electroencephalographic recordings, the EEG manifested itself as an apparently random or aperiodic signal. The most simple system which produces aperiodic signals is a linear stochastic process. A stationary stochastic process can be described in the time domain by mean and variance of the observed time series. A better description, including the information about the time evolution of the system, is given by the so-called *autocorrelation* function, which measures the linear correlation between data points. The same system can be equivalently approached using *Fourier transform*, a mathematical tool which is used to decompose a signal into a set of sinusoidal components whose amplitudes and phases are represented in the frequency domain. In the frequency domain the system is described by the *power spectral density* which represents how the power of the signal is distributed with frequency. The fruitful connection existing between the autocorrelation function and the power spectral density is provided by the Wiener-Khinchin theorem. The Wiener-Khinchin theorem states that the power spectral density of a wide-sense stationary stochastic process is equal to the Fourier transform of the corresponding autocorrelation function. Hence, using Parseval's theorem, the total power of the signal can be calculated equivalently in the time or in the frequency domain. If the system properties change over time, producing nonstationary signals, the *short-time Fourier transform* is used to produce the spectrogram which provides a time-frequency representation of the system. As many other aperiodic signals, the EEG has been widely analyzed as the output of a stationary stochastic process. Traditional linear analysis of the EEG mainly involves the estimation of the power carried by the different rhythms characterizing the signal (Tab. 1).

The introduction of chaos theory provided a new approach to the analysis of irregular time series. According to chaos theory, random behavior can arise also in deterministic nonlinear dynamical system with just a few dynamical variables. New methods were introduced to cap-

ture the unusual behavior of irregular time series, including the EEG. After a brief overview of nonlinear dynamical systems and their representation in the phase space, this chapter introduces the basics about chaos theory, including the concepts of unpredictability and strange attractor. The measures for quantifying the properties of a chaotic system, including largest Lyapunov exponent and correlation dimension are then presented. The chapter finally addresses the problem of phase space reconstruction, which is required for the calculation of the aforementioned parameters. The notions provided in this chapter are adapted from Henry *et al.* [2001] and Kantz and Schreiber [2004].

3.1 NONLINEAR DYNAMICAL SYSTEMS

Nonlinear dynamical system

The concept of dynamical system is applied to any system that evolves in time. Dynamical systems evolving continuously in time are mathematically defined by a coupled set of first-order autonomous ordinary differential equations:

$$\frac{d}{dt}\mathbf{x}(t) = \mathbf{F}(\mathbf{x}(t)) \tag{1}$$

while a coupled set of first-order autonomous difference equations describes dynamical systems whose behavior changes at discrete time intervals:

$$\mathbf{x}_{n+1} = \mathbf{G}(\mathbf{x}_n) \tag{2}$$

The components of the vectors $\mathbf{x}$ are the dynamical variables of the system evolving in continuous time ($t \in \mathbb{R}$) or in discrete time ($n \in \mathbb{Z}$) and the components of the vector fields $\mathbf{F}$ and $\mathbf{G}$ represent the dynamical rules governing the evolution of the dynamical variables. The term *autonomous* refers to the property of the vector fields of being not explicitly dependent on time. It should be noted that there is no loss of generality in the restriction to autonomous systems since a nonautonomous systems can be transformed into an autonomous systems by the introduction of additional degrees of freedom.

Deterministic nonlinear dynamical system

Under modest smoothness assumptions about the evolution rules, the mathematical theory of ordinary differential (or difference) equations ensures the existence of unique solutions. Thus, the dynamical system is *deterministic*, that is, once the current state is determined, the state at any future time is determined as well. However, despite the existence of unique solutions, there may be no explicit algebraic representation of the state of the system at a given point in time.

3.2 PHASE SPACE AND ATTRACTORS

Phase space

Phase space is an abstract mathematical space in which each possi-

ble state of a dynamical system is represented by a point. Thus, if the systems is defined by a set of n first-order autonomous ordinary differential (or difference) equations, then the phase space is a finite dimensional vector space in $\mathbb{R}^n$. A sequence of points $\mathbf{x}_n$ or $\mathbf{x}(t)$ solving the equations is a *trajectory* of the dynamical system in the phase space. As dynamical variables evolve in time, the representative point of $\mathbf{x}_n$ and $\mathbf{x}(t)$ traces out a continuous curve or a sequence of points in the phase space, respectively. As time proceeds, trajectories in the phase space can run away to infinity or remain in a bounded area. If a dynamical system is also dissipative, that is, on average the phase space volume contracts as the system evolves, a set of initial conditions will be attracted to some sub-set of the phase space. This sub-set, invariant under the dynamical evolution, is called the *attractor* of the system. Simple examples of attractors are fixed points and limit cycles.

Trajectory

Attractor

3.3 DETERMINISTIC CHAOS AND STRANGE ATTRACTORS

The solutions of many nonlinear dynamical systems are apparently random. Even though these systems are deterministic, with no random elements involved, they result highly unpredictable. However, random signals generated by noise are fundamentally different from those generated by low order deterministic dynamics. The behavior of such systems, highly sensitive to initial conditions, is known as *deterministic chaos*. Geometrical counterpart of the sensitivity to initial conditions is the complex structure exhibited by the attractors. These attractors are known as *strange attractors*.

Deterministic chaos

Strange attractors

One of the first examples of three-dimensional nonlinear dynamical system evolving continuously in time and showing chaotic behavior is the Lorenz oscillator [Lorenz, 1963]. The Lorenz oscillator is governed by the following differential equations:

$$\begin{aligned} \frac{dx}{dt} &= \sigma(y - x) \\ \frac{dy}{dt} &= x(\rho - z) - y \\ \frac{dz}{dt} &= xy - \beta z \end{aligned} \tag{3}$$

Figure 3a shows Lorenz strange attractor for $\rho = 28$, $\sigma = 10$ and $\beta = \frac{8}{3}$.

A two-dimensional discrete dynamical system is the Hénon map [Hénon, 1976]. The difference equations that describe the Hénon map are:

$$\begin{aligned} x_{n+1} &= y_n + 1 - \alpha x_n^2 \\ y_{n+1} &= b x_n \end{aligned} \tag{4}$$

The strange attractor of the canonical Hénon map, built with $\alpha = 1.4$ and $b = 0.3$, is shown in Fig 3b.

A strange attractor is characterized by the following properties:

(a) Lorenz attractor. **(b)** Hénon map.

Figure 3: Strange attractors of a 3D continuous and a 2D discrete dynamical system.

- phase space trajectories through all points on the attractor diverge exponentially on average;
- the dimension of the set of points delimited by the attractor is noninteger.

The next two subsections discuss more in detail the aforementioned properties.

3.3.1 Sensitivity to initial conditions: Lyapunov exponents

Lyapunov exponents

The dynamical property of a chaotic system manifests itself in the unpredictability of the future states due to the sensitive dependence on its initial conditions. Nearby trajectories separate very fast, or more precisely, exponentially fast over time. The average exponential separation between nearby phase space trajectories, related to the strength of chaos, is quantified by Lyapunov exponents. Although a dynamical system in $\mathbb{R}^n$ has associated n Lyapunov exponents, the overall predictability of the system is determined by the largest Lyapunov exponent, λ. Consider two points in the phase space with Euclidean distance $\delta_0 \ll 1$ at time $n = n_0$ and denote with $\delta_{\Delta n}$ the Euclidean distance between the two trajectories emerged from these points at time $n = n_1$. The largest Lyapunov exponent λ is then determined by:

$$\delta_{\Delta n} \simeq \delta_0 e^{\lambda \Delta n}, \quad \delta_{\Delta n} \ll 1, \quad \Delta n \gg 1 \tag{5}$$

where $\Delta n = n_1 - n_0$. A positive value of λ implies an exponential divergence of nearby trajectories, i.e., chaos (Tab. 2).

3.3.2 Noninteger dimension: correlation dimension

Correlation dimension

Attractors of dissipative chaotic systems have an apparently complex structure showing details on all length scales. One of the early way to quantify the strangeness of a strange attractor by a dimension was proposed by Grassberger and Procaccia [1983]. They called this notion

Table 2: Possible types of motion and corresponding largest Lyapunov exponent.

Type of motion	Largest Lyapunov exponent
stable fixed point	$\lambda < 0$
stable limit cycle	$\lambda = 0$
chaos	$0 < \lambda < \infty$
noise	$\lambda = \infty$

correlation dimension. The correlation sum for a set of points $\mathbf{x}_n$ in some vector space is defined as the fraction of all possible pairs of points whose distance ρ is less than or equal to a given distance r:

$$C(r, N) \approx \frac{2}{N(N-1)} \sum_{i=1}^{N} \sum_{j=i+1}^{N} \Theta(r - \rho(\mathbf{x}_i, \mathbf{x}_j)) \tag{6}$$

where the Heaviside step function is defined as:

$$\Theta(s) = \begin{cases} 1, & \text{if } s \geqslant 0 \\ 0, & \text{if } s < 0 \end{cases} \tag{7}$$

The sum counts the pair ($\mathbf{x}_i$,$\mathbf{x}_j$) whose distance ρ is smaller than r. The correlation dimension D is defined as:

$$D = \lim_{r \to 0} \lim_{N \to \infty} \frac{\log C(r, N)}{\log r} \tag{8}$$

Since both limits cannot be realized in practical applications, Grassberger and Procaccia proposed to deduce D from the law $C(r) \propto r^D$ as the slope of the straight line fitting $\log C(r)$ versus $\log(r)$. The notion of dimension is important because it is related to the minimum number of dynamical variables required to describe the dynamics of the strange attractor.

3.4 PHASE SPACE RECONSTRUCTION

The largest Lyapunov exponent and the correlation dimension provide information about the dynamics of the trajectories and the geometry of the strange attractor, respectively. Thus, to better understand the nature of a chaotic system, knowledge of the trajectories in phase space is desirable. Unfortunately, in most practical cases one does not have direct access to the system but what he observes is a single time series. The essential problem in the study of deterministic dynamical systems is the reconstruction of the state vectors in phase space from a given

Phase space reconstruction

observation in time. The method of phase space reconstruction, developed by Packard *et al.* [1980], has been rigorously justified by the embedding theorems of Takens [1981] and Sauer *et al.* [1994].

Embedding theorem

According to Takens, if the observed time series is one component of an attractor that can be represented by a smooth d-dimensional manifold (with d an integer) then the topological properties of the attractor (such as the largest Lyapunov exponent and the correlation dimension) are equivalent to the topological properties of the embedding formed by the m-dimensional phase space vectors:

$$\mathbf{s}_n = (s_{n-(m-1)\tau}, s_{n-(m-2)\tau}, ..., s_{n-\tau}, s_n) \tag{9}$$

whenever $m \geqslant 2d + 1$. In Eq. 9 τ is the time delay and m is the embedding dimension. Sauer extended Takens' theorem to the case of strange attractors with noninteger dimension D.

To optimize the measurements of the largest Lyapunov exponent and the correlation dimension, there is the need to specify the optimum value for the embedding dimension m and the time delay τ. Although for many practical purposes the most important embedding parameter is the product $m\tau$, the embedding dimension and the time delay are commonly chosen separately.

3.4.1 Optimal m

Embedding dimension

The main problem of phase space reconstruction is the choice of the optimal embedding dimension. As asserted by the aforementioned embedding theorems, a phase space is correctly reconstructed if the embedding dimension is chosen as $m \geqslant 2D + 1$. In this terms, if a m embedding dimension provides a good representation of the phase space, every m' embedding dimension greater than m would be as much correct. However, the choice of an arbitrary large m value will result in an increased computational effort required by the algorithms for the analysis of the dynamical system. Thus, the main problem in phase space reconstruction is the choice of the optimal embedding dimension.

False nearest neighbors

Kennel *et al.* [1992] developed a method for determining the embedding dimension introducing the concept of *false nearest neighbors*. Consider two neighboring states in the phase space at a given time. Under smoothness assumptions about the dynamical rules governing the system, the two trajectories emerging from the two points should be still close after a short time interval δ_n despite the sensitivity to initial conditions. If two neighboring states in a m_i-dimensional space diverge exponentially in the m_{i+1}-dimensional space, then they are defined "false neighbors" for the chosen m_i embedding dimension. The algorithm compares the distances between neighboring trajectories at successively higher dimensions. When the ratio between the distances in dimension m_i and in dimension m_{i+1} is greater than a fixed threshold, large enough to allow for exponential divergence due

to deterministic chaos, then the considered trajectories are false neighbors. As i increases, the percentage r of false neighbors decreases and the optimal embedding dimension is chosen where r approaches zero.

3.4.2 Optimal τ

Time delay

The embedding theorems consider data with infinite precision. Thus, embedding with the same dimension m but different time delay τ are equivalent in the mathematical sense for noise-free data. However, if τ is small compared to the internal time scales of the system, consecutive phase space points are strongly correlated. On the other hand, for large values of time delay successive elements are already almost independent. One of the most common methods for determining the optimal time delay is based on the behavior of the *autocorrelation* function of the signal. According to this method, the first zero of the autocorrelation function represents a good value of τ. Another proposal is based on the more refined concept of *mutual information* introduced by Fraser and Swinney [1986]. The optimal value of time delay corresponds to the first local minimum of the mutual information which is a quantity that measures how much information on the average can be predicted about one time series point given full information about the other.

Autocorrelation

Mutual information

4 FRACTAL GEOMETRY OF THE EEG

CONTENTS

The measures presented in the preceding chapter for the characterization of a dynamical system producing irregular time series require the reconstruction of the phase space, a procedure which may be computationally expensive.

A new perspective to approach the study of such systems without reconstructing the attractor is offered by the concept of fractal geometry. Complexity is a theme shared by many physiological systems in all areas of medical research. The classical notion of scaling is not able to describe the irregular structures seen in lungs and brain, as well as the irregular patterns of electroencephalographic and heart rate variability signals. In this chapter, the main features of fractal shapes are firstly presented in the more intuitive space domain and then adapted for the characterization of fractal processes in time. Fractional Brownian motion, the most used mathematical model for natural fractal processes, including the EEG, is then described. Finally, the fractal approach adopted by the Author during the PhD course for the analysis of the EEG is presented. The theoretical concepts presented in this chapter are adapted from Peitgen and Saupe [1988].

4.1 FRACTALS AND SELF-SIMILARITY

Within the last 30 years fractal geometry has become a central concept in most of the natural sciences, among which physics, chemistry, physiology and meteorology. Although fractal objects are complex in appearance, they arise from simple rules and contrarily to Euclidean shapes, they represent more suitable models for natural phenomena.

Euclidean versus fractal geometry

To understand the major differences between Euclidean and fractal geometry, consider a three-dimensional Euclidean shape, for example a sphere. A sphere is characterized by one size (the radius r), is

completely described by a simple algebraic formula ($(x-x_0)^2+(y-y_0)^2+(z-z_0)^2=r^2$) and provides an accurate description of many artificial objects. Fractals, on the contrary, have no characteristic size (they are self-similar or independent of scale), are usually the result of a recursive construction procedure and provide a good description of many natural shapes, processes or phenomena (coastlines, turbulence, snowflakes, etc.).

Consider the von Koch curve, one of the first mathematical fractals described in literature [von Koch, 1904]. Figure 4 shows the first four steps of the recursive procedure for constructing this famous fractal curve. A line segment is first divided into three equal segments (n=0). The middle segment is replaced by two equal segments forming two sides of an equilateral triangle (n=1). This procedure is then repeated on each of the four segments, whose middle third is replaced by two equal segments forming two sides of an equilateral triangle (n=2). On each iteration, the number of the segments is multiplied by four while the length of the segments is divided by three. Thus, the length of the curve increases by a factor of $\frac{4}{3}$ with each iteration. The von Koch curve is the limiting curve obtained by iterating the construction rule an infinite number of times.

The von Koch curve has no characteristic size. It exhibits an exact *self-similarity*, meaning that each small portion, when magnified, is exactly identical to the original one. The curve is said to be independent of scale because there will be an equivalent level of detail at every scale. Moreover, the limiting curve obtained after an infinite number of iterations would compress an infinite length into a finite area of the plane without intersecting itself. The von Koch curve, though apparently complex, is produced by the iteration of a very simple rule. However, there is no algebraic formula that can describe its points in the plane. Based on the von Koch curve, the fractal shape of Fig. 5 provides a good description of the snowflake.

4.2 SELF-SIMILARITY AND DIMENSION

Self-similarity

One of the central concepts of fractal geometry is the property of self-similarity, also known as *scaling* or *scale-invariance*. Although every fractal exhibits some form of self-similarity, it is not true that, if an object is self-similar, then it is fractal. Consider a one-dimensional Euclidean object like a line segment. It can be divided into N identical segments each reduced by a scaling factor $r=\frac{1}{N}$. A two-dimensional Euclidean object, for example a square area, can be divided into N smaller squares, each scaled down by a factor $r=\frac{1}{\sqrt[2]{N}}$. Similarly, a three-dimensional Euclidean object, such as a solid cube, can be divided into N self-similar copies, each scaled down by a factor $r=\frac{1}{\sqrt[3]{N}}$. It can be deduced that, in the same way, a D-dimensional self-similar object can be divided into N identical parts each of which is reduced

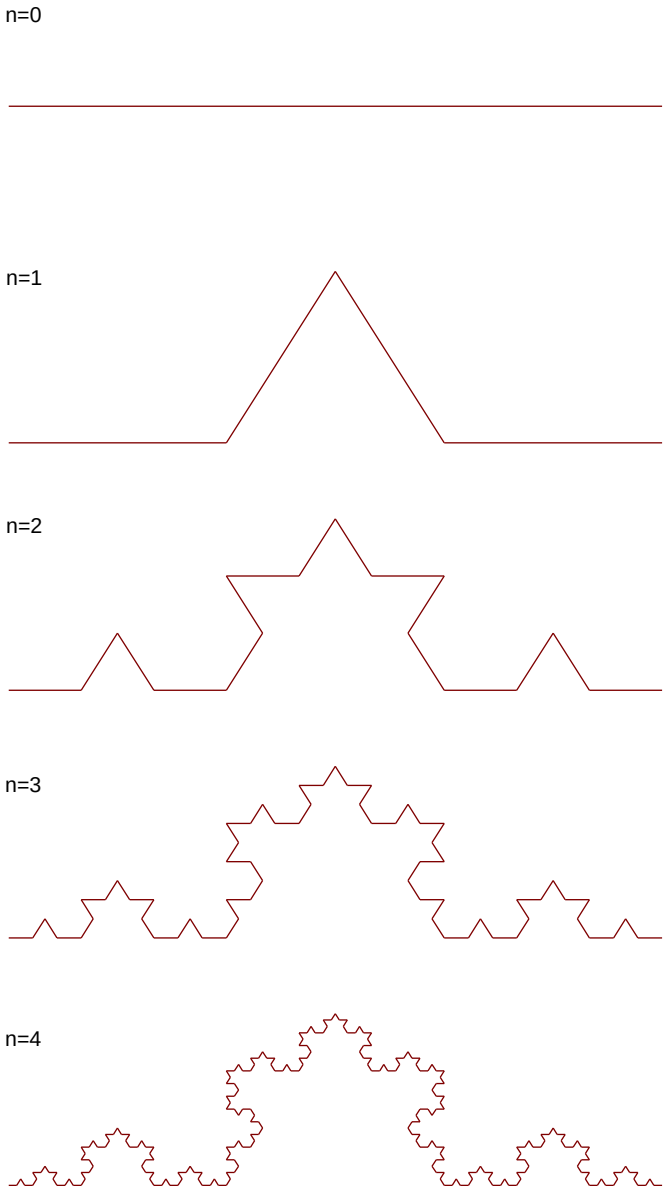

Figure 4: Initiator (n=0) and generator (n=1) of the von Koch curve, and next steps in the construction.

by a factor $r = \frac{1}{\sqrt[D]{N}}$. The relation between the number N of rescaled D-dimensional objects and the reduction factor r is given by:

$$N = \frac{1}{r^D} \tag{10}$$

Thus, given a Euclidean self-similar object divided into N parts scaled down by a factor r from the whole, its *dimension* is equal to:

$$D = \frac{\log N}{\log \frac{1}{r}} \tag{11}$$

Dimension

The concept of self-similarity is intimately connected with the intuitive notion of dimension. However, the dimension of a self-similar object needs not to be an integer. Consider the von Koch curve of Fig. 4. Each segment is composed by 4 sub-segments, each scaled down by a factor of $r = \frac{1}{3}$ from its parent. By using Eq. 11 it derives that $D = \frac{\log 4}{\log 3}$, i.e., the dimension of the von Koch curve is non integer. Thus, the von Koch curve is a self-similar object with *fractal dimension* $FD = 1.2619$. The fractal dimension reflects the unusual property of the von Koch curve of filling more space than a Euclidean line segment ($D = 1$) but less than a Euclidean area ($D = 2$). In this terms, as FD increases from 1 toward 2, the self-similar curves progress from being "line-like" to "area-like", though remaining curves with a topological dimension of 1.

Statistical self-similarity

Exact self-similar objects would be inaccurate models for most fractals in nature. A coastline, for example, does not exhibit the exact scale invariance of the von Koch curve. When magnified, smaller parts of a coastline show the same statistical properties of the whole but never look like the whole. Fractals in the real world are, to be more precise, *statistically self-similar*. Moreover, whereas a mathematical fractal object has an infinitely repeatedly self-similarity when magnified, fractals in nature are statistical self-similar only over a finite number of scales. Scale-invariance is an approximation of the real world, from a physicist's point of view, and vice versa, from the mathematician's perspective.

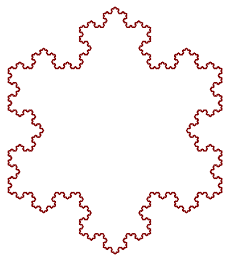

Figure 5: Von Koch snowflake, derived from the von Koch curve.

4.3 TIME–DOMAIN SELF–SIMILARITY

Although fractal geometry is generally meant in space, self-similar behavior can be observed also in time. Randomness in time is generally ascribed to *noise*. The correlation between successive points in a random process is determined by the "color" of the noise, which is related to the slope of the power spectral density. The most famous noise is represented by *white noise* (Fig. 6). White noise is characterized by flat power spectral density, representing equal amounts of power at all frequencies within a fixed bandwidth. In a statistical sense, white noise is an uncorrelated process that could be produced by a random number generator. A highly correlated process is the *Brownian motion*, also known as red noise or brown noise, which is characterized by a power density proportional to $\frac{1}{f^2}$ (Fig. 6). It can be produced by a random walk process or by integrating white noise. The process having a power spectral density proportional to $\frac{1}{f}$ is the *pink noise*, whose name arises from being intermediate between white noise and red noise (Brownian motion). Within the scientific literature, the term $\frac{1}{f}$-noise is often use to refer to any process characterized by a power spectral density proportional to $\frac{1}{f^\beta}$. For the sake of clarity, in this thesis the Author will refer to $\frac{1}{f^\beta}$ behavior with the term $\frac{1}{f}$*-like* noise. $\frac{1}{f}$-like noise is claimed to be the most common noise found in nature. A time series showing $\frac{1}{f}$-like power spectrum has no characteristic time scale. The property of having no characteristic time scale can be better understood by considering, for example, periodic phenomena. A periodic process has a specific time scale which generates a characteristic peak in the power spectrum. Viewing such a process on a different time scale would dramatically alter its appearance. On the contrary, the fluctuations of a $\frac{1}{f}$-like process, *with appropriate y-axis rescaling*, will appear similar under temporal magnification in the same way that the structure of a fractal shape appears similar under spatial magnification. The underlying temporal process of $\frac{1}{f}$-like time series is fractal in nature [Pritchard, 1992].

$\frac{1}{f^\beta}$ *behavior*

4.4 FRACTIONAL BROWNIAN MOTION

Fractals in nature have been traditionally described with *fractional Brownian motion* (fBm) of Mandelbrot and Van Ness [1968]. Fractional Brownian motion is derived from the mathematical model of Brownian motion, widely used in physics and finance to characterize random fluctuations over time. It is the only self-similar nonstationary process with stationary Gaussian increments. Figure 7 shows three examples of fBm traces with different scaling behavior. As can be inferred, the scaling property of fractional Brownian motion ($B_H(t)$) is determined by H, the Hurst exponent, whose values range between 0 and 1. The more H is close to 0, the rougher are the traces. On the contrary, as H approaches 1 the traces become relatively smooth. The variations of

Fractional Brownian motion

the function, $\Delta B = B(t_2) - B(t_1)$, are related by H to the variations of time, $\Delta t = t_2 - t_1$, according to the simple scaling law:

$$\Delta B \propto \Delta t^H \tag{12}$$

Since the displacements of Brownian motion are proportional to the square root of the elapsed time, a value of $H = \frac{1}{2}$ generates a trace of Brownian motion.

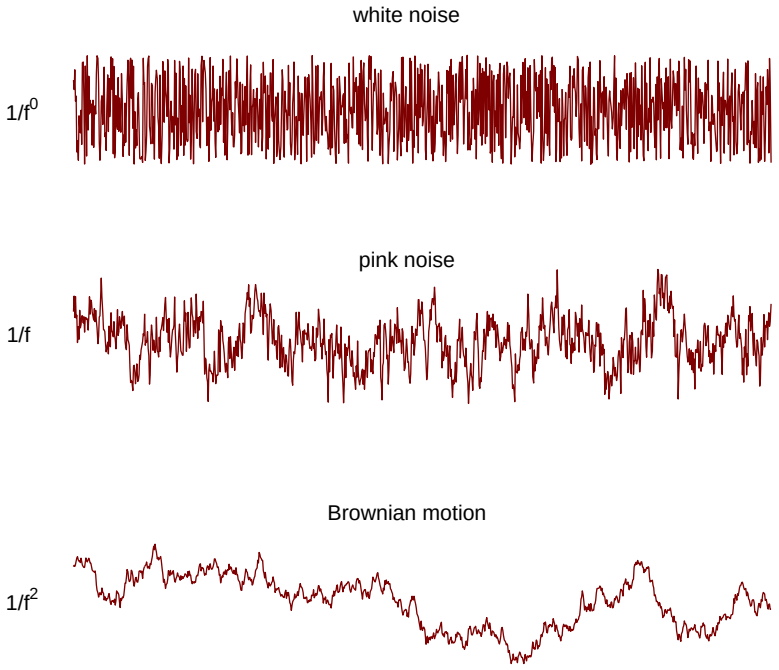

Figure 6: Examples of typical noise processes.

4.5 SELF-AFFINITY

The scaling behavior exhibited by fBm is quite similar but different from the above mentioned exact and statistical self-similarity. Consider, as an example, the Weiestrass function $X_H(t)$ [Bassingthwaighte *et al.*, 1994] (Fig. 8). This function consists of an infinite summation of periodic terms, each of which has a frequency that is a factor γ larger than the preceding term and an amplitude that is γ^H times smaller:

$$X(t) = \sum_{n=0}^{\infty} \frac{\cos(2\pi\gamma^n t)}{\gamma^{Hn}} \tag{13}$$

with γ>1. Whereas self-similar objects repeat identically under magnification, X_H and t must be scaled down by different amounts (ΔX_H and Δt, respectively) to obtain two identical views. In particular, the magnified curve results indistinguishable from the whole only if $\Delta X_H = \Delta t^H$. The property of fractal time series that need such anisotropic scaling in the x- and y-axis, in order to appreciate their self-similarity, is known as *self-affinity*.

Self-affinity

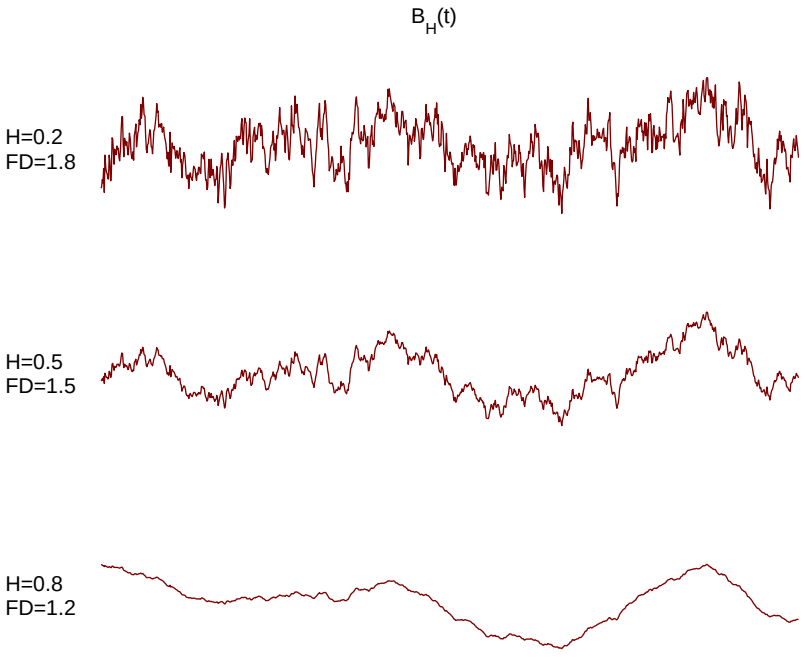

Figure 7: Examples of fractional Brownian motion $B_H(t)$ for different values of H and FD.

4.6 STATISTICAL SELF-AFFINITY: FRACTAL DIMENSION, HURST INDEX AND β EXPONENT

Since fractional Brownian motion traces repeat *statistically* when B_H becomes $\Delta t^H B_H$, fBm scaling property is known as *statistical self-affinity*. As can be seen by comparing Figs. 6 and 7, the roughness of the noises changes with the spectral exponent β similarly to how the roughness of fBm traces changes with H index. A fruitful connection exists be-

Statistical self-affinity

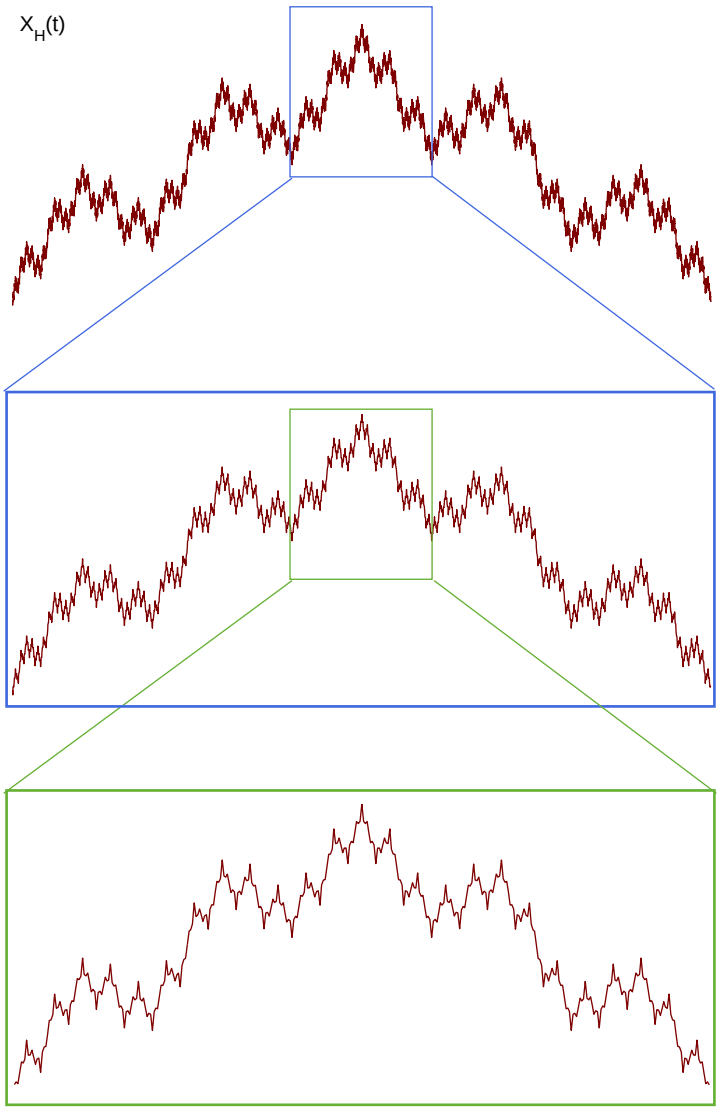

Figure 8: Self-affine structure of the Weierstrass fractal function.

tween the three equivalent characterization FD, H and β of a fBm function:

$$FD = 2 - H = \frac{5-\beta}{2} \tag{14}$$

For $H \in (0,1)$, FD is in the range 1-2 and $1 < \beta < 3$.

4.7 MODELING EEG WITH FBM

The so-called $\frac{1}{f}$-like behavior is a ubiquitous property of complex biological systems. In such scaling, the power spectral density of a time series is governed by an inverse power-law:

$$PSD \propto \frac{1}{f^{\beta}} \tag{15}$$

where the exponent β is related to the color of the series, that is, to the degree of autocorrelation. The human EEG reflects the ongoing activity of the underlying complex system: the human brain. In one of the first studies on the fractal-like behavior of the EEG, Pritchard [1992] reported that the EEG exhibits significant $\frac{1}{f}$-like power scaling, suggesting that the human brain is fractal in time. Moreover, he observed that the EEG displays "more color" than a truly $\frac{1}{f}$ process, meaning that the EEG is autocorrelated to a greater degree. The particular broad-band power spectrum of the EEG could be generated by a high dimensional stochastic system where a large number of multiplicative subprocesses switch from log-normal to $\frac{1}{f}$-like. However, the unpredictability of the EEG could also be attributed to the sensitive dependence on initial conditions of a low dimensional system governed by deterministic chaos and described by a few nonlinear differential (or difference) equations [Pritchard, 1992].

Although the origin of the $\frac{1}{f}$-like behavior of EEG power spectrum still remains a mystery, the fractal analysis of the signal has become a powerful tool for the characterization of many physiological and pathological mechanisms involving complexity changes. Given the typical $\frac{1}{f^{\beta}}$ power spectrum of the EEG (example in Fig. 22), with β in the range 1-3, fractional Brownian motion turned out to be the most suitable mathematical model for its description. In these terms, EEG statistical self-affinity can be equivalently characterized by the three scaling parameters: the the Hurst index (H), the fractal dimension (FD) and the power-law exponent (β).

4.8 TIME DOMAIN FRACTAL APPROACH

The study of the fractal-like behavior of the EEG can be approached both in the time-domain and in the frequency-domain. In this thesis the attention is focused on the time-domain analysis, i.e., on the

Fractal dimension

characterization of the EEG in terms of fractal dimension, to meet the growing need for real-time systems. Several methods have been proposed to estimate the fractal dimension of a time series. One of the early techniques for calculating the fractal dimension of a waveform is the box-counting method [Mandelbrot, 1982], based on counting how many 2D cells of size ϵ are required to cover the total length of the curve. A similar method, based on the morphological covering of the curve, was proposed by Maragos and Sun [1983]. Two of the most used algorithms were developed in the late '80s by Higuchi [1988] and Katz [1988], the latter improved by Petrosian [1995] to reduce the execution time. More recently, Sevcik [2006] and Paramanathan and Uthayakumar [2008] proposed new procedures to estimate the fractal dimension of waveforms.

Algorithms for direct estimation

In order to identify the most accurate and reliable algorithm, the Author firstly selected three of the most used methods for the estimation of EEG fractal dimension: the box-counting method, Katz's algorithm and Higuchi's algorithm. The algorithms were then compared by evaluating not only the ability to provide accurate estimates but also their sensitivity to parameters like the sampling frequency of the EEG and the estimation time window length. The results of this research, presented in Chapter 5, are guidelines that will be applied to the experimental investigations presented in Part II for the correct fractal analysis of the EEG.

fBm model for indirect estimation

Despite the plethora of algorithms available for the fractal analysis of the EEG directly in the time domain, the use of the relationship 14 to derive FD from the calculated β exponent is widespread among physicians. Conversely, sometimes the scaling exponent β is obtained from the fractal dimension estimated in the time-domain to describe the power-law of the EEG. The accuracy of the estimates obtained by the application of Eq. 14 relies on the accuracy of the fBm model. At present, a detailed model of the system that generates the EEG is far from being feasible. Deviations from $\frac{1}{f}$-like behavior may occur more often than thought, not only owing to abnormalities introduced by pathological states. Pritchard [1992], for example, observed that deviations from log-log linearity are associated with the eyes-closed alpha rhythm in resting state EEG. From this perspective, the values obtained using the scaling relationship 14 may be inaccurate estimates of the real parameters. A further research carried out during the PhD course, aimed at empirically verifying the relationship existing between FD and β to establish how much the EEG deviates from fBm, is presented in Chapter 6.

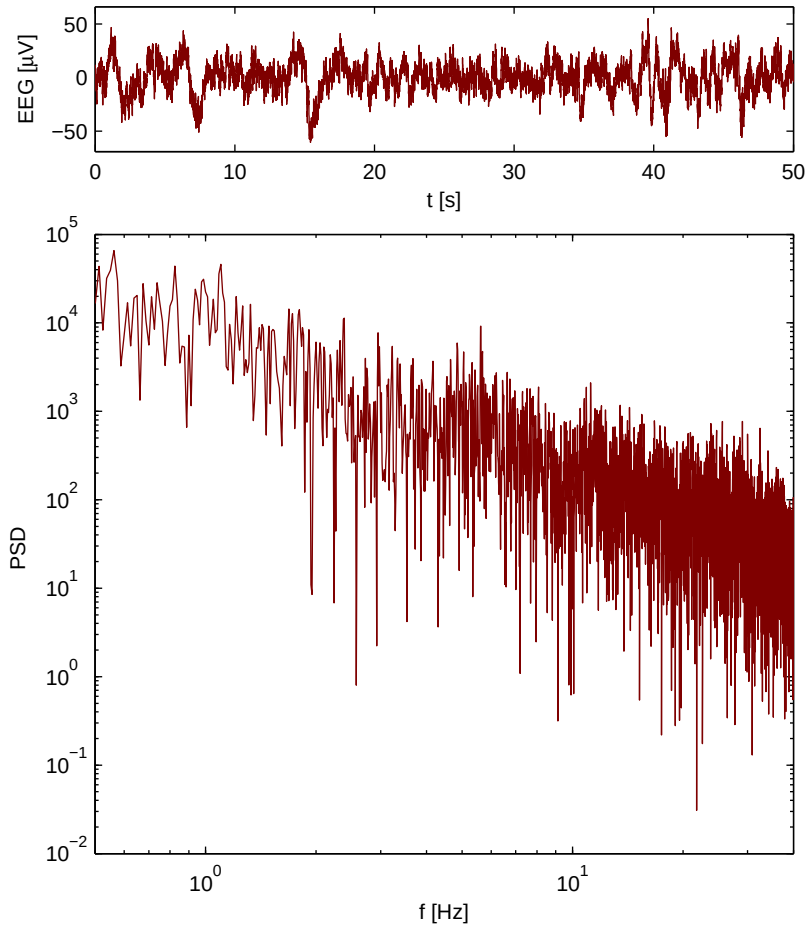

Figure 9: Example of EEG signal and its $\frac{1}{f}$-like power spectrum.

5 FRACTAL DIMENSION ESTIMATION ALGORITHMS

CONTENTS

This chapter provides the description of three algorithms widely used for the estimation of the fractal dimension of waveforms: the box-counting method [Mandelbrot, 1982], Katz's algorithm [Katz, 1988] and Higuchi's algorithm [Higuchi, 1988]. The performances of the aforementioned algorithms are compared in terms of accuracy, sensitivity to the sampling frequency and dependence on the estimation time window length. Aim of the study is the identification of the most reliable algorithm to be applied for the fractal analysis of the EEG. The investigation is performed in two steps: the algorithms are firstly applied to three synthetic series of known fractal dimension and then used for the analysis of EEG traces acquired from twenty full-term sleeping newborns. The chapter is based on Author's publications 2 and 4.

5.1 INTRODUCTION AND MOTIVATION

As mentioned in Chapter 4, the complexity of many physiological systems can be assessed through the analysis of the irregular time series they generate. Such time series, apparently random or aperiodic in time, are frequently independent of scale and self-similar under magnification [Mandelbrot, 1982]. The particular non-uniform scaling of a time series which is invariant under a transformation that scales different coordinates by different amounts is known as self-affinity [Mandelbrot, 1985]. Self-affine time series are characterized, in the frequency domain, by a power-law spectrum. Among the plethora of indexes that can describe the irregularity of waveforms showing self-affinity in time and power-law spectrum, the fractal dimension (FD) has gained wide acceptance.

The electroencephalogram is a fractal-like signal whose underlying mechanisms reflect the complexity of brain activity [Acharya *et al.*, 2005; Bosl *et al.*, 2011; Catarino *et al.*, 2011; Chouvarda *et al.*, 2011; Mizuno *et al.*, 2010]. For this reason it represents a rich source of information about several pathophysiological phenomena. The fractal dimension, for example, is a powerful EEG index in the monitoring of the depth of anesthesia [Ferenets *et al.*, 2006, 2007] as well as in the identification of wake/drowsy states [Bojic *et al.*, 2010; Inouye *et al.*, 1994] and of different sleep stages [Acharya *et al.*, 2005; Carrozzi *et al.*, 2004; Chouvarda *et al.*, 2011]. It also represents a useful parameter for the characterization of psychiatric brain diseases like schizophrenia [Raghavendra *et al.*, 2009] and autism [Ahmadlou *et al.*, 2010], for the diagnosis and monitoring of neurological disorders like Alzheimer's disease [Ahmadlou *et al.*, 2011] and for epileptic seizure detection and prediction [Accardo *et al.*, 1997; Daneshyari *et al.*, 2010; Polychronaki *et al.*, 2010].

The practice of obtaining FD estimates from spectral analysis by using the scaling relationship derived from Eq. 14, i.e., $FD = (5-\beta)/2$, with β representing the exponent of the power-law, is widespread [Phothisonothai and Nakagawa, 2009; Rankine *et al.*, 2007]. However, many methods have been proposed in order to estimate the fractal dimension of waveforms directly in the time-domain, allowing the analysis of biological events also of brief duration [Higuchi, 1988; Katz, 1988; Paramanathan and Uthayakumar, 2008; Petrosian, 1995].

Although some comparison studies [Accardo *et al.*, 1997; Esteller *et al.*, 2001; Paramanathan and Uthayakumar, 2008; Raghavendra and Dutt, 2009] have demonstrated that Higuchi's algorithm [Higuchi, 1988] is the most accurate in estimating the fractal dimension of waveforms, other techniques, like box-counting method [Mandelbrot, 1982] and Katz's algorithm [Katz, 1988], have often been used to calculate EEG fractal dimension. Moreover, regardless of the chosen algorithm, no enough attention has been paid on the possible influence of the signal sampling frequency and the estimation time window length on FD values.

As regard the sampling frequency, EEG traces are commonly acquired at various rates ranging from about 100 Hz to 1024 Hz or higher. Sometimes, especially to increase frequency resolution in spectral analysis, EEG signals are oversampled. Generally the oversampling does not affect visual or traditional linear analysis of the EEG, provided that a suitable filtering has been used. As far as the time window length used for FD estimation, it is usually set according to the events to be analyzed and therefore it is also very variable. However, it is still unclear if oversampling of different time windows could produce significant changes in the fractal analysis, which is based on geometric characteristics of signals.

State of the art

Raghavendra and Dutt [2009] compared the performances of Higuchi's and Katz's algorithms on four synthetic functions of known fractal dimension and on one EEG sleep trace, testing the sensitivity of the estimates to the sampling frequency only for one of the four synthetic

functions and for three values of fractal dimension. However, the sampling frequency of the synthetic functions was not set according to the Nyquist-Shannon sampling theorem causing an undesired undersampling. The study of Esteller *et al.* [2001] also compared the performances of Higuchi's and Katz's algorithms on one synthetic function of known fractal dimension and on 16 intracranial EEGs of epileptic patients. The effect of the estimation time window length was tested only on the synthetic function. However, the window length increment did not correspond to an effective time increment but rather to a sampling frequency increment. Moreover, also in this case, the conditions of the Nyquist-Shannon sampling theorem were not fulfilled. A similar procedure, applied also on EEG signals, was followed in the study of Paramanathan and Uthayakumar [2008] for the comparison of Higuchi's and Katz's algorithms.

In all the aforementioned studies the dependence of the algorithms on the time window length was not correctly assessed and the investigation of their sensitivity to the sampling frequency could be invalidated by an inappropriate sampling procedure.

Algorithms comparison

In order to circumvent the problems that may arise from an incorrect selection either of the length of the time window or of the sampling frequency, in the present study a detailed comparison of three methods commonly used for the estimation of EEG fractal dimension (the box-counting [Mandelbrot, 1982], the Katz's [Katz, 1988] and the Higuchi's [Higuchi, 1988] algorithms) was carried out at the appropriate sampling frequencies (greater than the Nyquist rate) and on different time windows. The sensitivity to both the sampling frequency and the time window length was evaluated for all algorithms. The study was performed in two steps: the algorithms were at first tested on three synthetic functions of known fractal dimension for different values of fractal dimension (FD), sampling frequency (FS) and time window length (TWL). In the second step, the results were compared with those achieved from the analysis of 20 neonatal EEGs for different values of FS and TWL.

5.2 MATERIALS AND METHODS

5.2.1 Fractal dimension estimation algorithms

5.2.1.1 *Box-counting algorithm*

One of the most common ways to measure the fractal dimension of a time series is the box-counting method [Mandelbrot, 1982]. It consists in covering the waveform with small cells of size ϵ. If $M(\epsilon)$ denotes the number of such cells required to cover the waveform, then the

box-counting dimension FD_B (also known as Kolmogorov capacity or capacity dimension) is defined as:

$$FD_B = \lim_{\epsilon \to 0} \frac{\log M(\epsilon)}{\log \frac{1}{\epsilon}} \tag{16}$$

In this work the procedure is repeated for cells whose size ϵ ranges from 10 to 20 points. An estimate of FD_B can be obtained by calculating the slope of the regression line when $\log M(\epsilon)$ is plotted against $\log \frac{1}{\epsilon}$.

5.2.1.2 *Katz's algorithm*

According to Katz [1988], the fractal dimension of a planar curve can be in general defined as:

$$FD = \frac{\log L}{\log d} \tag{17}$$

where L is the total length of the curve and d is its planar extent (or diameter). For a N-points time series $x(1)$,$x(2)$,...,$x(N)$ the index FD can be calculated considering L as the sum of the distances between successive points, i.e., $L = \text{sum}(\text{distance}(i, i+1))$ for $i = 1$,...,N and d as the farthest distance between the first point and any other point of the series, i.e., $d = \max(\text{distance}(1, i))$ for $i = 1$,...,N. Under this formulation, the fractal dimension is dependent on the particular unit of measure used and cannot easily be compared. To overcome the problem, Katz introduced a yardstick $\bar{a}$, a standard unit of measure defined as the average distance between successive points, i.e., $\bar{a} = \text{mean}(\text{distance}(i, i+1))$. Normalizing distances by $\bar{a}$ and defining $n = L/\bar{a}$ as the number of steps in the series (one less the number of points, i.e., $n = N-1$), the fractal dimension is estimated as:

$$FD_K = \frac{\log n}{\log n + \log \frac{d}{L}} \tag{18}$$

5.2.1.3 *Higuchi's algorithm*

Let $x(1)$,$x(2)$,...,$x(N)$ be the N-points time series under investigation and construct k new sequences as follows:

$$x_k^m = \left[x(m), x(m+k), x(m+2k), ..., x\left(m + \left\lfloor \frac{N-m}{k} \right\rfloor k\right)\right] \tag{19}$$

$$m = 1, 2, ..., k,\ k \in \mathbb{N}_0$$

where m represents the initial time and k, ranging from 1 to k_{max}, indicates the time delay. In this work, following the study of Accardo *et al.* [1997], k_{max} was set equal to 6. The symbol $\lfloor a \rfloor$ denotes the

integer part of a. For each x_k^m constructed series the length $L_m(k)$ is calculated as:

$$L_m(k) = \left[\left(\sum_{i=1}^{\lfloor \frac{N-m}{k} \rfloor} |x(m+ik) - x(m+(i-1)k)| \right) \frac{N-1}{\lfloor \frac{N-m}{k} \rfloor k} \right] \frac{1}{k} \quad (20)$$

where the term

$$\frac{N-1}{\lfloor \frac{N-m}{k} \rfloor k}$$

is a normalization factor. An average length is computed for all time series having the same delay k as the mean of the k lengths $L_m(k)$ for $m = 1,2,...,k$. This procedure is repeated for each k ranging from 1 to k_{max}. If $L(k) \propto k^{-FD_H}$, the time series x is fractal with dimension FD_H. Thus, if $L(k)$ is plotted against $1/k$ on a double logarithmic scale, the slope of the straight line fitting the data represents Higuchi's estimate of the fractal dimension [Higuchi, 1988].

5.2.2 Synthetic series analysis

Material

The performances of the three algorithms were firstly evaluated on three synthetic functions of known fractal dimension. Two deterministic waveforms (Weierstrass-Mandelbrot cosine function and Takagi-Landsberg function) and one stochastic process (fractional Brownian motion) were employed in the study.

Methods

The fractal dimension FD of each function was varied from 1.1 to 1.9 in steps of 0.1. Each function, for each FD value, was firstly constructed with the minimum number of points per second, fs_1, in order (for a band-limited signal) to obey the Nyquist-Shannon sampling theorem. Then, to evaluate the dependence on the sampling frequency (FS) by producing oversampling, the number of points of all functions was increased by a factor of 2, 3 and 4, considering fs_2, fs_3 and fs_4 points per second, respectively. To evaluate the effect of the time window length (TWL), each function sequence was divided into segments of four different lengths with no overlap. Considering that EEG features are commonly analyzed in time intervals ranging from 1 to 30 seconds, the window lengths chosen for EEG analysis were: 1 s, 5 s, 10 s and 30 s. This choice corresponds to select the shortest TWL (wl_1) as $\frac{0.4}{f_{min}}$ being EEG's lowest frequency f_{min} of about 0.4 Hz, and the other three windows as 5, 10 and 30 times the shortest TWL, respectively. Thus, in order to perform a consistent comparison between synthetic series analysis and EEG evaluation, synthesized function were firstly divided into successive segments of $wl_1 = \frac{0.4}{f_{min}}$ s. Then, the TWL was increased by a factor of 5, 10 and 30, considering estimation intervals of wl_2, wl_3 and wl_4 seconds, respectively. For each segment, FD_B, FD_K and FD_H values were estimated and then averaged on the whole function obtaining the mean values $\bar{FD}_B$, $\bar{FD}_K$ and $\bar{FD}_H$. Globally, sixteen mean values of fractal dimension, one value for each (fs_i, wl_j) pair, were obtained for each function

and for each considered algorithm. Finally, the relationship between FD and FS was evaluated for each wl_j and the relationship between FD and TWL was calculated for each fs_i.

5.2.2.1 *Weierstrass-Mandelbrot cosine function*

Weierstrass-Mandelbrot cosine function [Berry and Lewis, 1980] is derived from the complex Weierstrass-Mandelbrot function, defined by:

$$W(t) = \sum_{n=-\infty}^{\infty} \frac{(1 - e^{i\gamma^n t})e^{i\phi_n}}{\gamma^{(2-FD)n}} \tag{21}$$

where FD, the fractal dimension, must be in the range $1 < FD < 2$, $\gamma > 1$ and ϕ_n is an arbitrary phase that can be chosen to make $W(t)$ exhibit deterministic or stochastic behavior. Let $\phi_n = 0$; the Weierstrass-Mandelbrot cosine function is obtained as the real part of $W(t)$:

$$C(t) = \Re W(t) = \sum_{n=-\infty}^{\infty} \frac{1 - \cos(\gamma^n t)}{\gamma^{(2-FD)n}} \tag{22}$$

Following the study of Raghavendra and Dutt [2009], γ was set equal to 1.5. Although $C(t)$ calculation involves the sum of an infinite number of components, all practical applications introduce both low and high frequency cutoffs. If the infinite series is truncated so that the summation is done only for $|n| = n_{max}$ with $n_{max} = 10$, the function results in the superimposition of $2n_{max}+1$ frequency components centered at $\gamma^n/2\pi$ Hz. In this way, since $f_{max} = \gamma^{n_{max}}/2\pi$, the number of points per second required to correctly construct $C(t)$ is $fs \geqslant 2f_{max} = 2(\gamma^{n_{max}}/2\pi)$. In this work the minimum sampling frequency was set to 2.02 times f_{max}. Thus, being $\gamma = 1.5$ and $n_{max} = 10$, it resulted that $fs_1 = 19$. To oversample the function, the same curve was built with $fs_2 = 38$, $fs_3 = 57$ and $fs_4 = 76$ points per second, corresponding to 2, 3 and 4 times fs_1, respectively. Since $f_{min} = \gamma^{-n_{max}}/2\pi = 0.0028$ Hz, the $C(t)$ longest period was of $T = 362$ s and thus, the shortest window length was set to $wl_1 = 0.4T = 145$ s. The other three windows were therefore $wl_2 = 725$ s, $wl_3 = 1450$ s and $wl_4 = 4350$ s wide, corresponding to 5, 10 and 30 times wl_1. In order to estimate the fractal dimension in all the considered windows, the function was constructed considering 50 cycles of the longest period, i.e., for t in the range [1,18100] seconds. An example of the considered function, for $FD = 1.4$ in the time range [0,362] seconds, is shown in Fig. 10.

5.2.2.2 *Takagi-Landsberg function*

The Takagi-Landsberg function, explored by Takagi [1903], is a curve constructed by positive mid-point displacements of straight line segments. It is defined on the unit interval by:

$$T(t) = \sum_{n=0}^{\infty} a^n \Delta(b^n t) \tag{23}$$

where $a \in [0,1]$, b is an integer greater than 1 and $\Delta(x)$, defined by $\Delta(x) = \min_{k \in \mathbb{Z}} |x - k|$, represents the distance from x to the nearest integer. This function is everywhere continuous but nowhere differentiable if $ab \geqslant 1$. In this work, following the study of Raghavendra and Dutt [2009], $b = 2$ and $a \in [0.5,1]$ so that the fractal dimension $FD = \frac{\log 4a}{\log b}$ could be varied from 1.1 to 1.9 in steps of 0.1. If the infinite summation is approximated by the finite superimposition of the few first terms and $n_{max} = 10$, the function is the result of the summation of $n_{max}+1$ triangular waves of frequency b^n Hz (neglecting harmonic terms). In this way, being f_{max} about equal to $b^{n_{max}}$, the number of points required to correctly construct one period of $T(t)$ is $fs \geqslant 2b^{n_{max}}$. The minimum number of points per second was chosen as $fs_1 = 2.02 f_{max} = 2068$. To oversample the function, the same curve was built with $fs_2 = 4136$, $fs_3 = 6204$ and $fs_4 = 8272$ points per second. Since $f_{min} = 1$ Hz, TWLs were set to $wl_1 = 0.4$ s, $wl_2 = 2$ s, $wl_3 = 4$ s and $wl_4 = 12$ s. In order to estimate FD for all window lengths, the function was constructed considering 50 periods, i.e., for t in the range [1,50] seconds. An example of the considered function, for $FD = 1.4$ in the time range [0,1] seconds, is shown in Fig. 10.

5.2.2.3 *Fractional Brownian motion*

The fBm traces used in this work were generated following the wavelet-based synthesis method proposed by Abry and Sellan [1996]. The original time-series was built with 128 points per second, the same rate that will be used to resample EEG traces, in order to produce a spectral content limited to about 50 Hz and therefore similar to that of the electroencephalogram. The series with sampling frequency $fs_1 = 128$ Hz was then interpolated to obtain oversampled $fs_2 = 256$ Hz, $fs_3 = 384$ Hz and $fs_4 = 512$ Hz sequences with about the same frequency content. Since $f_{min} = 1$ Hz, as observed from the spectra of synthesized signals, the shortest TWL was set to $wl_1 = \frac{0.4}{f_{min}} = 0.4$ s. The other three windows were therefore $wl_2 = 2$ s, $wl_3 = 4$ s and $wl_4 = 12$ s wide, corresponding to 5, 10 and 30 times wl_1. An example of the considered function, for $FD = 1.4$ in the time range [0,1] seconds, is shown in Fig. 10.

5.2.3 EEG analysis

Material

EEGs analyzed in the present study were recorded from 20 healthy

Methods

full-term newborns (10 males and 10 females) for an investigation of neonatal sleep-stage characteristics [Carrozzi *et al.*, 2004]. Eight unipolar derivations (Fp1, Fp2, C3, C4, T3, T4, O1, O2), common reference Cz, were recorded by means of Ag/AgCl electrodes according to the International 10-20 System. The EEGs were acquired within the first week of life, during diurnal sleep. The signals were digitally filtered (Butterworth band-pass) between 0.4 and 50 Hz, sampled at 1024 Hz and digitalized with a resolution of 12 bit. Since brain activity during sleep was symmetric in the two hemispheres, the analysis was carried out only on the four derivations of the left hemisphere (Fp1, C3, T3 and O1). For each derivation, four signals EEG_i $(i = 1,...,4)$ where obtained by resampling the original time series at $fs_1 = 128$ Hz, $fs_2 = 256$ Hz, $fs_3 = 384$ Hz and $fs_4 = 512$ Hz. For each EEG_i signal, a stationarity test was performed by means of the nonlinear cross prediction error algorithm [Schreiber, 1997]. The stationary sub-sequences of each signal were then divided into successive segments of $wl_1 = 1$ s, $wl_2 = 5$ s, $wl_3 = 10$ s and $wl_4 = 30$ s, being EEG's minimum frequency of about 0.4 Hz. For each stationary sub-sequence, FD_B, FD_K and FD_H values were computed on each contained segment and then averaged on the sub-sequence to obtain $\bar{FD}_B$, $\bar{FD}_K$ and $\bar{FD}_H$ mean values. In this way, sixteen mean values of fractal dimension, one value for each (fs_i, wl_j) pair, were obtained for each considered algorithm in each stationary sub-sequence. Since $FD_{H_{14}}$ fractal dimensions (i.e., Higuchi's estimates calculated on 30 s-windows for 128 Hz-sampled EEG) showed a limited range of values (Fig. 11), the longest segments with $\bar{FD}_{H_{14}} \sim 1.3$ and $\bar{FD}_{H_{14}} \sim 1.4$ were selected for each subject for the successive analysis (Fig. 11). Finally, for both groups, the relationship between the fractal dimension and the sampling frequency, for each TWL and that between the fractal dimension and the time window length, for each FS, were calculated.

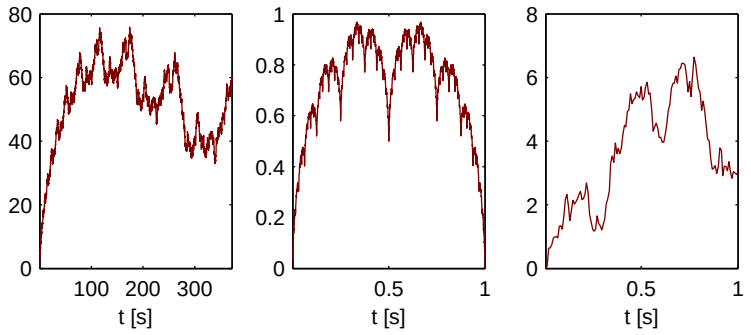

Figure 10: Fractal synthetic waveforms with FD = 1.4: Weierstrass-Mandelbrot cosine function (left), Takagi-Landsberg function (middle) and fractional Brownian motion (right).

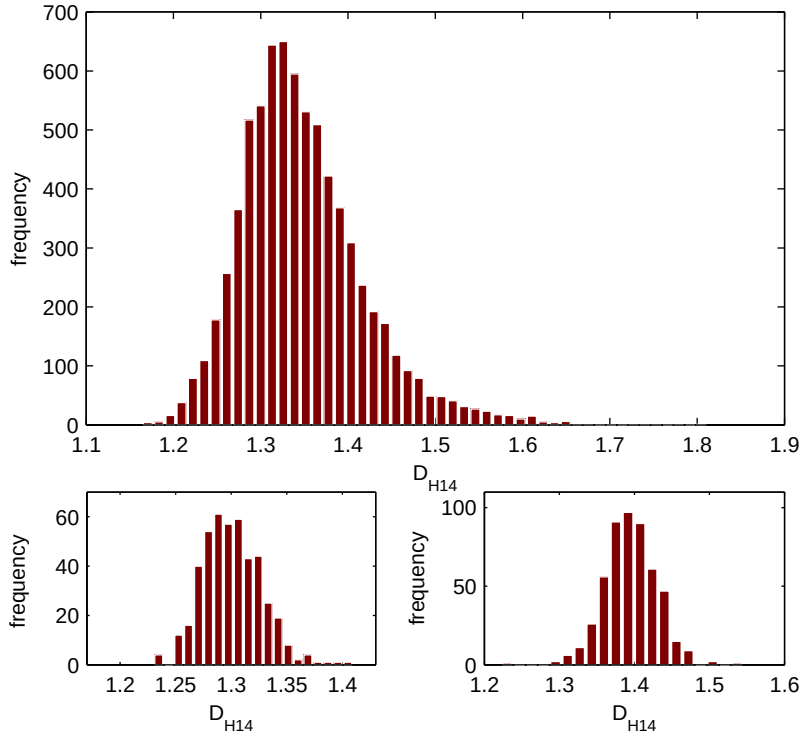

Figure 11: Histogram of FD_H values estimated in all stationary sub-sequences of all EEG derivation resampled at fs_1 Hz and divided into successive segments of wl_4 s (top), histogram of $FD_{H_{14}}$ values estimated in the selected intervals of the EEG with $\overline{FD}_{H_{14}} \sim 1.3$ (bottom left) and histogram of $FD_{H_{14}}$ values estimated in the selected intervals of the EEG with $\overline{FD}_{H_{14}} \sim 1.4$ (bottom right).

5.3 RESULTS

5.3.1 Results on synthetic series

Figure 12 shows the plot of the estimated FD (obtained with the three algorithms) versus the theoretical FD for the three considered synthesized waveforms. The curves were generated with fs_1 points per second and the fractal dimension was obtained as the average of the values estimated in sliding windows of wl_1 seconds. A perfect reproduction of the true fractal dimension should yield a straight line of slope 1 (solid gray line). The results show that Higuchi's algorithm provided the most accurate estimates of the fractal dimension for each considered function. Both Katz's algorithm and box-counting method, on the contrary, showed a nonlinear trend with large overestimation and underestimation of the fractal dimension. The worst results, for both algorithms, were found for the Weierstrass-Mandelbrot cosine function. In the next sections the effects of the sampling frequency (FS)

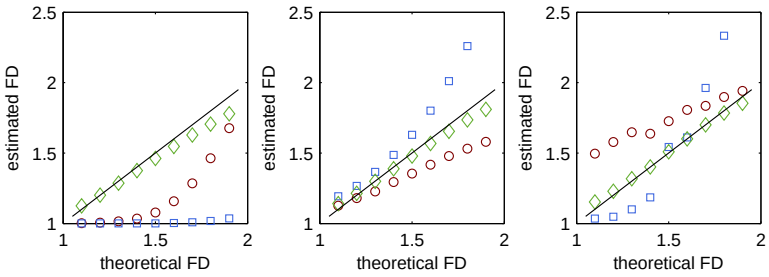

Figure 12: Plot of estimated versus theoretical fractal dimension values for Weierstrass-Mandelbrot cosine function (left), Takagi-Landsberg function (middle) and fractional Brownian motion (right). The functions were generated with fs_1 points per second and the fractal dimension was obtained as the average of the values estimated in sliding windows of wl_1 seconds by using the box-counting (red circles), the Katz's (blue squares) and the Higuchi's (green diamonds) algorithms.

and of the time window length (TWL) are presented for each considered algorithm and function.

5.3.1.1 *Effect of waveform sampling frequency*

The sensitivity of the algorithms to the sampling frequency was tested by varying the number of points per second, FS, of each base waveform from fs_1 to fs_4. By using a TWL of wl_1 seconds and the Takagi-Ladsberg function, the values estimated by the box-counting method, FD_B, slightly decreased when FS increased, underestimating in all cases the theoretical FD (Fig. 13). The Katz's algorithm showed a slight overestimation for FD values in the 1.1-1.5 range and a strong sensitivity to the sampling frequency for FD values greater than 1.5 (Fig. 13) overestimating, at all the considered FS, the theoretical FD and showing a linear relationship between FD_K and FS (example in Fig. 14 for $FD = 1.8$). The Higuchi's estimates, FD_H, strongly decreased as sampling frequency increased, for all FD values, following a linear law as shown in the example of Fig. 14 for $FD = 1.8$. Higuchi's most accurate estimates were those obtained on the function generated with the minimum number of points, that is, with the minimum required sampling frequency (Fig. 13). Higuchi's algorithm was the only one that showed the same behavior also for both Weierstrass-Mandelbrot cosine function and fractional Brownian motion. Similarly to the behavior for the Takagi-Landsberg function, Katz's algorithm, produced underestimation for FD in the range 1.1-1.5 and overestimation for greater values of FD also for fractional Brownian motion, even if FD_K estimates resulted to be linearly related to $1/FS$. However, the algorithm resulted almost insensitive to FS for Weierstrass-Mandelbrot function, always underestimating theoretical FD. Finally, the box-counting method mainly underestimated FD for both functions, always resulting almost independent from FS.

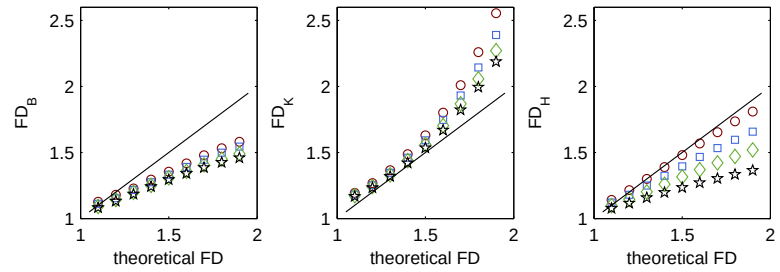

Figure 13: Plot of estimated versus theoretical fractal dimension for the Takagi-Landsberg function, for different values of FS, obtained with box-counting method (left), Katz's algorithm (middle) and Higuchi's algorithm (right) on estimation windows of wl_1 seconds. fs_1: red circles, fs_2: blue squares, fs_3: green diamonds, fs_4: black pentagrams.

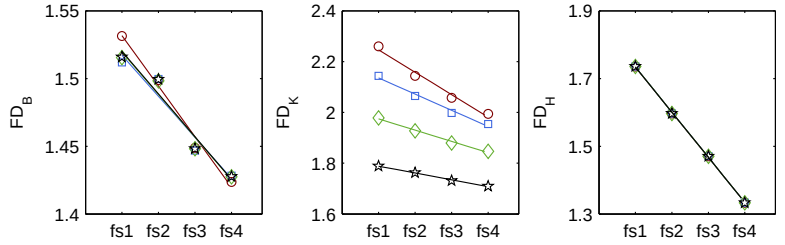

Figure 14: Plot of estimated fractal dimension versus FS, for different values of TWL, for the Takagi-Landsberg function of FD = 1.8, obtained with box-counting method (left), Katz's algorithm (middle) and Higuchi's algorithm (right). wl_1: red circles, wl_2: blue squares, wl_3: green diamonds, wl_4: black pentagrams.

5.3.1.2 *Effect of estimation time window length*

The dependence on the time window length was studied by varying TWL from wl_1 to wl_4 seconds considering a FS value of fs_1. The box-counting method turned out to be sensitive to the time window length only for fBm function, with FD_B slightly decreasing with TWL, while it underestimated the theoretical FD for the other two functions independently from TWL (examples for the Takagi-Landsberg function in Figs. 15 and 16). On the contrary, a clear dependence on the TWL was exhibited by Katz's algorithm for both fractional Brownian motion and Takagi-Landsberg function (examples in Figs. 15 and 16) producing underestimation and overestimation of theoretical FD, respectively. In both cases the FD_K estimates decreased as TWL increased following a nonlinear law. For the Weierstrass-Mandelbrot cosine function FD_K values were very close to 1 for all the considered TWL. Finally, Higuchi's algorithm turned out to be independent from the TWL for all the considered functions (examples in Figs. 15 and 16).

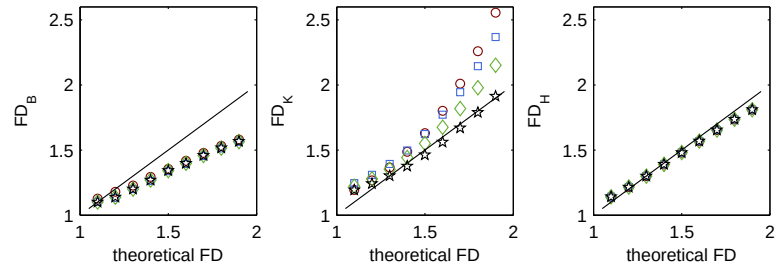

Figure 15: Plot of estimated versus theoretical fractal dimension for the Takagi-Landsberg function, built with fs_1 points per second, for different values of TWL, obtained with box-counting method (left), Katz's algorithm (middle) and Higuchi's algorithm (right). wl_1: red circles, wl_2: blue squares, wl_3: green diamonds, wl_4: black pentagrams.

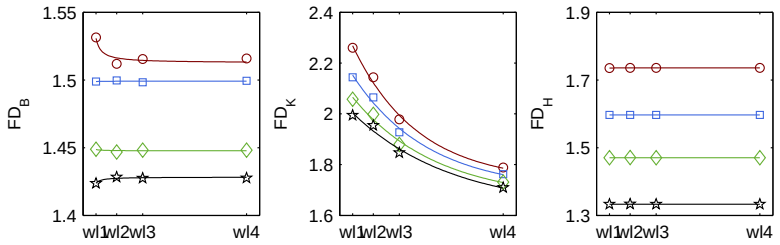

Figure 16: Plot of estimated fractal dimension versus TWL, for different values of FS, for the Takagi-Landsberg function of FD = 1.8, obtained with box-counting method (left), Katz's algorithm (middle) and Higuchi's algorithm (right). fs_1: red circles, fs_2: blue squares, fs_3: green diamonds, fs_4: black pentagrams.

5.3.2 Results on the EEG

Based on the results on the synthetic series, the performances of the three considered algorithms were evaluated on EEG traces in terms of sensitivity to both the FS and the TWL, considering the estimates of the Higuchi's algorithm as the most reliable ones.

5.3.2.1 *Effect of EEG sampling frequency*

Figure 17 (left column) shows that the box-counting estimate, FD_B, calculated on the segments in which the Higuchi's estimate $\bar{FD}_{H_{14}}$ was of about 1.3 (or 1.4), decreased as FS increased in a different way for each wl_j value. On the other hand, both Katz's and Higuchi's estimates linearly decreased with $1/fs$ according to the following relationship:

$$FD_j = \frac{m_j}{fs} + q_j \tag{24}$$

for $j = 1,...,4$. The values of the $\bar{m}_j$ and $\bar{q}_j$ coefficients, obtained by using Katz's ($\bar{m}_{Kj}$,$\bar{q}_{Kj}$) and Higuchi's ($\bar{m}_{Hj}$,$\bar{q}_{Hj}$) algorithms by averaging on the subjects, for fractal values ($\bar{FD}_{H_{14}}$) of about 1.3 and 1.4, are listed in Tab. 3 and in Tab. 4, respectively.

Table 3: Mean coefficients $\pm\sigma$ of the relationship 24 for $\bar{FD}_{H_{14}} \sim 1.3$.

	Katz		Higuchi	
	$\bar{m}_K$	$\bar{q}_K$	$\bar{m}_H$	$\bar{q}_H$
$wl_1 = 1$ s	32.44±3.18	1.39±0.02	44.92±1.37	0.97±0.01
$wl_2 = 5$ s	14.52±1.52	1.30±0.02	43.29±1.26	0.97±0.01
$wl_3 = 10$ s	10.02±1.03	1.25±0.02	42.90±1.18	0.97±0.01
$wl_4 = 30$ s	5.86±0.86	1.19±0.02	42.39±1.27	0.97±0.01

Table 4: Mean coefficients $\pm\sigma$ of the relationship 24 for $\bar{FD}_{H_{14}} \sim 1.4$.

	Katz		Higuchi	
	$\bar{m}_K$	$\bar{q}_K$	$\bar{m}_H$	$\bar{q}_H$
$wl_1 = 1$ s	38.98±2.88	1.44±0.02	59.73±2.41	0.95±0.01
$wl_2 = 5$ s	16.20±1.32	1.33±0.02	57.87±2.03	0.96±0.01
$wl_3 = 10$ s	11.48±0.82	1.27±0.02	57.06±1.89	0.96±0.01
$wl_4 = 30$ s	6.31±0.60	1.21±0.02	56.22±2.20	0.96±0.02

5.3.2.2 *Effect of EEG estimation time window length*

In Fig. 17 (right column) the relationships between FD and TWL for the considered fs_i are shown for a fractal dimension $\bar{FD}_{H_{14}}$ of about 1.3. The non linear relationship between TWL and both FD_B and FD_K estimates, with values decreasing as the sampling frequency increased, can be expressed in terms of an exponentially decreasing function in the form:

$$FD_i = a_i e^{-b_i wl} + c_i \tag{25}$$

for $i = 1,...,4$. The values of the $\bar{a_i}$, $\bar{b_i}$ and $\bar{c_i}$ coefficients, obtained by using the box-counting method ($\bar{a_{Bi}}$, $\bar{b_{Bi}}$, $\bar{c_{Bi}}$) and Katz's algorithm ($\bar{a_{Ki}}$, $\bar{b_{Ki}}$, $\bar{c_{Ki}}$), as the average on the subjects for fractal values ($\bar{FD}_{H_{14}}$) of 1.3 and 1.4, are listed in Tab. 5 and in Tab. 6, respectively. The figure confirms that Higuchi's algorithm is not appreciably sensitive to the time window length also on EEG signals.

Table 5: Mean coefficients $\pm\sigma$ of the relationship 25 for $\bar{FD}_{H_{14}} \sim 1.3$.

	Box-counting			Katz		
	$\bar{a}_B$	$\bar{b}_B$	$\bar{c}_B$	$\bar{a}_K$	$\bar{b}_K$	$\bar{c}_K$
$fs_1 = 128$ Hz	0.11±0.01	0.19±0.05	1.21±0.03	0.48±0.04	0.20±0.01	1.24±0.02
$fs_2 = 256$ Hz	0.11±0.01	0.25±0.02	1.18±0.02	0.36±0.03	0.18±0.01	1.22±0.02
$fs_3 = 384$ Hz	0.04±0.01	0.25±0.00	1.17±0.01	0.32±0.02	0.21±0.11	1.22±0.03
$fs_4 = 512$ Hz	0.08±0.01	0.24±0.00	1.14±0.01	0.29±0.02	0.19±.08	1.20±0.02

Table 6: Mean coefficients $\pm\sigma$ of the relationship 25 for $\bar{FD}_{H_{14}} \sim 1.4$.

	Box-counting			Katz		
	$\bar{a}_B$	$\bar{b}_B$	$\bar{c}_B$	$\bar{a}_K$	$\bar{b}_K$	$\bar{c}_K$
$fs_1 = 128$ Hz	0.12±0.01	0.18±0.05	1.24±0.02	0.58±0.04	0.21±0.02	1.27±0.02
$fs_2 = 256$ Hz	0.13±0.01	0.27±0.03	1.22±0.02	0.44±0.03	0.19±0.02	1.24±0.02
$fs_3 = 384$ Hz	0.05±0.01	0.21±0.07	1.21±0.01	0.37±0.03	0.18±0.02	1.23±0.02
$fs_4 = 512$ Hz	0.09±0.01	0.25±0.02	1.19±0.01	0.34±0.03	0.18±0.02	1.22±0.02

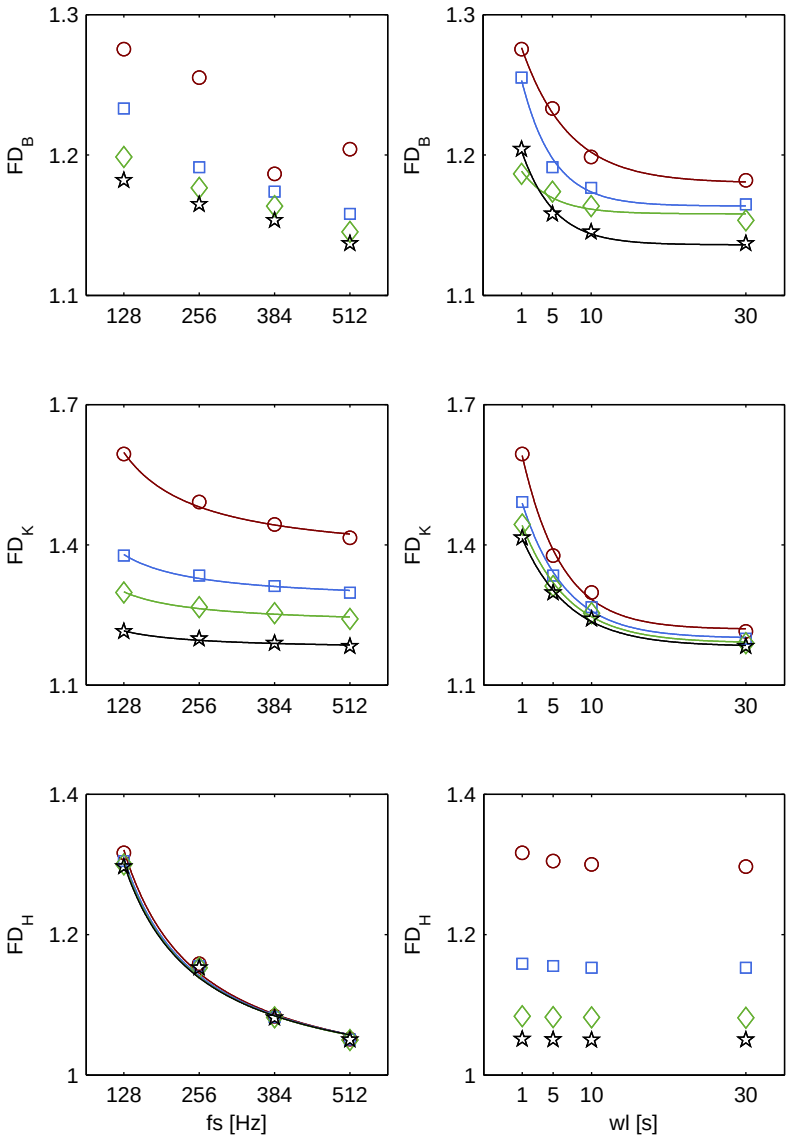

Figure 17: Left column: plot of estimated EEG fractal dimension versus FS for wl_1 (red circles), wl_2 (blue squares), wl_3 (green diamonds) and wl_4 (black pentagrams). Right column: plot of estimated EEG fractal dimension versus wl for fs_1 (red circles), fs_2 (blue squares), fs_3 (green diamonds), fs_4 (black pentagrams). Example for subject 1 with $\bar{FD}_{H_{14}} \sim 1.3$.

5.4 DISCUSSION

The test on the synthetic functions of known fractal dimension, performed at the appropriate sampling frequency observing Nyquist-Shannon sampling theorem without oversampling, partially confirmed the results of previous studies [Accardo *et al.*, 1997; Esteller *et al.*, 2001; Paramanathan and Uthayakumar, 2008; Raghavendra and Dutt, 2009], i.e., Higuchi's algorithm provides the most accurate estimates of the fractal dimension. However, some conflicting results have been obtained when analyzing the dependence of FD estimates on the two considered factors: the sampling frequency and the time window length.

Sensitivity to FS

Contrary to the results of Raghavendra and Dutt [2009], in which Higuchi's algorithm estimation accuracy improved as the sampling frequency increased, with FD_H values slightly affected by the sampling frequency, the reported results showed that Higuchi's method is strongly dependent on the sampling frequency and FD_H estimates improved as the sampling frequency decreased toward the Nyquist rate, i.e., to the lower bound for aliasing-free signal sampling. On the other hand, in agreement with the aforementioned study, Katz's algorithm turned out to be dependent on the sampling frequency, providing estimates that decreased with the sampling frequency.

Sensitivity to TWL

With regard to the sensitivity to the time window length, the study of Esteller *et al.* [2001] showed that the fractal dimension estimates obtained with Higuchi's algorithm improved as the window length increased, while the study of Paramanathan and Uthayakumar [2008] did not report any dependence on TWL. The analysis performed in the present study indicated that Higuchi's estimates are correct independently from the time window length, provided that a suitable sampling frequency is used. Both the aforementioned studies highlighted a slight sensitivity to TWL of Katz's algorithm while the present study showed a strong dependence on the time window length.

The fractal analysis of the EEG basically confirmed the results of the investigation carried out on the synthetic functions. The box-counting method turned out to be sensitive to both the sampling frequency and the time window length, although a clear relationship could be expressed only between FD_B and TWL. Moreover, the results supported the dependence of Katz's estimates on both factors and confirmed that Higuchi's algorithm is sensitive only to the sampling frequency.

Thus, although the fractal dimension of the EEG signals is not known a priori, based on the results on synthetic signals it can be asserted that the most correct estimates were those provided by Higuchi's algorithm at the lowest considered sampling frequency (128 Hz). This value, observing the Nyquist-Shannon sampling theorem, is about 2.5 times the LP cut-off frequency, which was chosen according to the frequency content of the EEG recorded from sleeping newborns, which is limited to about 40 Hz. Hence, in order to conduct an accurate fractal analysis, it is of primary importance to adapt the sampling frequency to the bandwidth of the considered EEG and, therefore, to the selected low-pass cutoff frequency. A sampling frequency close to 2.5 times

the cutoff frequency of a third order low-pass filter could represent an optimal choice to avoid underestimation of the fractal dimension due to oversampling. This solution also prevents the reduction of the dynamic range of the fractal dimension. Higuchi's algorithm, being not sensitive to the time window length, it is also preferable for real-time applications in which short epochs have to be examined.

It is nonetheless true that in some investigations it might be not interesting the true value of the fractal dimension, but rather its fluctuation over time or the differences among the values estimated in different conditions. In this cases, methods different from Higuchi's algorithm could be also used for the fractal analysis. In any case, whenever two or more studies have to be compared, it is necessary to take into account the sampling frequency and the time window length used in each investigation.

5.5 CONCLUSION

In this study the performances of three algorithms commonly used for the estimation of EEG fractal dimension were compared in terms of accuracy and sensitivity to the sampling frequency and to the time window length. The investigation was carried out firstly on three synthetic functions of known fractal dimension and then on 20 EEGs recorded from as many sleeping newborns. Results indicate that the box-counting algorithm is the least reliable method, providing incorrect estimates also dependent on both the sampling frequency and the estimation window length. The Katz's algorithm, though sensitive to both factors, turned out to be more reliable and produced some accurate estimates. However, the study suggests that Higuchi's algorithm is the most accurate of the considered methods, provided that the signals are not oversampled. Furthermore, it is appropriate to estimate the fractal dimension of events of both brief duration as well as longer EEG traces, being the estimates not dependent on the time window length. In any case, information about the sampling frequency and the time window length should always accompany the results of the fractal analysis, since it is relevant for its correct interpretation.

6 EEG VS FBM SCALING LAW

CONTENTS

This chapter presents an investigation carried out to verify the accuracy of fractional Brownian motion to model the EEG. The study is inspired by the widespread practice of using fBm theoretical relationships of Eq. 14 to equivalently characterize the scaling properties of the EEG. The fractal dimension (FD) and the power-law exponent (β) are independently estimated on 536 EEG traces acquired from healthy full-term sleeping newborns, children, young adults and elderly adults. Experimental relationships between FD and β are calculated and compared among the populations to detect possible scaling differences related to age. Mean experimental relationships are then calculated within each group and compared with the scaling relationship of Eq. 14 in order to detect possible deviations from fBm. The chapter is partially based on Author's publication 3.

6.1 INTRODUCTION AND MOTIVATION

The scaling behavior of self-affine time series can be equivalently characterized by the fractal dimension (FD), the power-law exponent (β) and the Hurst index (H). Whereas the fractal dimension and the Hurst index are related by the simple equation, $FD = 2 - H$, the relationship existing between FD and β is unsettled [Higuchi, 1990]. Consider, for example, the Weierstrass function, $X_H(t)$ [Bassingthwaighte *et al.*, 1994], of Fig. 8. As described in Chapter 4.5, this function consists of an infinite summation of periodic terms, each of which has a frequency that is a factor b larger than the preceding term and an amplitude that is a times smaller. Whereas self-similarity represents the property of the shapes to be identical under magnification, self-affinity expresses the necessity to scale down X_H and t by different amounts (ΔX_H and Δt, respectively) to obtain two identical views. In particular, if $a, b > 1$ and $b^H = a$ then $\Delta X_H = \Delta t^H$, whit H ranging from 0 to 1. The relationship between the fractal dimension and the power-law exponent

for the Weierstrass function can be easily calculated and expressed as follows:

$$FD = \frac{4-\beta}{2} \tag{26}$$

The possibility to calculate only one of the two parameters and then easily obtain the other one using a relationship like Eq. 26 may be useful in some circumstances. For real-time analysis, for example, when the number of available data is limited, time domain fractal analysis could be a more efficient alternative to frequency domain fractal analysis [Rankine *et al.*, 2007]. More often, the β exponent is estimated from the power spectrum to subsequently obtain the fractal dimension, FD [Phothisonothai and Nakagawa, 2009]. To correctly characterize EEG by either FD or β indexes it is necessary to have a model that accurately describes the considered process. The fractal dimension and the power-law exponent of fractional Brownian motion, the mathematical model for the EEG, are interrelated by the following equation:

$$FD = \frac{5-\beta}{2} \tag{27}$$

This scaling relationship, derived from Eq. 14, is widely used among physicians and researchers to equivalently characterize the irregularity of the EEG in terms of fractal dimension or power-law exponent. However, since a complete model of the EEG has not been found yet, deviations of the EEG from $\frac{1}{f}$-like behavior occur more often than thought also in non-pathological EEG [Pritchard, 1992]. To verify the accuracy of such a practice, in this study the relationship between the fractal dimension and the β exponent was calculated on 8-channel EEGs collected from healthy subjects belonging to 4 populations: full-term sleeping newborns, children, young adults and elderly adults. The obtained relationships were evaluated within the groups and among the groups, in order to highlight possible age-related differences. The mean relationship of each group was finally compared with that of Eq. 27 in order to assess the accuracy of fractional Brownian motion model.

6.2 MATERIALS AND METHODS

Materials

Data analyzed in the present study were collected from 4 populations of healthy subjects composed by 20 full-term newborns (NB), 15 children (CH), 21 young adults (YA) and 12 elderly adults (EA), respectively. Sleep EEG (NB) or resting state EEG (CH, YA and EA) was acquired at 256-1024 Hz from 8 unipolar channels (Fp1, Fp2, C3, C4, T3, T4, O1 and O2, referenced by Cz) with Ag/AgCl electrodes positioned according to the 10-20 system. All signals were resampled at 128 Hz, following the guidelines of Chapter 5, and digitally filtered between

Methods

0.4 and 40 Hz with a second order high-pass and a third order low-pass Butterworth filter, respectively. Nonstationarities were identified using nonlinear cross prediction [Schreiber, 1997] and then rejected from the analysis. The stationary intervals of each derivation were divided into 50% overlapping segments of 10 s in which the fractal dimension (FD) was estimated with Higuchi's algorithm [Higuchi, 1988]. Each segment was then fast Fourier transformed applying Hamming windows to subsequently obtain the power spectral density (PSD) using the periodogram method. The β exponent was finally calculated as the slope of the linear best fit of the PSD on a double logarithmic scale. For each signal, FD values were plotted against β exponents to assess whether a linear correlation was present in the considered populations. After visual confirmation, slope and intercept of the least-squares regression lines were calculated for all derivations of all subjects. Box-and-whiskers plots were created in order to compare the calculated coefficients among the 4 groups. The assumption of normality was checked for each coefficient with the Kolmogorov-Smirnov test. Then, slope and intercept were averaged, within each population, to obtain a mean regression line. The four obtained relationships were finally compared with that valid for the fractional Brownian motion [Berry, 1979; Mandelbrot and Van Ness, 1968].

6.3 RESULTS

A linear relationship between the fractal dimension and the power-law exponent of the EEG was observed in each subject independently from the population to which the subject belongs. Figure 18 shows, as an example, how FD is linearly related to β in all derivations of a sleeping newborn EEG. However, visual analysis suggested that the observed relationships are slightly different from the theoretical one valid for the fBm process (Eq. 27). Moreover, subjects belonging to different populations exhibited different relationships. The notched box-and-whisker plots of the calculated coefficients grouped by population are shown in Fig. 19. As can be seen, the medians of both the slope and the intercept are very similar among CH, YA and EA populations. On the contrary, since the notch of NB do not overlap with those of CH, YA and EA, in both box-plots, the medians of both coefficients are significantly different with 95% confidence. Since the Kolmogorov-Smirnov test proved normal distribution of both coefficients in all groups, although the box-plots of Fig 19 revealed slight skewness in some cases, their probability density functions were calculated within each population (Fig. 20). Mean and standard deviation of both the slope and the intercept are provided in Tab. 7. The mean regression lines obtained with the mean coefficients are plotted in Fig. 21 for a visual comparison with the line representing the relationship of Eq. 27 valid for fractional Brownian motion.

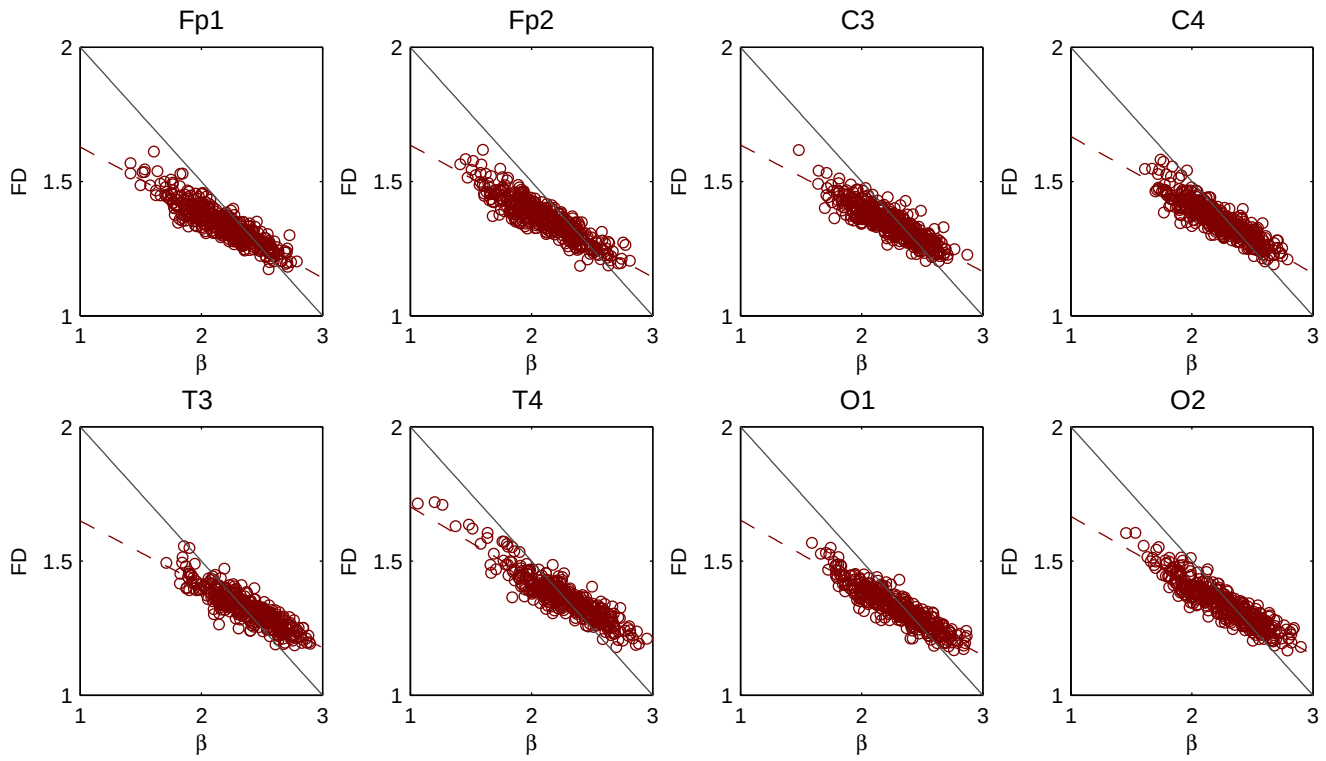

Figure 18: Fractal dimension against power-law exponent for the 8-channel EEG acquired from a sleeping newborn. The dashed red lines are the calculated relationships while the solid gray lines, from left top corner to right bottom corner, represent the relationship of Eq. 27 valid for the fBm process (slope = -0.5, intercept = 2.5).

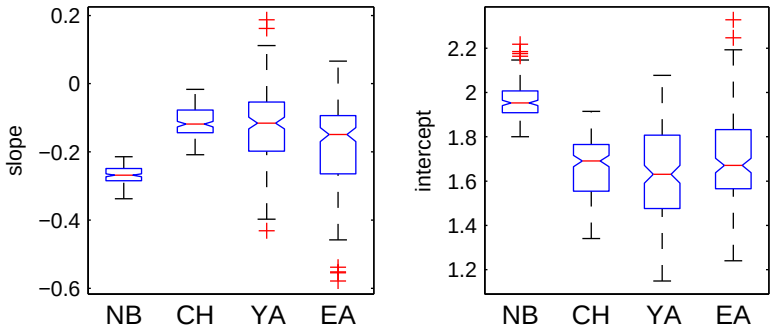

Figure 19: Notched box-and-whiskers plots of slope and intercept values in the four considered groups.

6.4 DISCUSSION

In the hypothesis that the EEG evolves like a fractional Brownian motion process, the scaling relationship of Eq. 27 is widely used by physicians and researchers in particular to indirectly estimate the fractal dimension from the power-law exponent.

As hypothesized, the experimental relationships between FD and β are different from the scaling relationship of fractional Brownian motion. As can be seen in Fig. 21, for calculated β values lower than approximately 2.2 (CH), 2.4 (NB and YA) or 2.5 (EA) the use of the theoretical relationship causes FD overestimation. On the contrary, as the power-law exponent approaches 3, the obtained fractal dimension becomes more and more underestimated.

However, an interesting observation can be made based on the results. Considering the distributions of Fig. 20 and the correspondent mean coefficients reported in Tab. 7, a clear distinction can be made between the scaling behavior observed in the neonatal EEG and that found in the EEG of all other groups. This result may find an explanation in the fact that neonatal EEG has significantly different characteristics compared with that of children and adults. In support of this hypothesis, low differences were found among the coefficients of children, young adults and elderly adults. The mean regression line, obtained as the average of the relationships of all CH, YA and EA subjects, is:

$$FD = -0.14\beta + 1.66 \tag{28}$$

Before to conclude that the proposed fBm model does not accurately describe the EEG, it would be interesting to understand the reason why the experimental relationship 28 does not match the theoretical one (27). A possible explanation could concern the phase distribution of the EEG. According to Higuchi [1990] and Penn and Loew [1997], the phase distribution of a series, at constant power-law, may strongly

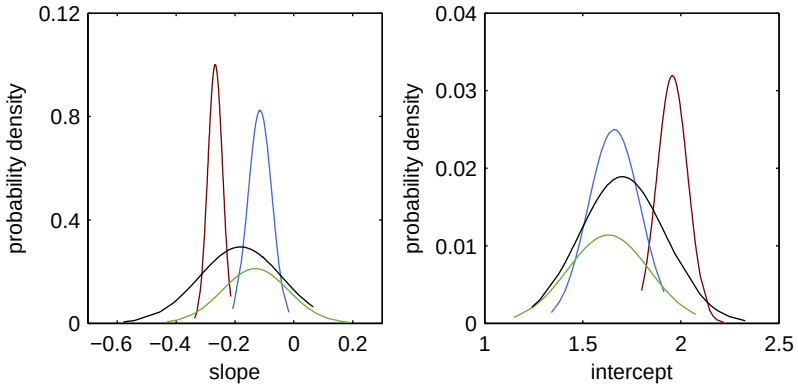

Figure 20: Distributions of slope and intercept values: red for newborns, blue for children, green for young adults and black for elderly adults.

Table 7: Mean and standard deviation of the distributions of Fig. 20.

	$\bar{m} \pm \sigma$	$\bar{q} \pm \sigma$
Newborns	-0.27±0.02	1.96±0.08
Children	-0.11±0.04	1.66±0.13
Young adults	-0.13±0.11	1.63±0.21
Elderly adults	-0.18±0.14	1.70±0.22

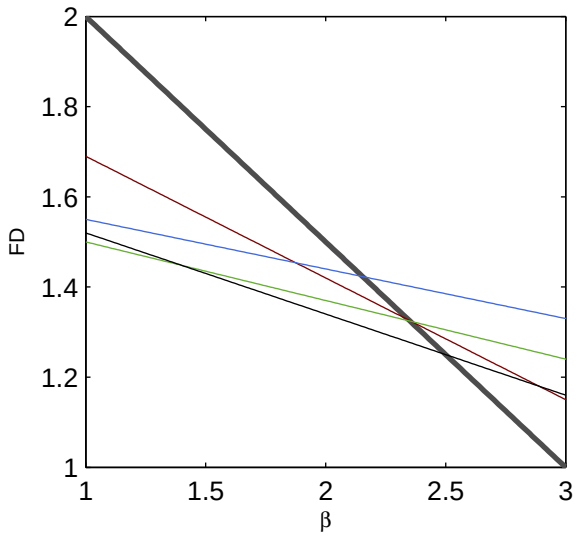

Figure 21: Mean regression line built for each population with the coefficients of Tab. 7: red for newborns, blue for children, green for young adults and black for elderly adults. The thick gray line represents the relationship of Eq. 27 valid for fractional Brownian motion.

affect its behavior in the time domain, producing very different values of fractal dimension. Future investigation should attempt to explore the possible influence of EEG phase distribution on the scaling relationship between FD and β.

6.5 CONCLUSION

The self-affinity of the EEG can be characterized equivalently by either fractal dimension or power-law beta exponent. Fractional Brownian motion, applied to the modeling of the EEG, provides a useful relationship between FD and β, which is currently exploited by many researchers and physicians. The results of the study presented in this chapter highlight the inaccuracy of the adopted model which introduces errors in the quantitative description of the scaling properties of the EEG. Every time absolute values of FD are required for analysis purposes, direct estimation provides more correct values than those indirectly obtained by applying the fBm relationship 27 with lower computational effort. Further investigations are necessary to assess how would the experimental relationships presented in this work change, for example, with pathology or according to the mental task. Based on the preliminary results reported in this chapter, there is little chance that a single scaling relationship could be found for the description of the fractal-like behavior of the EEG.

Part II

Clinical applications

7 MONITORING CAROTID ENDARTERECTOMY

CONTENTS

EEG monitoring during carotid endarterectomy is the commonest method used to reduce the risk of intraoperative brain ischemia. Beside visual assessment of the EEG, some quantitative parameters, based on spectral information, have been recently suggested as additional criteria for shunt need decision. This chapter explores new linear (HLF ratio) and nonlinear parameters (ZC and FD) which can assist the physician in real-time decision whether a shunt is required or not. The results obtained with the proposed parameters are compared with those achieved by means of three previously explored measures: the desynchronization index, the sBSI and the tBSI. This chapter is based on Author's publication 1.

7.1 INTRODUCTION AND MOTIVATION

Carotid endarterectomy

Carotid endarterectomy (CEA) is a well-known surgical procedure for the prevention of stroke in patient with high-grade carotid stenosis and is generally performed with selective shunting [Kalkman, 2004].

Intraoperative ischemia

Intraoperative ischemia during carotid cross-clamping in patients undergoing CEA is a major complication and prompt recognition of insufficient collateral blood supply is crucial (occlusion of the controlateral internal carotid artery is considered to have a significant impact on the outcome of CEA).

State of the art

Different methods have been used to prevent intraoperative stroke: the measurement of carotid back pressure [Moore *et al.*, 1973], the assessment of the awake patient under regional anaesthesia [Shah *et al.*, 1994], the transcranial Doppler measurement [Ghali *et al.*, 1997], the monitoring of somatosensory evoked potentials [Schweiger *et al.*, 1991], and the continuous EEG monitoring [McFarland *et al.*, 1988; Pinkerton, 2002; Plestis *et al.*, 1997; Salvian *et al.*, 2012; Visser *et al.*, 1999]. The latter is still the most used form of monitoring cerebral hypoperfusion

during CEA. As EEG visual analysis is subject to human error and makes quantification of signal's alterations difficult, it is evident that a quantitative measure should identify more reliably those patients who need a shunt during carotid clamping. To this aim, several parameters based on EEG spectral analysis, producing reasonable results, have been recently proposed for the monitoring of CEA [Cursi *et al.*, 2005; van Putten, 2006; van Putten *et al.*, 2004]. They are supported by the fact that a decrease in relative alpha and beta band powers as well as possible hemispheric asymmetry represent clear signs that the brain is at risk during CEA [Minicucci *et al.*, 2000; Visser *et al.*, 2001]. In order to support the physician in a prompt decision whether or not shunting is needed, the possibility of reliable real-time evaluation and the ease of interpretation represent specific characteristics that quantitative EEG measures should have.

Adopted approach

Based on these requirements, in this chapter some linear and nonlinear EEG parameters that could be useful to monitor the cerebral response to significant blood flow reduction are investigated and compared with those proposed in the literature [Cursi *et al.*, 2005; van Putten, 2006; van Putten *et al.*, 2004]. The new linear parameter (HLF ratio) is based on the observation that in presence of brain suffering the spectral power decrease in the 8-15 Hz band is very often associated to a power increase in the low frequency band. In order to take into account both behaviors, the ratio between the signal power in the 8-15 Hz and in the 0.5-5 Hz will be considered. The nonlinear parameters that will be examined are Higuchi's fractal dimension (FD) and the zero-crossings (ZC), an index for the description of nonlinear systems which is dependent on the dominant frequency (or band) of the signal.

Proposed parameters

7.2 MATERIALS AND METHODS

7.2.1 Patients

A total of 140 patients who underwent carotid endarterectomy at the AOTS Hospital of Trieste in 2003-2006 were retrospectively examined. Since artifacts, well recognized by the human observer, are not trivially eliminated or compensated for by computer programs, the 5 cases in which the EEG was so corrupted to make unreliable also the expert assessment were rejected from the study. The remaining 46 female and 89 male patients (age of 70±8 years) were considered for the investigation. All CEAs were performed under general anesthesia and decision to shunt was based on intraoperative EEG monitoring. Selective shunt was advised (21 patients) if the visual inspection of EEG, as interpreted by an experienced neurophysiologist during clamping procedure, showed significant mono- or bilateral EEG changes. These alterations included a decrease in fast activity and/or an increase in slow activity (slowing down in running EEG), or an attenuation of the whole EEG activity (voltage reduction). The accurate EEG off-line reanalysis finally permitted to reclassify two patients who belonged to

the non-shunted group as to be shunted. Hence, on the whole, 112 non-shunted and 23 shunted patients were considered for the classification.

7.2.2 EEG recording and analysis

Recording

EEGs were recorded according to the international 10-20 system with Ag/AgCl electrodes. The acquisition was performed using Galileo System (EBNeuro, Florence, Italy) with a 128 or 512 Hz sampling frequency. Ten bipolar derivations were used for the analysis (F4-C4, C4-P4, P4-O2, F8-T6, T6-O2, F3-C3, C3-P3, P3-O1, F7-T5, T5-O1). Although some EEG derivations may be more sensitive to anomalies during carotid endarterectomy than others [Laman *et al.*, 2012], in this work all EEG derivations were equally weighted in order to simplify the procedure. The off-line investigation was carried out during the 3 min before and 3 min after the artery clamping, separately for right and left hemisphere derivations.

Pre-processing

The signal coming from each derivation was resampled (if necessary) at 128 Hz, according to the guidelines of Chapter 5 for the estimation of the fractal dimension, digitally processed with a Butterworth band-pass filter between 0.4 and 40 Hz and divided into 50% overlapping segments of 20 s (2560 points), each of which was detrended and Hamming windowed.

Parameters calculation

All parameters were calculated in these epochs and averaged among all the derivations of the same hemisphere, obtaining one value per parameter and hemisphere every 10 seconds. The baseline for all parameters was evaluated from the first 3 min preceding the clamping procedure (reference period), using the median value in this period. Finally, possible variations of the parameters after clamping with respect to the baseline value were quantified by calculating for each parameter and hemisphere, at each step t, two different functions: the percent relative variation, $R(t)$, and the Z -score, $Z(t)$, defined as:

$$R(t) = \frac{P(t) - \bar{P}}{\bar{P}} \cdot 100 \tag{29}$$

and

$$Z(t) = \frac{P(t) - \bar{P}}{\sigma} \tag{30}$$

where $P(t)$ represents the generic parameter value at step t; $\bar{P}$ and σ correspond to the median and the standard deviation values, respectively, of the parameter P calculated in the reference period. The $R(t)$ function determines the percent parameter change during clamping compared to the reference period, while the $Z(t)$ function measures the significance of the difference between post-clamping and reference period values. Linear analysis considered some spectral parameters

calculated from the power spectral density (PSD) estimated using periodogram method:

$$PSD = \frac{1}{N}|DFT|^2 \tag{31}$$

Spectral parameters

DFT being the Discrete Fourier Transform of the EEG. From PSD, the power in the traditional EEG sub-bands (delta 0.5-4 Hz, theta 4-8 Hz, alpha 8-13 Hz and beta 13-18 Hz) and the power in a low frequency band (LF: 0.5-5 Hz) and in a high frequency band (HF: 8-15 Hz) were computed. In addition also the ratio HF/LF (HLF ratio) was calculated. The HLF ratio and the HF index were used in the following. It should be underlined that the HF parameter is basically identical to the desynchronization index described by [Cursi *et al.*, 2005]. Beside these linear parameters, Higuchi's fractal dimension (FD) and the zero-crossings (ZC) were calculated on the same epochs. The ZC count is a nonlinear parameter used in the analysis of random signals [Kedem, 1986]. Due to the fruitful connections existing between ZC and the dominant frequency, ZC index is expected to be able to identify possible changes in dominant spectral components during carotid clamping. The algorithm for the calculation of this parameter is described in Appendix A.

Zero-crossings

Fractal dimension

The FD was computed by means of Higuchi's algorithm as described in Chapter 5.2.1.3. The estimation of both nonlinear parameters is faster than spectral analysis and can be reliably performed also on short epochs. The behavior of the three proposed indexes (HLF ratio, ZC and FD) was compared to that of the HF (or desynchronization index) [Cursi *et al.*, 2005] and of the sBSI and tBSI parameters suggested by van Putten *et al.* [2004] and van Putten [2006]. The sBSI index is a normalized measure for interhemispheric spectral symmetry defined as:

Previously proposed indexes

$$sBSI = \frac{1}{N}\sum_{i=1}^{N}\left\|\frac{1}{M}\sum_{j=1}^{M}\frac{R_{ij}-L_{ij}}{R_{ij}+L_{ij}}\right\| \tag{32}$$

where R_{ij} (L_{ij}) are the Fourier coefficients belonging to frequency $i = 1,...,N$ of the right (left) hemispheric bipolar derivations $j = 1,...,M = 5$. In the present study $N = 50$ (frequency range 1-25 Hz, with spectral bandwidth of 0.5 Hz). Before calculating the FFT transform, the EEG data were resampled at 256 Hz in order to replicate the work of van Putten [2006]. On the other hand the tBSI index is sensitive to diffuse EEG changes. With the aim of eliminating the contribution of a possible spatial asymmetry the tBSI is calculated as:

$$tBSI = \frac{2tBSI' - sBSI}{2} \tag{33}$$

with tBSI′, a measure of temporal EEG changes, defined as:

$$tBSI' = \frac{1}{N}\sum_{i=1}^{N}\left\|\frac{1}{K}\sum_{j=1}^{K}\frac{S_{ij}-Sref_{ij}}{S_{ij}+Sref_{ij}}\right\| \tag{34}$$

where S_{ij} are the Fourier coefficients belonging to frequency $i = 1,...,N$ of the right and left hemispheric bipolar derivations $j = 1,...,K = 2M$, and $N = 50$ as before [van Putten, 2006]. All van Putten's parameters were calculated on 10 s intervals.

7.2.3 Patients classification

Automatic classification criteria

To decide if a subject should be identified as to be shunted or not, the values for each hemisphere of the four parameters (HF, HLF ratio, ZC and FD) during the post-clamp period were compared with suitable thresholds. Different thresholds for $R(t)$ functions were manually tested starting from values that visually could discriminate the pre-post clamp changes when present (see for example Subject3 in Fig. 23). The thresholds that produced the best classification (in terms of accuracy) are reported in Tab. 8. For $Z(t)$ functions a threshold of -1.2, very poor for the significance level ($p > 0.23$) but representing a good compromise to achieve the best accuracy, was set for the parameters. It was established that shunting has to be advised if the parameter exceeds, at least in one of the two hemisphere, the threshold value for at least 30 s. A procedure was then implemented in order to automatically recognize each CEA as belonging to "shunted group" or to "non-shunted group". For the tSBI and sBSI indexes the classification criterion followed the thresholds on ΔtBSI and ΔsBSI reported in van Putten [2006]. To estimate the effectiveness of a correct patient classification (shunted or not), for each parameter a truth table (scheme in Tab. 9) was calculated by comparing the parameter classification with that of the electroencephalography expert (this corresponds to the real-time clinical choice followed by off-line re-analysis). Starting from each truth table the results were statistically described in terms of sensitivity (true positive/[true positive+false negative]), specificity (true negative/[true negative+false positive]), and accuracy ([true positive+true negative]/total number of maps), which are classical statistical measures of the performance of a binary classification test related to the concepts of type I and type II errors.

7.3 RESULTS

The analysis of the EEGs showed that hypoperfusion was generally associated to a decrease (monolateral or diffuse) of the power in the alpha, beta and HF bands and frequently also to an increment in the delta band, confirming previous results [Minicucci *et al.*, 2000; Visser *et al.*, 1999]. The HLF ratio also decreased during suffering while FD

Table 8: Threshold values for the parameters used in the subject classification. The values are expressed in terms of percent relative variation, $R(t)$, during clamping compared to the pre-clamp reference period. For the sBSI and tBSI parameters the thresholds described in van Putten [2006] were used.

	$R(t)$ threshold
FD	-5%
ZC	-15%
HLF ratio	-40%
HF/desync index	-35%
ΔsBSI	0.05
ΔtBSI	0.02

showed different behavior during clamping: for more than 50% of shunted cases it increased rather than decreasing even if it was able to point out asymmetries (as shown, for example, in the Subject2 of Fig. 23). Examples of EEG traces and corresponding parameters time courses in typical patients who underwent a CEA are shown in Figs. 22 and 23, respectively. Figure 22 presents 5 s during the pre-clamping and 5 s during the post-clamping periods of EEG traces of a patient who did not need the shunt (Subject1) and of two patients showing, after clamping, monolateral changes (Subject2) or mainly diffuse suffering (Subject3). While the EEG changes are evident in Subject3, for all the EEG channels, these are visible only on the left derivations in Subject2; in Subject1 the EEG remains substantially unchanged. In Fig. 23 the $R(t)$ function trends of FD, ZC, HLF ratio, HF, sBSI and tBSI parameters during 3 min before and after the clamp, in the three typical patients of Fig. 22, are shown. The vertical line corresponds to the clamp start time while the horizontal lines represent the threshold values reported in Tab. 8. Points below (for FD, ZC, HLF ratio and HF parameters) or above the threshold (for sBSI and tBSI parameters) are considered as indicators of suffering. For FD, ZC, HLF ratio and HF parameters, the selected thresholds correspond to those that produced the best subject classification (in terms of accuracy); the thresholds for sBSI and tBSI parameters were selected following the criteria reported in van Putten [2006]. These refer to a difference between the actual value during clamp and the mean value during pre-clamp period. Left column of Fig. 23 shows that in five of the six monitored parameters, changes due to clamping are not able to exceed the threshold, confirming that no changes occurred in the EEG analysis (Subject1 in Fig. 22). Only the tBSI parameter fluctuates around the threshold, which proves to be too low. In a second example shown in Fig. 22 (Subject2), visual EEG analysis recognizes severe changes in the left hemisphere, correctly reflected in a more or less asymmetric reduction in four of the examined parameters (central column of Fig. 23). In this case both the tBSI and sBSI parameters correctly point out the monolateral suffering. In the third case, a decision to shunt was based

Table 9: Scheme of the truth table used in the classification process. A and D represent the number of true positive and true negative cases, respectively. B is the number of false negative and C is the number of false positive cases.

		Automatic classification based on the thresholds of Tab. 8	
		Shunted	Non-shunted
Neurophysiologist classification	Shunted	A	B
	Non-shunted	C	D

on the appearance of alterations in the activity of both hemispheres, detectable in the curves shown in Fig. 22 (Subject3) as well as in the behavior of the three new proposed parameters and of the HF index (right column of Fig. 23). In this case the sBSI parameter alone is not able to identify the suffering, showing its intrinsic limitation due to the demand of an altered EEG symmetry in order to operate in a correct way. On the contrary, the tBSI parameter well highlights the situation. It should be noted that even if the FD parameter shows the presence of asymmetry (Fig. 23, central column) or of evident gap (Fig. 23, right column), it does not exceed beyond doubt the preset threshold. Behaviors similar to those of the $R(t)$ functions are presented by the four parameters expressed in terms of Z-score functions. In the latter case a fixed threshold of -1.2 was used for all the considered parameters. Table 9 shows the truth table scheme used in the classification process.

In order to analyze the classification outcomes, the results obtained from each examined parameter by using both the $R(t)$ and the $Z(t)$ functions are shown in Tab. 10. The classification is expressed in terms of number of subjects correctly classified in the two classes (shunted: true positive and non-shunted: true negative) to which they were assigned by the visual EEG analysis. In the same table, the sensitivity, the accuracy and the specificity of each parameter are also displayed. The classification obtained from the $R(t)$ functions is slightly better than that gained from the $Z(t)$ ones, and hereafter only the $R(t)$ functions were considered. The ZC and HLF ratio parameters presented the best results, correctly classifying all the considered subjects, demonstrating a complete correlation with hypoperfusion complications. Also the HF parameter showed a very good discrimination power producing only four false positives. The FD parameter as well as the sBSI index, though having maximum specificity (100% of non-shunted cases correctly classified), unfortunately were not able to correctly identify the cases to be shunted (60-70% of wrong cases). On the contrary, the tBSI index permitted to recognize all the shunted cases but produced a large quantity (25%) of false positives.

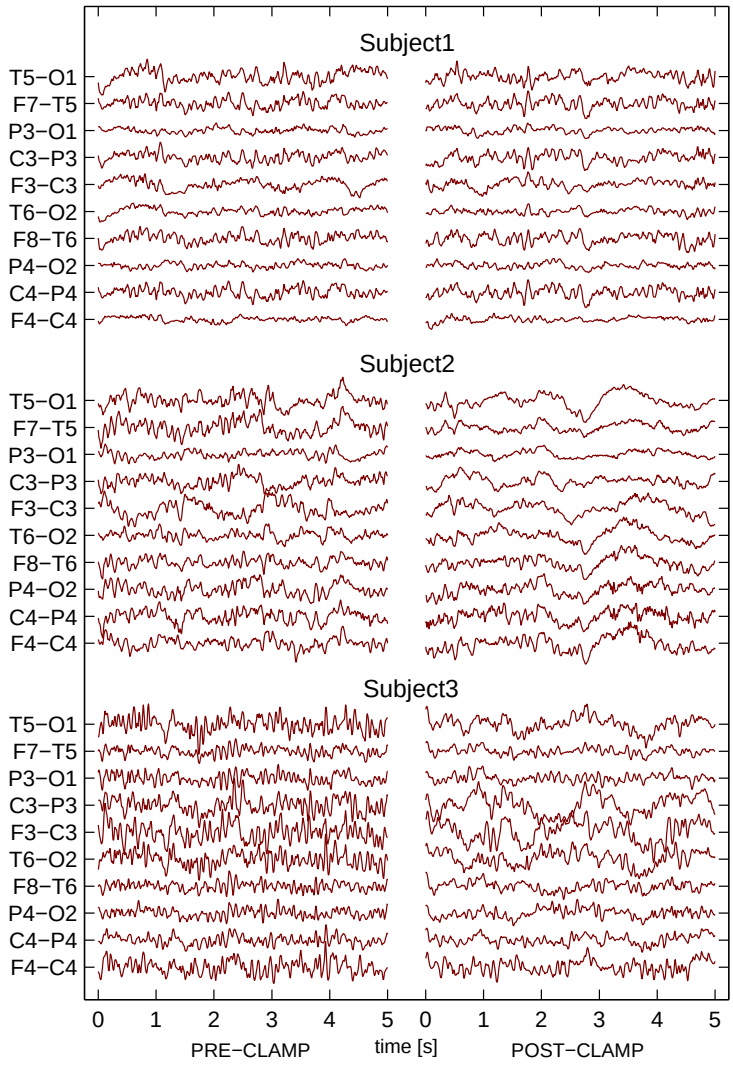

Figure 22: Five seconds of EEG traces during pre- (left column) and post-clamp (right column) periods in three typical patients presenting no changes (Subject1), monolateral differences (Subject2), and mainly diffuse suffering (Subject3). Subject1 was not shunted while the remaining two were shunted.

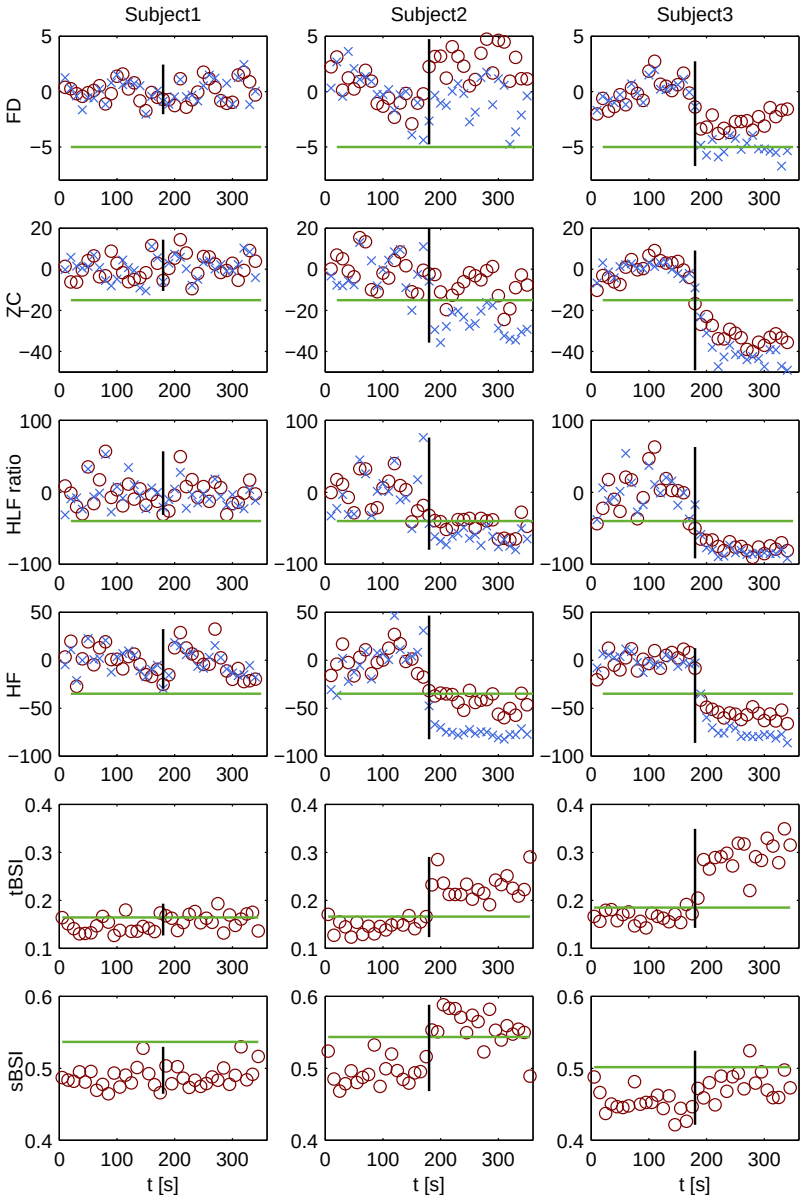

Figure 23: Percent relative variation, $R(t)$, time courses of the considered parameters, corresponding to the three typical situations in Fig. 22. Left column: Subject1 presenting no changes; central column: Subject2 with asymmetric differences; right column: Subject3 showing mainly diffuse suffering. For the FD, ZC, HLF ratio and HF parameters 'x' represents the right hemisphere and 'o' the left hemisphere. Vertical lines: clamping start; horizontal lines: threshold values.

Table 10: Sensitivity, accuracy and specificity together with the number of shunted (TP=true positive) and of non-shunted (TN=true negative) subjects correctly classified on 23 and 112 total cases, respectively. The values refer to each considered parameter and to both the percent relative variation, $R(t)$, and the Z-score, $Z(t)$, functions.

Parameter	TP	TN	Sensitivity	Accuracy	Specificity
FD-R(t)	7	112	0.30	0.88	1.00
FD-Z(t)	8	110	0.35	0.87	0.98
ZC-R(t)	23	112	1.00	1.00	1.00
ZC-Z(t)	22	112	0.96	0.99	1.00
HLF ratio-R(t)	23	112	1.00	1.00	1.00
HLF ratio-Z(t)	21	112	0.91	0.99	1.00
HF-R(t)	23	108	1.00	0.97	0.96
HF-Z(t)	23	106	1.00	0.96	0.95
sBSI	9	112	0.39	0.90	1.00
tBSI	23	84	1.00	0.79	0.75

7.4 DISCUSSION

Although visual analysis of the EEG represents the standard methodology to decide when the shunt is necessary during CEA, it is current opinion that this procedure is subject to human error and requires great experience in interpreting the graphs' alterations. This is the reason why quantitative real-time EEG analysis becomes every day more and more required, representing a useful additional information assisting in the decision for selective shunting. In the literature some parameters, e.g., BSI [van Putten *et al.*, 2004], sBSI and tBSI [van Putten, 2006], have been proposed even if their validity has been evaluated only preliminarily on few cases [Cursi *et al.*, 2005; van Putten, 2006; van Putten *et al.*, 2004]. In this study three new parameters (HLF ratio, ZC and FD) for the monitoring of cerebral hypoperfusion due to artery clamping, were proposed and evaluated, on a large number of CEA cases, and their performances and reliability were compared with those of the indexes suggested in the literature. The HLF ratio and ZC parameters yielded the best results with 100% correct identification of both shunt and non-shunt situations, while FD did not yield satisfactory results and produced many (about 70%) false negatives. At first, the differences in the classification (Tab. 10) obtained by using $R(t)$ and $Z(t)$ functions were examined: for all the parameters, $R(t)$ functions allowed the correct classification of one or two more cases than by using $Z(t)$ functions. This very small difference may be due to the use, for the $Z(t)$ functions, of a single threshold value (i.e., -1.2) for all the parameters while, for the $R(t)$ ones, the thresholds were optimized for each index (see Tab. 8). This fixed value represented only a compromise to achieve the best accuracy; in fact a threshold of 1.96, corresponding to a significant ($p < 0.05$) difference between pre- and post-clamp mean values, is more correct from a statistical point of view

but is inappropriate for a good classification. However, the $Z(t)$ functions are also influenced by the signal variability and consequently by the noise present on the EEG: more noise produces larger variance and smaller $Z(t)$ changes, making harder to exceed the threshold. Another remark concerns the EEG derivations used in the parameter calculation: even if some authors [Laman *et al.*, 2012] suggest to use selected derivations because of their higher sensitivity in detection of anomalies occurring during carotid surgery than others, in this work good results were also obtained using equally weighted bipolar EEG channels; consequently, a channel selection was not considered necessary. A main result of this work is to show that the $R(t)$ functions of two of the new examined parameters, i.e., the ZC and the HLF ratio, were able to correctly identify all cases presenting either mono- (asymmetric) or bilateral (diffuse) hemispherical suffering (as suggested by visual EEG analysis). In these cases the left and right $R(t)$ time courses presented, for no less than 30 s, a significant decrease below a threshold of -15%, for ZC, and of -40%, for the HLF ratio, of the pre-clamp mean values, thus providing precise indications of possible cerebral ischemia. In addition, the two parameters were also able to correctly discriminate all the cases in which the shunt was not required, corresponding to no significant EEG changes, showing they could capture EEG variations due to any kind of intra- or interhemispheric suffering. Furthermore, the simultaneous use of two $R(t)$ curves, one for each EEG side, permits to immediately identify possible asymmetries present in the EEG changes during CEA.

HLF ratio

The HLF ratio was based on the hypothesis, described in the literature [Blume *et al.*, 1986; Minicucci *et al.*, 2000; Salvian *et al.*, 2012], that alpha and beta EEG spectral powers decrease in presence of brain hypoperfusion followed by an increase of delta power, the latter being frequently not significant. Based on a similar idea, but limited only to the alpha and beta bands, Cursi *et al.* [2005] suggested the desynchronization index (corresponding in this study to the $R(t)$ function of the HF parameter). As reported in the results, the HF was able to correctly identify all the subjects to be shunted and only four cases of non-shunted patients were wrongly classified. Moreover, the optimal threshold value found in this study for the HF index is the same suggested in [Cursi *et al.*, 2005]. Adding the information coming from lower frequencies (0.5-5 Hz band), used as the denominator in the HLF ratio parameter, improves the HF performance: exact subject classification is achieved. This work confirms that the 8-15 Hz frequency range is the band which is most sensitive to possible cerebral suffering during CEA [Cursi *et al.*, 2005; Minicucci *et al.*, 2000]. Moreover, the results support the hypothesis that the utilization of the information included into the 0.5ñ5 Hz band may slightly improve the specificity, producing a more accurate identification of the cases that do not require shunting.

Zero-crossings

The ZC parameter, recently proposed for studying dementia, sleep-stage characteristics and background activity [Carrozzi *et al.*, 2004; Henderson *et al.*, 2006; Lin *et al.*, 2006] from EEG series, turned out to be capable of sensing reduction of fast activity as well as possible slow

activity changes, thus producing an indicator that can assist in the decision whether to proceed with shunting during CEA. The ZC parameter, measuring possible dominant frequency (or band) modifications, proved to be strongly correlated with the visual assessment of the EEG changes due to brain suffering. It is underlined that the ZC parameter is very easily calculated directly from temporal signals and it does not require power spectrum evaluation of the EEG (as the HLF ratio or the HF index do). Hence, it is suitable for a real time implementation and its time course, added as a further signal in the visualization of the EEG derivations, may permit the successful outcome of the surgical procedure.

Fractal dimension

The third examined new parameter, FD, did not yield satisfactory results. It produced many (about 70%) false negatives (i.e., it did not identify many subjects to be shunted), even if it correctly recognized all the subjects that did not need shunting. This situation was mainly due to an uncertain decrement of the FD values in many cases of cerebral hypoperfusion: the FD changes were too small and an increase of the threshold value produced a very large increment of false positive cases. The FD parameter, measuring the fractal behavior of the EEG signal, was not able to recognize generalized EEG decreases, since it does not change if the signal is merely rescaled in amplitude; thus it produced many classification errors. Furthermore, the EEG complexity changes sensed by the FD were so small they did not exceed the threshold.

sBSI

The sBSI parameter produced slightly better results than FD. The index corresponds to the previously proposed [van Putten *et al.*, 2004] brain symmetry index (BSI) and it should quantify hemispheric changes in spectral symmetry. Unfortunately, the sBSI index excluded about 60% of the subjects to be shunted (false negative), confirming the limits already underlined by [van Putten, 2006] even if on a limited number of cases (4). In fact, the sBSI parameter was able to detect only the cases presenting asymmetric spatial changes in the EEG, showing on the contrary insensitivity to distributed attenuation of fast activity or to diffuse increase of delta activity.

tBSI

In order to overcome this limitation and to be also sensitive to temporal changes in spectral characteristics, a further index (tBSI) was proposed by van Putten [2006]. The tBSI index yielded 28 wrongly classified cases, on a total of 112 (25% of false positive), suggesting shunt when it was not necessary. It should be noted that the combined use of the sBSI and tBSI indexes did not improve the results; probably both sBSI and tBSI parameters are able to identify asymmetric changes. It is evident that the equation 33 used by van Putten could be not sufficient to cancel the influence of spatial asymmetries on tBSI, or (alternatively but improbably) all the cases here considered showing asymmetry also included diffuse EEG changes sensed by the tBSI parameter. However, in all the examined subjects the tBSI index alone produced the same classification result as when used with the sBSI contribution. Furthermore, since the tBSI index calculation considers the absolute value of the pre/post-clamp difference (Eq. 34), it is modified not only by a signal decrease but also by a signal increase that

generally indicates activation [Visser *et al.*, 1999], as it could happen when the haematic flow increases or anesthesia becomes less deep. This situation is signaled by the tBSI parameter as a need of shunt when it is actually not required; this fact could explain some of the false positives obtained with this index.

7.5 CONCLUSION

Since routine shunting may increase the risk of perioperative stroke [Salvian *et al.*, 2012], EEG monitoring, based on quantitative measures of the EEG changes, proved to be a useful tool for shunt decision during CEA. In this study the R(t) functions of some new parameters, in particular the HLF ratio and the ZC indexes, showed to be able to correctly identify cases presenting mono- or bilateral hemispheric changes capturing both asymmetric and diffuse suffering situations. As proved by the retrospective analysis, in those patients where the mean value of the HLF ratio or the ZC parameters go below -40% and -15% thresholds, respectively, in the 3 min before clamping, visual EEG analysis showed significant changes, and shunting was advised. Slightly worse results (4% of false positives) had been achieved with the HF/desynchronization index (previously proposed by Cursi *et al.* [2005]) while the pair of sBSI/tBSI parameters (or the tBSI alone) produced about 25% of false positives. Finally, the FD parameter and the sBSI index alone did not yield good results, and generated large classification errors. In conclusion, the R(t) function of the ZC parameter represents the best choice both for a correct classification and for the possibility of real-time implementation. The contemporary utilization of the R(t) left and right functions permits an immediate quantification of possible asymmetries as well as, when used as continuous display beside the EEG derivations, the identification of EEG changes due to artifacts or anesthesia. Thus, the Author proposes to use the ZC parameter to support the visual assessment of the EEG during CEA, offering a quantitative measure for EEG alterations due to cerebral hypoperfusion.

8 MONITORING THE DEPTH OF ANESTHESIA

CONTENTS

The assessment of the depth of anesthesia based on the analysis of the EEG is an active field of research. Although many methods, including BIS^{TM}system, have been developed over the years to quantify unconsciousness during anesthesia, intraoperative awareness is still a major clinical problem. This chapter explores an alternative approach, based on the nonlinear analysis of the EEG, aimed at reducing both the incidence of intraoperative awareness and the computational complexity of BIS. The standalone fractal dimension (FD) and zero-crossings (ZC), as well as the burst suppression compensated FD (bsFD) and ZC (bsZC), as measures of the depth of anesthesia, are evaluated in this preliminary study and compared with BIS index. The chapter is based on Author's publication 5.

8.1 INTRODUCTION AND MOTIVATION

The monitoring of anesthesia based on EEG parameterization is intended to help anesthesiologists maintain suitable level of hypnosis in order to provide optimal working conditions to surgeons and to ensure patient's safety. While, on the one hand, too deep anesthesia must be avoided in order to prevent over dosing side effects, on the other hand, low doses of hypnotic agents can cause some form of intraoperative awareness. In this situation patients may hear conversations, have visual perceptions, feel pressure or pain and be unable to communicate their sensations [Schwender *et al.*, 1998]. After operation, patients can recall all of the details of the procedure and can experience unpleasant further effects like anxiety, sleep loss, nightmares and panic attacks. A severe anxiety disorder, namely the post-traumatic stress disorder (PTSD), can develop as a result of these postoperative effects [Jones, 1994; Osterman *et al.*, 2001].

Intraoperative awareness

Several depth-of-hypnosis assessment methods, based on linear and nonlinear measures of the EEG, have been proposed in the last decade

State of the art

to provide a quantitative objective measure of the depth of anesthesia. Multiscale rescaled range analysis [Liang *et al.*, 2011], wavelet-based bicoherence [Li *et al.*, 2011], spectral entropy [Ferenets *et al.*, 2007; Klockars *et al.*, 2011], approximate entropy and Lempel-Ziv complexity [Jordan *et al.*, 2006] are mentioned as examples. Some commercial systems, based on the Patient State Index (PSI) [Drover *et al.*, 2002], the Narcotrend monitoring [Kreuer *et al.*, 2003] and the Entropy^{TM}method [Viertiö-Oja *et al.*, 2004] have been recently introduced in the operating room. The benchmark comparator for all these monitors is the Bispectral Index Score BIS^{TM} of Aspect Medical Systems (Newton, MA) [Kelley, 2010]. Bispectral index is a parameter that integrates several electroencephalographic measures into a unit-less number between 100 (fully awake) and 0 (flat line EEG). Although the exact algorithm used to synthesize the index is still unknown, some studies referenced in Morimoto *et al.* [2004] brought new insight into the BIS-calculation process. After artifacts removal, the EEG is firstly analyzed for suppression detection and quantification through the burst suppression ratio. Then the signal is fast Fourier transformed (FFT) to compute a relative beta ratio and to derive the bispectrum, from which the relative synchrony of fast and slow waves is calculated. These parameters are combined to generate the BIS index, whose values, updated every second, should be maintained within the recommended range (40 to 60) for patient safety during surgery.

BIS^{TM}index

Rationale

Despite the use of such monitors, the incidence of awareness during general anesthesia that can be recalled explicitly after operation has been reported to be 1.1% in total intravenous anesthesia (TIVA) and 0.59% in balanced anesthesia [Errando *et al.*, 2008]. Sometimes anesthesiologists have to rely on objective autonomic measures such as heart rate, blood pressure, respiration pattern and body temperature [Miller, 2005] or even on subjective assessments based, for example, on the Ramsay sedation scale [Ramsay *et al.*, 2012]. For this reason, research in the field of EEG-based monitoring of anesthesia is still very active.

Adopted approach

The present study proposes an alternative methodology with the twofold aim of minimizing the incidence of intraoperative awareness and reducing the computational complexity of BIS [Miller *et al.*, 2004; Schneider *et al.*, 2004]. Two nonlinear indexes, the fractal dimension (FD) and the zero-crossings (ZC), are off-line calculated and then combined with the burst suppression ratio (BSR) to produce the bsFD and bsZC indexes. The indexes, proposed to monotonically quantify the depth of anesthesia, are compared with BIS by means of Pearson's correlation analysis. The comparison with BIS is made also in terms of ability to detect the onset of possible awareness.

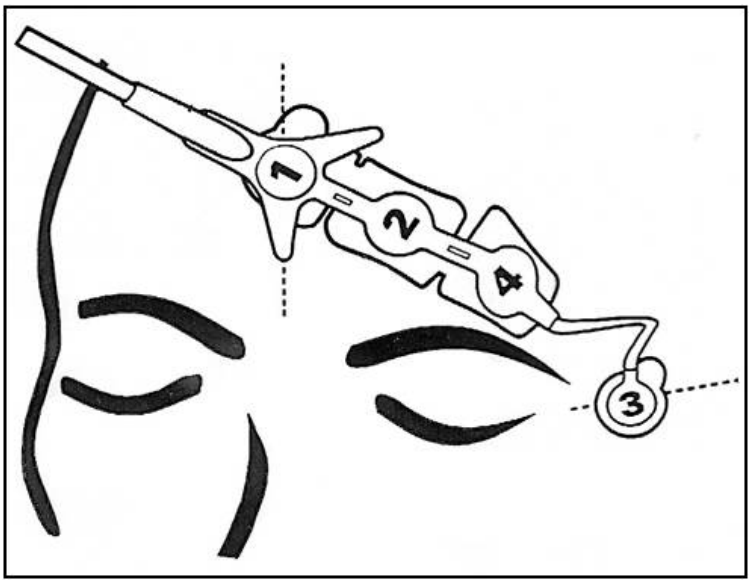

Figure 24: The BIS sensor^{TM}used for the recording of both BIS and raw EEG.

8.2 MATERIAL AND METHODS

8.2.1 Patients

The methodology proposed in the present research was applied to EEG recordings from 6 patients who underwent surgery under general anesthesia. The study was approved by the Ethics Committee of the IRCCS "Burlo Garofolo" Scientific Institute of Trieste. General anesthesia was induced by intravenous *propofol* (hypnotic agent), *fentanyl* (analgesic) and *rocuronium/vecuronium* (muscle relaxants). Anesthesia was maintained, under BIS control, by administration of inhalational agent *sevoflurane* (balanced anesthesia, 4 patients) or *propofol* (total intravenous anesthesia, 2 patients). Some patients were premedicated with 1-2 mg of *midazolam*.

8.2.2 EEG recording and analysis

Recording

In order to minimally interfere with the standard surgical procedure, the BIS sensor^{TM}(Aspect Medical Systems, Newton, MA), applied to the forehead of the patients before the induction of anesthesia, was used to acquire both the BIS index and raw EEG data (Fig. 24). The acquisition started at least 2 minutes before the induction of the hypnotic agent in order to have a baseline for the successive evaluations. At the end of the surgical procedure data were transferred from the BIS Monitor to a laptop computer via USB. EEG signals were A/D converted with a sampling frequency of 128 Hz, according to the guidelines of Chapter 5, and 16-bit accuracy. The EEG derivation selected for the analysis corresponds to the Fp1-Fpz bipolar derivation of the 10-20 sys-

Pre-processing

tem. EEG signals were processed with a Butterworth bandpass filter (second order high-pass and third order low-pass) between 6 and 50 Hz. The choice of removing low frequencies was made in order to preserve and highlight high-frequency oscillations considered as a marker of the conscious state [Sleigh *et al.*, 2001]. EEG traces were then divided into 50% overlapping segments of 10 s. Higuchi's fractal dimension (FD) and the zero-crossings (ZC) were calculated in these epochs as explained in Chapter 5.2.1.3 and Appendix A, respectively. To detect and quantify possible EEG suppression, that would heavily modify the characteristics of the signal, the burst suppression ratio (BSR) was calculated as explained by Doyle and Matta [1999]. EEG suppression is defined as those epochs longer than 500 ms during which EEG voltage does not exceed ± 5 μV (example of burst suppression pattern in Fig. 25). The BSR is defined as the percentage of the suppression time, T_s, against the time duration of the segment under investigation, T:

Parameters calculation

$$BSR = \frac{T_s}{T} \cdot 100 \tag{35}$$

The BSR is calculated on the same segments used for the estimation of FD and ZC, therefore on intervals of $T = 10$ s. A burst suppression ratio of 100% implies isoelectric EEG. Supposing that EEG's parameterization could be corrupted by EEG burst suppression, compensated fractal dimension (bsFD) and zero-crossings (bsZC) were calculated as proportional reductions of FD and ZC, respectively:

$$bsFD = FD \cdot \left(1 - 0.8 \cdot \frac{BSR}{100}\right) \tag{36}$$

$$bsZC = ZC \cdot \left(1 - 0.8 \cdot \frac{BSR}{100}\right) \tag{37}$$

In correspondence to the large artifacts introduced in the EEG by the automatic impedance check performed every ten minutes on the electrodes, the values of the parameters were replaced by the last value preceding the artifact. FD, ZC, bsFD and bsZC parameters were then monitored in all phases of anesthesia: pre-induction, induction, burst suppression (if present), maintenance and recovery, in order to compare the performances of the proposed parameters with the BIS index. Pearson's correlation coefficient was used to assess and quantify dependence between each parameter and BIS index.

8.3 RESULTS

As can be seen in the example of Fig. 26, both FD and ZC decreased as BIS decreased and increased as BIS increased for BIS $\geqslant 35$. However, erroneous behavior is exhibited by both parameters for lower values

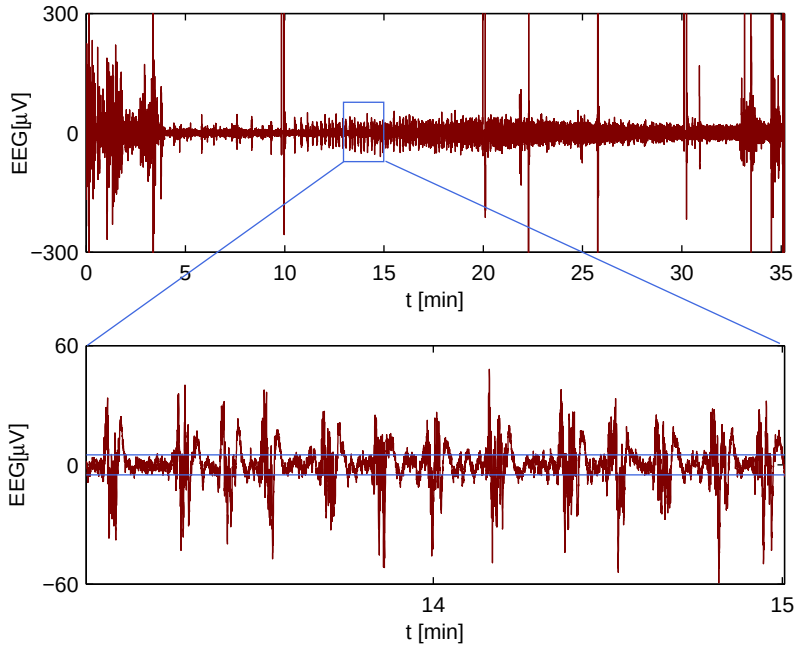

Figure 25: Example of EEG burst suppression pattern.

of BIS. On the other hand, BIS values in the range 30-0, as reported by Bruhn *et al.* [2000], are linearly correlated with BSR $\geqslant$ 40%. The compensation of both FD and ZC parameters with BSR circumvents the sensitivity of the measures to the burst suppression, as shown by bsFD and bsZC indexes in Fig. 27. The combined parameters are able to follow the depth of hypnosis distinguishing all the phases that characterize a typical anesthesia: pre-induction (0-2 min), induction (2-3.3 min), burst suppression (3.3-20 min), maintenance (20-29.3 min) and recovery (29.3-35 min). The analysis conducted on the 6 patients confirmed that neither FD nor ZC standalone parameters are able to characterize all phases of anesthesia (Tab. 12). The compensation with BSR, obviously able to describe only burst suppression, improved, as expected, the performances of both parameters. Table 11 presents Pearson's correlation coefficients calculated for the relationships BIS-bsFD and BIS-bsZC observed in each patient. Both parameters were linearly correlated with BIS in almost all patients. Table 11 highlights that the linear correlation between bsFD (bsZC) and BIS was barely of 61% for Patient 6 (Tab. 11). Patient 6 is a subject who most likely experienced intraoperative awareness. As referred by the anesthesiologist, the patient showed marked movements and slurring of speech, twice during surgery, at about minute 22 and minute 28 of the operation. As shown in Fig. 29, while BIS index showed only slight increase in correspondence of the two episodes, bsFD and bsZC abruptly increased reaching values similar to those recorded before induction and after recovery of anesthesia. Moreover, to the strong decrease of BIS index

right before the first event did not correspond a significant reduction of none of the proposed parameters. The spectrogram of Fig. 30 revealed high EEG activity in the range 15-48 Hz, completely abnormal in anesthetized subjects. For comparison, the spectrogram of a typical EEG during anesthesia with no awareness is shown in Fig. 28. Although bsZC index showed the highest correlation with BIS, its discriminative power resulted lower than that of bsFD parameter. This fact may be explained considering that both pre-induction and recovery have short duration with respect to burst suppression and maintenance. Thus, they probably don't have much weight in the calculation of Pearson's correlation. Figure 31 shows the exponential relationship found between mean bsFD and BIS values, calculated for each subject in the available phases. Table 13 compares BIS and bsFD index ranges for each clinical state.

8.4 DISCUSSION

With the twofold aim of identifying a reliable index for the correct quantification of the depth of anesthesia and to reduce the computational complexity of BIS system, in this study 4 easy-to-calculate parameters based on nonlinear and fractal analysis of the EEG were explored. Standalone FD and ZC parameters and burst suppression compensated fractal dimension and zero-crossings (bsFD and bsZC) were evaluated on 6 EEG signals recorded under general anesthesia. To assess their ability to follow the depth of anesthesia, all parameters were compared with BIS index, off-line transferred to a laptop together with the EEG.

Since the amplitude of the high frequency components decreases as anesthesia deepens, with a concomitant increase of the amplitude of the low frequency waves [Rampil, 1998], FD was expected to decrease with *propofol* infusion. Similarly, according to the dominant frequency principle [Kedem, 1986], ZC was supposed to decrease with induction of anesthesia. However, both parameters failed to follow the depth of anesthesia for high doses of hypnotic agents which imply a burst suppression ratio greater than 40%. On the one side, the failure of FD may be explained by a loss of fractal-like geometry due to EEG suppression. On the other side, burst suppression patterns do not have a dominant frequency/band and therefore can't be described by zero-crossings count.

Since BSR $\geqslant$ 40% is linearly correlated with BIS in the range 30-0 [Bruhn *et al.*, 2000], it was decided to compensate FD and ZC with BSR. By using Eqs. 36 and 37 two new parameters, bsFD and bsZC, respectively, were defined. The compensation with BSR improved the performances of both the fractal dimension and the zero-crossings, allowing the quantification of the depth of anesthesia also in correspondence of burst suppression patterns, i.e., for high doses of hypnotic agents. Both parameters were linearly correlated with BIS with a mean Pearson's coefficient of 0.75$\pm$0.11 for bsFD and of 0.79 $\pm$0.11 for bsZC.

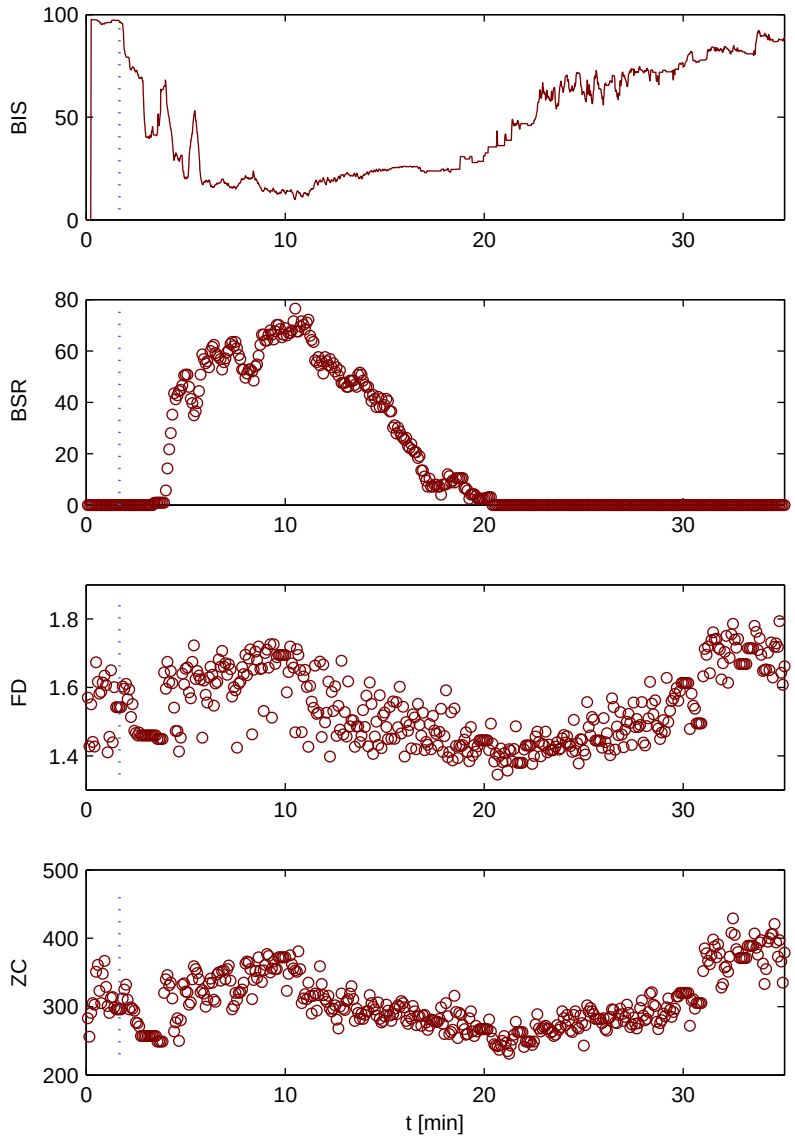

Figure 26: BIS index, burst suppression ratio (BSR), fractal dimension (FD) and zero-crossings (ZC) for patient 5 who underwent surgery under TIVA anesthesia. Dashed vertical lines represent the induction of anesthesia.

The lowest correlation coefficients were obtained for Patient 6, who, twice during the operation, showed marked movements and slurring speech. This form of awareness was caused by too light anesthesia, not accurately reflected by BIS index. The parameters proposed in

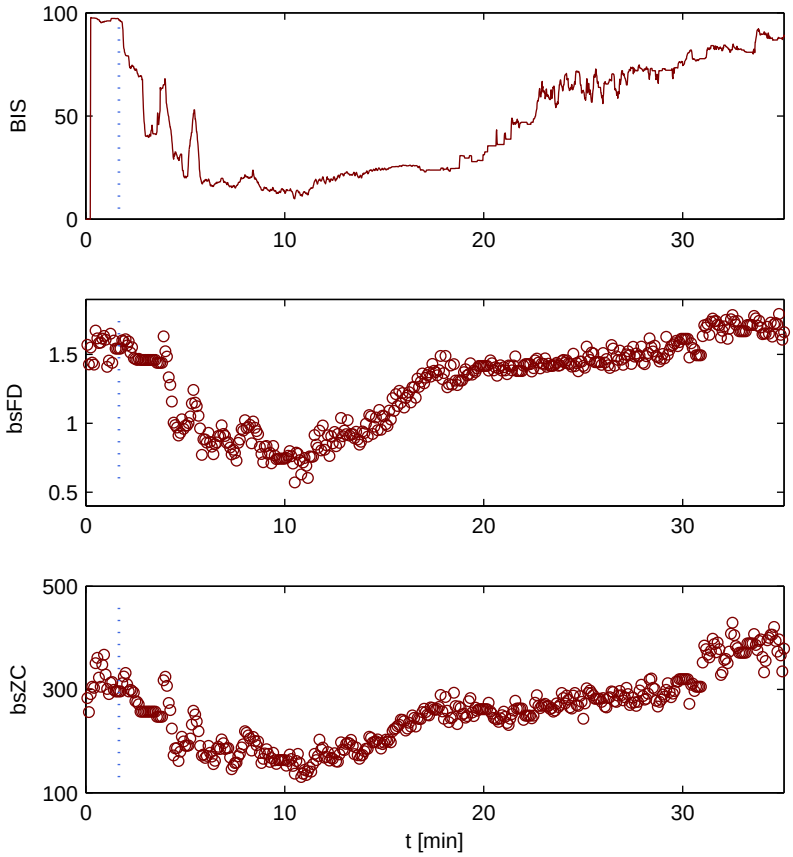

Figure 27: BIS, bsFD and bsZC indexes for the same patient of Fig. 26.

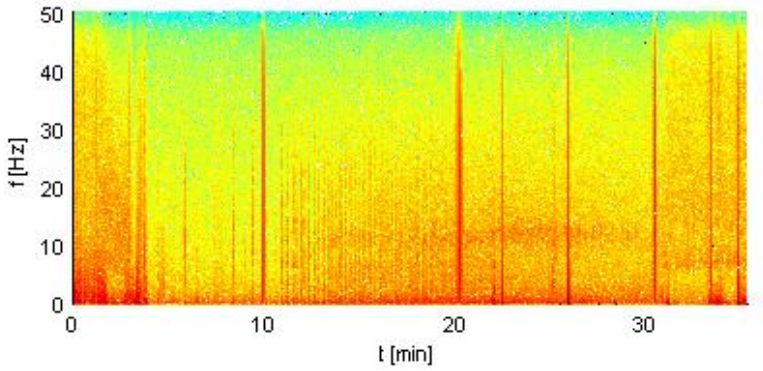

Figure 28: Spectrogram of the Fp1-Fpz derivation of the same patient of Figs. 26 and 27. All phases of anesthesia can be easily distinguished. Pre-anesthesia: 0-2 min; burst suppression: 3.3-20 min; maintenance: 20-29.3 min; recovery: 29.3-35 min.

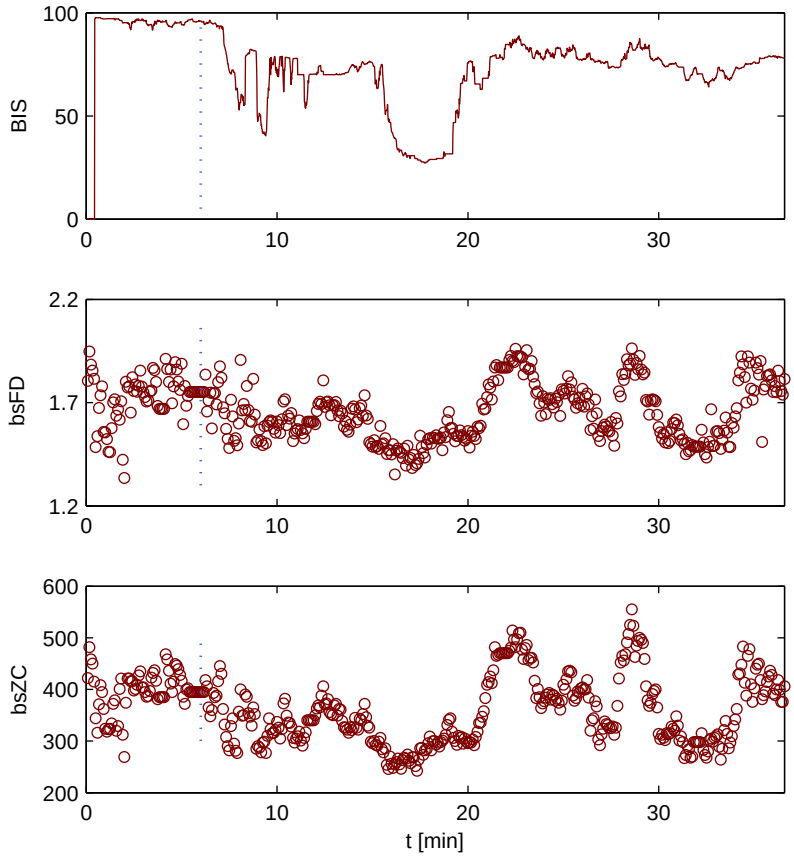

Figure 29: BIS, bsFD and bsZC indexes for patient 6 who experienced probable awareness under TIVA anesthesia.

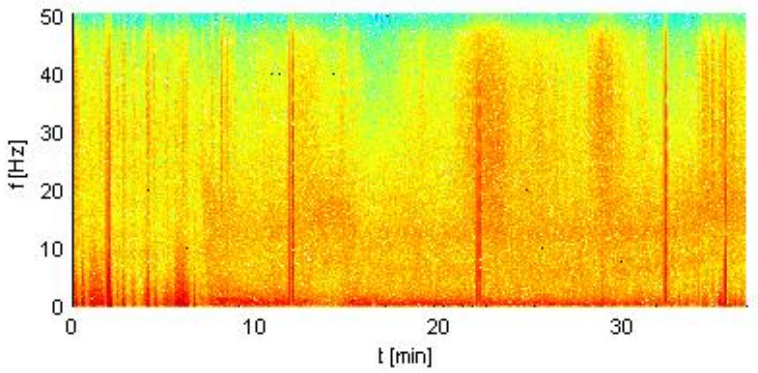

Figure 30: Spectrogram of Fp1-Fpz derivation of the same patient of Fig. 29. Abnormal activity in the range 15-45 Hz is evident at min 22 and 28. Similar activity was registered with the recovery of the patient.

Table 11: Pearson's correlation coefficients between BIS and both bsFD and bsZC parameters.

	BIS-bsFD	BIS-bsZC
Patient1	0.88	0.89
Patient2	0.71	0.77
Patient3	0.77	0.84
Patient4	0.64	0.75
Patient5	0.87	0.89
Patient6	0.61	0.61

Table 12: Ability to distinguish among the different phases of anesthesia of the considered parameters.

	pre-anesthesia	burst suppression	maintenance	recovery
BSR		√		
FD	√		√	√
ZC			√	
bsFD	√	√	√	√
bsZC		√	√	

this study, on the contrary, clearly increased in correspondence to both episodes (Fig. 29). The analysis of the spectrogram (Fig. 30) confirmed the presence of abnormal high activity in the range 15-48 Hz, which reflects changes in the conscious state [Sleigh *et al.*, 2001]. As can be seen in the spectrogram of a successful anesthesia (Fig. 28), maintenance is characterized by the presence of a 13 Hz oscillation with no high frequency activity observed.

One trend revealed by this preliminary study is the high variability of the proposed indexes in the pre-anesthesia phase. The reason for this behavior may be related to the concomitant administration of different drugs. Further investigations should attempt to clarify the cause of this variability since a more stable baseline is desirable.

Although bsZC had the highest correlation with BIS, the index that yielded the best results discriminating among all possible levels of sedation was bsFD. This information warrants further investigations to better establish whether bsFD or bsZC represents the most reliable monitoring tool. In any case, the power of the proposed parameters lies in the ability of reflecting changes occurring both in the low spectrum and in the high frequency range, though calculated directly in the time domain.

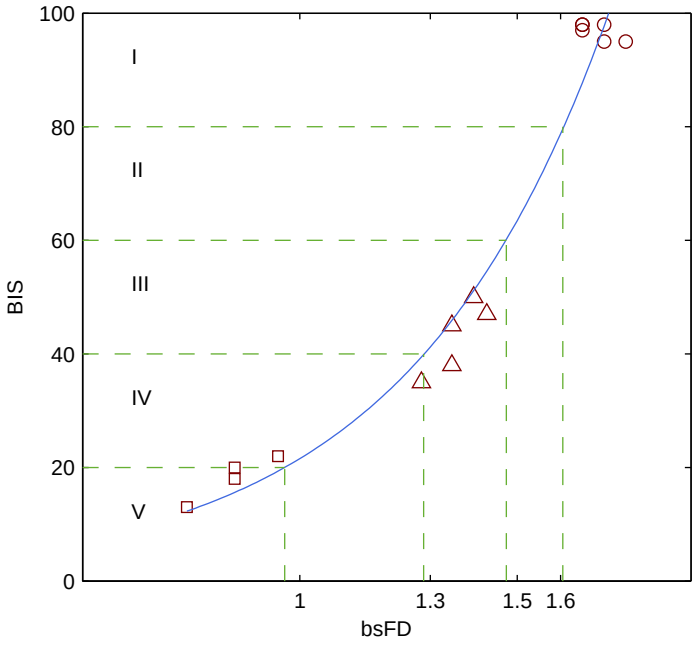

Figure 31: Mean BIS versus bsFD during pre-anesthesia (circles), burst suppression (squares) and maintenance (triangles). The solid blue line represents the exponential relationship between the two indexes. Dashed green lines separate the 5 ranges for the different clinical states listed in Tab. 13.

Table 13: Clinical state and correspondent index range for BIS and bsFD.

	Clinical state	BIS	bsFD
I	Awake	80-100	>1.6
II	Light/Moderate sedation	60-80	1.45-1.6
III	General anesthesia	40-60	1.3-1.45
IV	Deep hypnotic state	20-40	1-1.3
V	Bust-suppression	0-20	<1

8.5 CONCLUSION

A correct parameterization of the depth of anesthesia is necessary to ensure patient safety in operating room. Although several methods have been developed for the monitoring of anesthesia, the incidence of intraoperative awareness is still too high. This study proposes some nonlinear parameters and explores their ability in quantifying the hypnotic level during general anesthesia. The results presented in this chapter are preliminary as the number of patient is very limited. However, some interesting conclusions can be drawn. Similarly to BIS index, the fractal dimension of the EEG, properly combined with the

burst suppression ratio, is able to monitor the depth of anesthesia distinguishing among all different clinical states (Fig. 31 and Tab. 13). Moreover, bsFD index detects two episodes of intraoperative awareness whose onset was not clearly indicated by BIS monitor. The proposed parameter, combination of two time domain measures, is of low computational cost and therefore more suitable for real-time implementation. Should such preliminary results be confirmed on a larger sample, anesthesiologists could be provided with an easy-to-calculate reliable index for the monitoring of the depth of anesthesia and the reduction of the incidence of intraoperative awareness.

9 MACRO-STRUCTURAL EEG ORGANIZATION IN AUTISM

CONTENTS

The characterization of the macro-structural organization of the EEG in autism, with respect to that of mental retardation, has not been previously studied. Some preliminary investigations have been conducted to differentiate autistic and normal electroencephalographic activity. However, most of the studies carried on the autistic EEG principally aimed at analyzing the co-occurrence of autism and epilepsy. In this chapter the problem of autistic macro-structural neuronal organization is addressed through linear and nonlinear quantitative analysis of the EEG recorded in the three major electrical states: awake state, light sleep (stages 1 and 2) and deep sleep (stages 3 and 4). A statistical analysis is performed in order to identify the measures the best discriminate between the populations of autistic children and children with mental retardation. The chapter is based on Author's publication 6.

9.1 INTRODUCTION AND MOTIVATION

Autism

Autism is defined as a behavioral, cognitive and brain developmental disorder characterized by impairments in social interaction and communication, as well as by the presence of restricted and repetitive behaviors, interests and activities [Rapin, 1997]. Abnormalities in gross brain structure, neuronal growth patterns, abnormal connectivity and neurotransmitter profiles have been extensively studied [Belmonte *et al.*, 2004; Penn, 2006; Rippon *et al.*, 2007]. The study of the autistic brain has been approached with different investigation techniques such as EEG, MEG, magnetic resonance imaging (MRI) and functional MRI (fMRI) [Mengotti *et al.*, 2011; Philip *et al.*, 2012; Wilson *et al.*, 2007]. The search for objective measures that can help in screening for autistic children is of primary importance since, till now, most of the tools available to physicians rely on subjective observations. Autism belongs to the autism spectrum disorders (ASD), a broad classification

that includes also Asperger's Syndrome and pervasive developmental disorder not otherwise specified. Moreover, overlap among other behavioral and developmental disorders can produce false positives and subsequently poor test specificity. A correct early diagnosis would improve treatment and patient's longterm quality of life.

State of the art

The EEG represents a promising diagnosis tool, since it provides a low-cost description of brain activity dynamics with high temporal resolution. To date, most of the studies based on the EEG address the problem of the co-occurrence of autism and epilepsy [Tuchman *et al.*, 2010]. However, some investigations aimed at the characterization of autistic brain activity, with no reference to epileptic abnormalities, have been recently published. On the basis of conventional linear analysis, Grice *et al.* [2001] observed higher power for gamma sub-band of autistic EEG when compared with non-ASD signals. On the other hand, Chan *et al.* [2009] reported a significant reduction of theta activity in the anterior regions of the brain, while the results presented by Pop-Jordanova *et al.* [2010] indicated increased delta and theta power in the frontal derivations. However, the highly nonlinear and complex dynamics of the brain, brought to light in the last few decades, may not be exhaustively explained by traditional linear techniques. For this reason, chaos theory and fractal analysis have been recently introduced in ASD research as tools for the study of autistic brain features from a nonlinear perspective. Ahmadlou *et al.* [2010] recently proposed an automated EEG-based diagnosis methodology which combines wavelet decomposition, fractal analysis and neural networks. In the study of Catarino *et al.* [2011], EEG complexity of ASD patients is assessed by means of multiscale entropy analysis.

Adopted approach

This study represents an investigation of the macro-structural organization of the EEG in autism. To this extent, EEG signals were recorded in the three major electrical states: awake, light sleep (stages 1 and 2) and deep sleep (stages 3 and 4). The rationale for the inclusion of sleep EEG analysis lies in the fact that sleep disturbances are well-known correlates of autism disorder. On the one hand, irregular sleep, frequent night awakenings and severely reduced sleep time are the most referred problems [Malow, 2004]. On the other hand, REM sleep has recently been implicated in important cognitive functions like memory consolidation and emotions processing and hence it could represent an indicator of brain plasticity [Hobson and Pace-Schott, 2002; Maquet, 2001]. Thus, since abnormal sleep architecture may reflect abnormal neurotransmission, some investigations have been conducted in order to assess relative ratios or REM and non-REM sleep [Buckley *et al.*, 2010] or to investigate EEG synchronization during non-REM sleep [Kulisek *et al.*, 2008]. In this study, the issue was addressed from both a linear and a nonlinear point of view. Firstly, a linear spectral analysis was performed on the traditional EEG subbands in terms of percent power. Successively, both Higuchi's fractal dimension and the zero-crossings count were evaluated directly in the time domain. Mentally retarded children, matched with autistic patients for cognitive functioning, served as control group.

9.2 MATERIALS AND METHODS

9.2.1 Patients

A total of 19 autistic children and 19 children with mental retardation were included in the study. Participants were recruited at the Developmental Psychopathology Unit at the IRCCS "Eugenio Medea" Scientific Institute of Udine. The autism and comparison groups were matched for age (5-13 years), gender (17 boys and 2 girls) and IQ. None of the children were taking, or had ever taken, any psychotropic medication. Parental written informed consent was obtained for all the children. This research was approved by the local Ethics Committee.

9.2.2 EEG recording and analysis

Recording

Participants underwent an EEG assessment, in which a total of 3 recordings were collected. About 5 min of resting EEG in the awake state were firstly acquired. During data acquisition children were instructed to minimize head movements. Then, subjects underwent two further recordings during afternoon sleep after being sleep-deprived the night before the test. The first registration was performed under light sleep conditions (stages 1 and 2), while the second EEG was acquired when subjects fell into deep sleep (stages 3 and 4). Both sleep EEGs had a duration of about 10 minutes. Hereafter the first recording will be referred to as AW (awake) EEG, the second one as LS (light sleep) EEG and the third one as DS (deep sleep) EEG. Unfortunately, not all registrations were available for the analysis. Some recordings in the AW state had to be excluded because of the poor quality of registration either due to lack of cooperation or extensive movement artifact. On the other hand, sleep EEG was not acquired for those patients who could not achieve natural sleep (lack of both LS and DS recordings) or awoke before deep sleep was reached (lack of DS recording). The number of registrations available for each group in each state are summarized in Tab. 14. EEG signals were acquired with Ag/AgCl electrodes according to the 10-20 system of electrode positioning. Nineteen unipolar derivations (Fp1, Fp2, F7, F3, Fz, F4, F8, T3, C3, Cz, C4, T4, T5, P3, Pz, P4, T6, O1 and O2) and sixteen bipolar derivations (Fp1-F3, F3-C3, C3-P3, P3-O1, F7-T3, T3-T5, T5-O1, Fp2-F4, F4-C4, C4-P4, P4-O2, F8-T4, T4-T6, T6-O2, Fz-Cz and Cz-Pz) were used for the analysis. Signals were sampled at 256 or 512 Hz. In order to correctly compare

Pre-processing

Table 14: Number of subjects analyzed in the different electrical states.

	Autism	Mental retardation
AW	17	17
LS	14	15
DS	12	12

Table 15: Groups of unipolar derivations and corresponding brain regions considered for the analysis.

	Left	Right	Midline
Frontal	Fp1 F3 F7	Fp2 F4 F8	
Temporal	T3 T5	T4 T6	
Central-parietal	C3 P3	C4 P4	
Occipital	O1	O2	
Midline			Fz Cz Pz

Table 16: Groups of bipolar derivations and corresponding brain regions considered for the analysis.

	Left	Right	Midline
Anterior	Fp1-F3 F3-C3	Fp2-F4 F4-C4	
Frontal-temporal	F7-T3 T3-T5	F8-T4 T4-T6	
Central-parietal	C3-P3	C4-P4	
Posterior	P3-O1 T5-O1	P4-O2 T6-O2	
Midline			Fz-Cz Cz-Pz

Parameters calculation

EEG signals sampled at different rates, EEGs acquired at 512 Hz were resampled at 256 Hz. All EEGs were also resampled at 128 Hz for the successive fractal analysis according to the guidelines reported in Chapter 5. Both groups of 128 and 256 Hz EEGs were processed with a Butterworth bandpass filter between 0.5 and 60 Hz and with a 50 Hz notch filter. After detrending, each trace was then divided into 50% overlapping segments of 10 s. For the calculation of the spectral parameters, after Hamming windowing, each segment was fast Fourier transformed in order to derive the power spectral density (PSD) estimated by periodogram method using Eq. 31. From the PSD, the percent power in the traditional EEG sub-bands (delta 0.5-4 Hz, theta 4-8 Hz, alpha 8-13 Hz, beta 13-30 Hz and gamma 30-60 Hz) was calculated. Higuchi's fractal dimension (FD) and the zero-crossings (ZC) were calculated in the same segments as explained in Chapter 5.2.1.3 and Appendix A, respectively. For each unipolar and bipolar derivation, a mean value of each parameter was calculated as the average among all 10 s segments. The 19 unipolar derivations and the 16 bipolar derivations were then clustered into 9 unipolar and bipolar groups, respectively, according to the brain region as shown in Tabs. 15 and 16. Mean values within each of the 18 groups were finally calculated for each parameter. Pairwise differences between groups on all parameters were thus evaluated and statistical significance was assessed via the nonparametric Mann-Whitney U test. Tests were two-sided and a p-value < 0.05 was considered to indicate statistical significance.

Statistical analysis

9.3 RESULTS

For the sake of clarity, results will be presented for each electrical state (AW, LS and DS) separately. In the AW EEG, increased relative delta activity in the temporal and posterior bipolar derivations of the right hemisphere was revealed in autistic children with respect to the mentally retarded controls. Moreover, Higuchi's fractal dimension FD was higher in Fp1 channel as well as in the unipolar midline group (Fz Cz Pz) (Fig. 32). With respect to the comparison group, LS EEG of autistic children exhibited higher relative delta activity in the temporal bipolar derivation of the left hemisphere (T3-T5) with a contextual reduction of the percent beta power, observed also in the occipital and the parietal-occipital derivations of the same hemisphere (O1 and P3-O1). Moreover, higher relative gamma activity was registered for the autistic children in the left frontal bipolar derivation (Fp1-F3) and in the frontal bipolar region (Fp1-F3 F3-C3) (Fig. 33). Similar results were obtained for DS EEG, showing higher percent delta power in the T3-T5 bipolar derivation and concomitant reduction of relative beta activity in T3-T5 and P3-O1 bipolar derivations as well as in (P3-O1 T5-O1) bipolar region. The increased percent power of the gamma band was maintained in autistic children also in deep sleep and was registered in particular in the Fp1-F3 bipolar derivation (Fig. 34). Significant parameters, associated loci and corresponding p-values are presented in Tabs. 17, 18 and 19 for AW, LS and DS EEG, respectively. There were no statistically significant differences between the two groups for neither theta nor alpha percent power in none of the considered electrical states. Also ZC was unable to discriminate between autistic and mentally retarded children in all cases. The AW EEG could also not be described in terms of percent gamma and beta power while both light and deep sleep showed no significant differences also for FD. To summarize the results, higher complexity, quantified by FD, was registered in the left frontal-polar derivation and in the midline region of autistic children. At the same time, the autistic AW EEG showed an increased delta activity in the right posterior derivations. During sleep, almost independently from the stage, increased relative delta activity was observed in the temporal derivations of the left hemisphere with a contextual reduction of percent beta power also highlighted in the contiguous posterior derivations.

Awake state

Light sleep

Deep sleep

Table 17: Sites of the significant differences and correspondent *p*-values in the awake state (AW EEG).

	%PW delta			%PW beta	%PW gamma	FD		
unipolar derivation						Fp1 0.046	Cz 0.027	Pz 0.042
unipolar region						Fz Cz Pz 0.032		
bipolar derivation	P4-O2 0.027	T4-T6 0.046	T6-O2 0.030					
bipolar region	P4-O2 T6-O2 0.021							

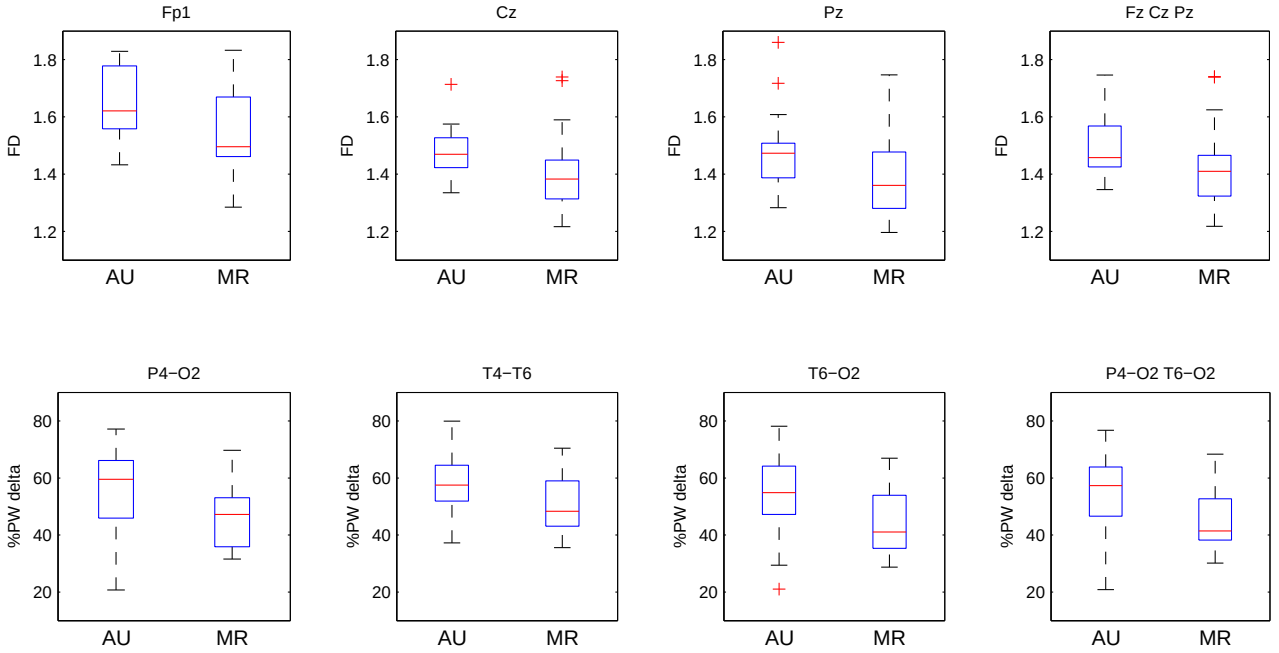

Figure 32: Box plots showing the statistically significant differences between autistic children group (AU) and mentally retarded group (MR) in the awake state with the indication of the site (derivation or group of derivations).

Table 18: Sites of the significant differences and correspondent *p*-values during light sleep (LS EEG).

	%PW delta	%PW beta		%PW gamma	FD
unipolar derivation		O1 0.014			
unipolar region		O1 0.014			
bipolar derivation	T3-T5 0.017	P3-O1 0.047	T3-T5 0.017	Fp1-F3 0.008	
bipolar region				Fp1-F3 F3-C3 *0.031*	

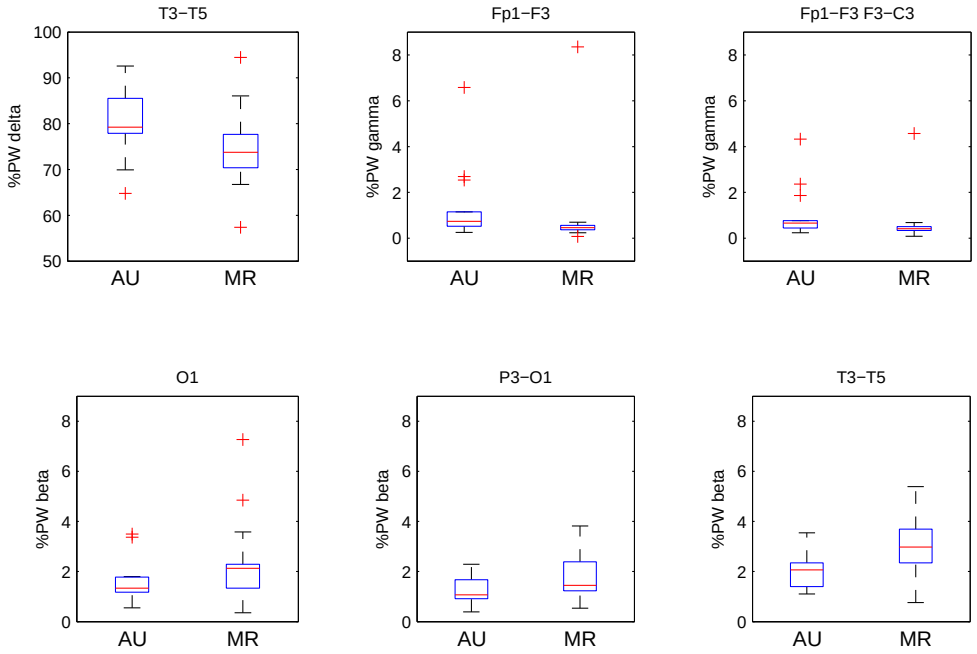

Figure 33: Box plots showing the statistically significant differences between autistic children group (AU) and mentally retarded group (MR) during light sleep with the indication of the site (derivation or group of derivations).

Table 19: Sites of the significant differences and correspondent *p*-values during deep sleep (DS EEG).

	%PW delta	%PW beta	%PW gamma	FD
unipolar derivation				
unipolar region				
bipolar derivation	T3-T5 0.019	P3-O1 T3-T5 0.023 0.012	Fp1-F3 0.001	
bipolar region		P3-O1 T5-O1 0.040		

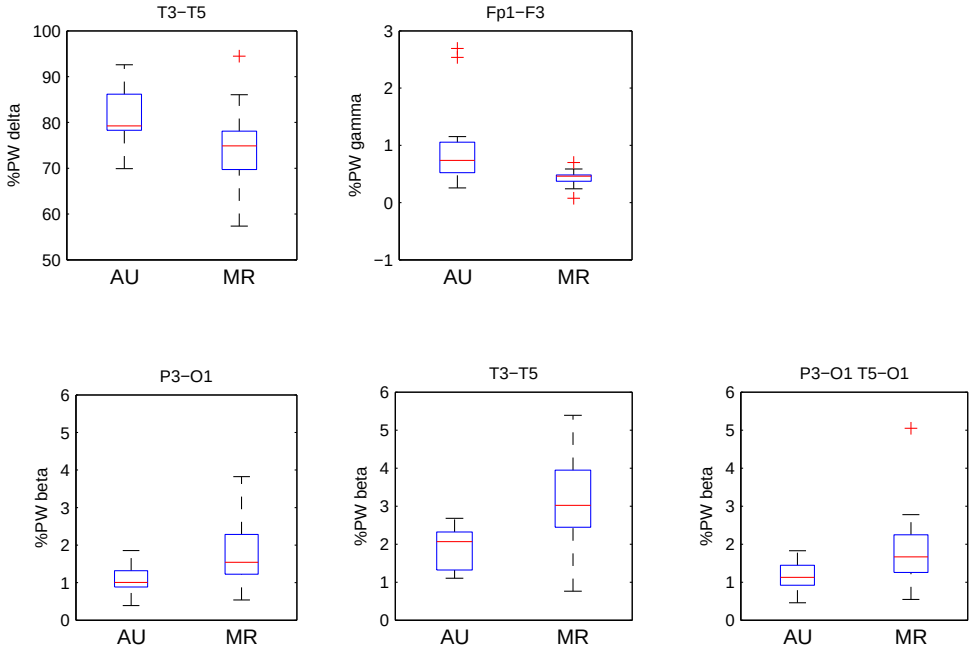

Figure 34: Box plots showing the statistically significant differences between autistic children group (AU) and mentally retarded group (MR) during deep sleep with the indication of the site (derivation or group of derivations).

9.4 DISCUSSION

The study presented in this chapter is the first one in which the EEG of autistic children is compared with that of mentally retarded subjects, matched for cognitive functioning, in the three major electrical states: awake state, light sleep and deep sleep. The relative power in the traditional EEG sub-bands (delta, theta, alpha, beta and gamma), Higuchi's fractal dimension and the zero-crossings were calculated and averaged for each unipolar/bipolar derivation and for each unipolar/bipolar group of derivations. Although available literature is very recent and limited, some preliminary studies on the comparison of autistic and normal EEG in the awake state have been published. Conflicting results, obtained with linear analysis, indicated increased gamma power [Grice *et al.*, 2001], reduced theta activity in the anterior regions of the brain [Chan *et al.*, 2009] and higher power of the delta and theta band in the frontal loci [Pop-Jordanova *et al.*, 2010]. The fractal analysis carried out by Ahmadlou *et al.* [2010] using Higuchi's algorithm showed significant differences in the frontal channels (F4, F7 and F8). Such results, difficult to interpret, have been presumptively correlated to the cognitive, social and communication impairment, typical of neurological and developmental disorders.

The results achieved by the present investigation indicated higher irregularity of autistic awake EEG, quantified by Higuchi's fractal dimension, in the left frontal-polar channel (Fp1) and in the unipolar midline group (Fz Cz Pz). This finding suggests that, for the same IQ, the neuronal activity is more organized in autistic subjects than in mentally retarded controls. As regards spectral analysis, the delta sub-band was the only one that provided percent power values discriminative in distinguishing among awake autistic and awake mentally retarded EEG. Significant higher relative delta activity was found averaging the bipolar derivations in the right posterior region (P4-O2 T6-O2). This result becomes more interesting when associated to those achieved by sleep EEG analysis. Although nonlinear parameterization did not highlight significant differences, linear analysis revealed increased relative delta activity in T3-T5 derivation and a concomitant reduction of beta percent power in the left posterior bipolar region (P3-O1 T5-O1). In other words, a shift in slow activity from right to left hemisphere was observed in the wake-to-sleep transition. Such a result, deserving further investigation, is not of immediate understanding. However, a possible explanation may concern information processing and memory consolidation deficits, as well as abnormal transcallosal transfer of information, which occur during sleep. Higher relative gamma oscillations during light sleep were observed in autistic children with respect to mentally retarded controls in the left anterior region of the brain. Since high frequency activity is related to perceptual and cognitive processes, partly impaired also in mental retardation, a higher percent power in the gamma sub-band may be an indicator for autistic perceptual and cognitive impairment.

9.5 CONCLUSION

The study presented in this chapter was conducted with the aim of characterizing the macro-structural organization of the EEG of autistic children with respect to that of mentally retarded controls. Fractal analysis suggests that the complexity of EEG signal in the awake state is higher for autistic children with respect to controls, although subjects were matched for cognitive functioning. Linear analysis revealed a posterior slow activity shift between awake and asleep states from the right to the left hemisphere, which may be related to autistic deficits in information processing and memory consolidation, as well as to abnormal transcallosal transfer of information. Moreover, higher relative gamma activity, associated with cognitive processes, was highlighted in autism. Future studies, to be performed on a larger sample of recruited subjects including also normal children, should attempt to clarify and hopefully confirm these findings. Quantitative EEG-based measures would be very important because early diagnosis allows early intervention with increased effectiveness.

10 CONCLUSION

For the purpose of EEG nonlinear analysis, the possibility of fruitfully exploring brain complexity directly in the time domain without the need for phase space reconstruction would undoubtedly be advantageous.

After a review of the methods available in the literature for the analysis of the fractal-like behavior of the EEG directly in the time domain, the Author selected and compared three widely used algorithms for the estimation of the fractal dimension of waveforms. Higuchi's algorithm outperformed box-counting and Katz's methods, producing correct estimates of the fractal dimension also on short traces, provided that minimum sampling rate required to avoid aliasing is used. The use of the scaling relationship of fractional Brownian motion to obtain indirect estimates of the fractal dimension from the power-law exponent is, on the contrary, not recommended, since deviations from fBm were observed by the Author. As long as a complete model of the EEG is lacking, direct estimation of the fractal dimension with Higuchi's algorithms is preferable.

Higuchi's fractal dimension was used to address three clinical issues: 1) the monitoring of carotid endarterectomy for the prevention of intraoperative stroke, 2) the assessment of the depth of anesthesia to monitor unconsciousness during surgery and 3) the analysis of the macro-structural organization of the EEG in autism with respect to mental retardation.

In the first study the fractal dimension was expected to reflect the possible complexity drop due to hypoperfusion caused by artery clamping. The efficacy of the parameter as a criterion to determine whether a shunt is indicated was evaluated on 140 surgical procedures. The parameter did not achieve satisfactory results since the threshold selected to minimize identification errors produced a sensitivity of barely 30% with 100% specificity. Higher thresholds improved sensitivity at the expense of a fall in specificity. Both HFL linear index and ZC nonlinear parameter, on the contrary, obtained 100% overall accuracy resulting better indicators of cerebral suffering.

In the second investigation the fractal dimension was expected to reflect the level of unconsciousness induced by the hypnotic agents during general anesthesia. The ability of the parameter to follow the depth of anesthesia from induction to recovery was assessed in 6 patients. Whereas the standalone parameter was not able to monitor too deep unconsciousness, characterized by burst suppression patterns, the fractal dimension compensated for burst suppression correctly quantified the depth of anesthesia in all its phases.

In the discrimination of autism from mental retardation, the fractal dimension was significantly different in the anterior regions of the brain and along the midline, while differences in some spectral parameters were observed mainly in the posterior areas, suggesting that linear analysis and fractal analysis capture complimentary information on brain functioning. The results of the fractal analysis, in particular, revealed that autistic children have more complex EEG sources with respect to mentally retarded controls.

The results of the clinical studies suggest that, although linear spectral analysis still represents a valuable technique for the investigation of the EEG, time domain fractal analysis provides additional information on brain functioning which traditional analysis cannot achieve, making use of techniques of low computational cost. In conclusion, nonlinear processing of the EEG based on the analysis of the fractal-like behavior of the signal represents a powerful tool for the comprehension of neuronal activity.

A APPENDIX

The zero-crossings (ZC) is a nonlinear parameter used in the analysis of random signals [Kedem, 1986]. It is computed by counting the number of baseline crossings in a fixed time interval. Let $x(1)$,$x(2)$,...,$x(N)$ be a zero-mean stationary Gaussian time series. Consider the associated clipped binary series $y_1(n)$ defined by:

$$y_1(n) = \begin{cases} 1, & \text{if } x(n) > 0 \\ 0, & \text{if } x(n) \leqslant 0 \end{cases} \tag{38}$$

with $n = 1,2,...,N$ and let $y_2(n)$ be the associated series defined as:

$$y_2(n) = y_1(n+1) \tag{39}$$

with $n = 1, 2, ..., N-1$, where $y_2(N) = y_2(N-1)$. Three further binary series are defined by:

$$\begin{array}{lcl} z_1(n) = y_1(n) & \text{OR} & y_2(n) \\ z_2(n) = y_1(n) & \text{NAND} & y_2(n) \\ z_3(n) = z_1(n) & \text{AND} & z_2(n) \end{array} \tag{40}$$

Then the ZC count is defined by the sum:

$$ZC = \sum_n z_3(n) \tag{41}$$

Fruitful connections exist between ZC count and dominant frequency. When a certain frequency band becomes dominant, it attracts the normalized expected zero-crossings and $\frac{ZC}{2(N-1)}$ admits values in this band. Likewise, when a certain frequency f_0 becomes significantly dominant then $\frac{ZC}{2(N-1)} \simeq f_0$. In the extreme case when only f_0 is present, $\frac{ZC}{2(N-1)} = f_0$. This tendency of zero-crossings was called the *dominant frequency principle*. As an example, consider the signal $x(n)$:

$$x(n) = A\cos(0.8n) + B\cos(1.25n)$$

for $n = 1,2,...,N$ with $N = 200$. ZC is a function of the weights A and B. When $A = B = 1$ there is no dominant frequency (Fig. 35). It results $ZC = 69$ and $\frac{\pi ZC}{199} = 1.095$ which is in the range 0.8-1.25 as expected. When $A = 0.8$ and $B = 1$, the frequency 1.25 is dominant (Fig. 35). It results $ZC = 79$ and $\frac{\pi ZC}{199} = 1.247$ which is very close to 1.25 in agreement with the dominant frequency principle.

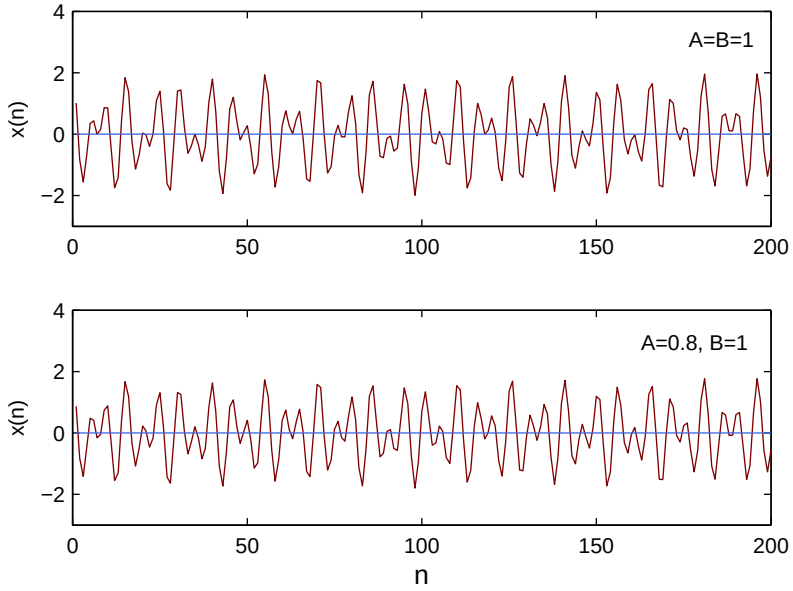

Figure 35: Demonstration of dominant frequency principle. Top plot: $x(n) = \cos(0.8n) + \cos(1.25n)$: none of the oscillations is dominant. Bottom plot: $x(n) = 0.8\cos(0.8n) + \cos(1.25n)$: 1.25 component is dominant. $\frac{\pi ZC}{199} = 1.247$.

Thus, ZC is an index that may reflect possible changes in dominant spectral components. Moreover, the calculation of this parameter is very fast and can be performed also on short epochs.

BIBLIOGRAPHY

Abry, P and F Sellan [1996], "The wavelet-based synthesis for fractional Brownian motion proposed by F. Sellan and Y. Meyer: remarks and fast implementation," *Appl and Comput Harm Anal*, 3, 4, pp. 377–383. (Cited on p. 39.)

Accardo, A, M Affinito, M Carrozzi, and F Bouquet [1997], "Use of the fractal dimension for analysis of electroencephalographic time series," *Biol Cybern*, 77, 5, pp. 339–350. (Cited on pp. 34, 36, 48.)

Acharya, UR, O Faust, N Kannathal, T Chua, and S Laxminarayan [2005], "Non-linear analysis of EEG signals at vaious sleep stages," *Comput Methods Programs Biomed*, 80, pp. 37–45. (Cited on p. 34.)

Ahmadlou, M, H Adeli, and A Adeli [2010], "Fractality and wavelet-chaos-neural network for EEG-based diagnosis of autistic spectrum disorder," *J Clin Neurophysiol*, 27, 5, pp. 328–333. (Cited on pp. 34, 88, 98.)

– [2011], "Fractality and wavelet-chaos-methodology for EEG-based diagnosis of Alzheimer disease," *Alzheimer Dis Assoc Disord*, 25, 1, pp. 85–92. (Cited on p. 34.)

Bassingthwaighte, JB, LS Liebovitch, and BJ West [1994], *Fractal physiology*, Oxford University Press, New York. (Cited on pp. 26, 51.)

Belmonte, MK, G Allen, A Beckel-Mitchener, LM Boulanger, RA Carper, and SJ Webb [2004], "Autism and abnormal development of brain connectivity," *J Neurosci*, 24, 42, pp. 9228–9231. (Cited on p. 87.)

Berry, MV [1979], "Diffractals," *J Phys A*, 12, pp. 781–797. (Cited on p. 53.)

Berry, MV and ZV Lewis [1980], "On the Weierstrass-Mandelbrot fractal function," *Proc R Soc Lond*, 370, 1743, pp. 459–484. (Cited on p. 38.)

Blume, WT, GG Ferguson, and DK McNeill [1986], "Significance of EEG changes at carotid endarterectomy," *Stroke*, 17, pp. 891–897. (Cited on p. 71.)

Bojic, T, A Vuckovic, and A Kalauzi [2010], "Modeling EEG fractal dimension changes in wake and drowsy states in humans - a preliminary study," *J Theor Biol*, 262, 2, pp. 214–222. (Cited on p. 34.)

Bonebakker, AE, M Jelicic, J Passchier, and B Bonke [1996], "Memory during general anesthesia: practical and methodological aspects," *Conscious Cogn*, 5, 4, pp. 542–561.

Bosl, W, A Tierney, H Tager-Flusberg, and C Nelson [2011], "EEG complexity as a biomarker for autism spectrum disorder risk," *BMC Med*, 9, p. 18. (Cited on p. 34.)

Bruhn, J, TW Bouillon, and SL Shafer [2000], "Bispectral index (BIS) and burst suppression: revealing a part of the BIS algorithm.," *J Clin Monit Comput*, 16, 8, pp. 593–596. (Cited on pp. 79, 80.)

Buckley, AW, AJ Rodriguez, K Jennison, J Buckley, A Thurm, S Sato, and S Swedo [2010], "Rapid eye movement sleep percentage in children with autism compared with children with developmental delay

and typical development," *Arch Pediatr Adolesc Med*, 164, 11, pp. 1032–1037. (Cited on p. 88.)

Carrozzi, M, A Accardo, and F Bouquet [2004], "Analysis of sleep-stage characteristics in full-term newborns by means of spectral and fractal parameters," *Sleep*, 27, 7, pp. 1384–1393. (Cited on pp. 34, 40, 71.)

Catarino, A, O Churches, S Baron-Cohen, A Andrade, and Ring H [2011], "Atypical EEG complexity in autism spectrum conditions: a multiscale entropy analysis," *Clin Neurophysiol*, 122, 12, pp. 2375–2383. (Cited on pp. 34, 88.)

Chan, AS, MC Cheung, YM Han, SL Sze, WW Leung, HS Man, and CY To [2009], "Executive function deficits and neural discordance in children with Autism Spectrum Disorders," *Clin Neurophysiol*, 120, 6, pp. 1107–1115. (Cited on pp. 88, 98.)

Chouvarda, I, MO Mendez, V Rosso, AM Bianchi, L Parrino, A Grassi, M Terzano, N Maglaveras, and S Cerutti [2011], "Predicting EEG complexity from sleep macro and microstructure," *Physiol Meas*, 32, 8, pp. 1083–1101. (Cited on p. 34.)

Cursi, M, MV Meraviglia, GF Fanelli, R Chiesa, A Tirelli, G Comi, and F Minicucci [2005], "Electroencephalographic background desynchronization during cerebral blood flow reduction," *Clin Neurophysiol*, 116, 11, pp. 2577–2585. (Cited on pp. 62, 64, 70, 71, 73.)

Daneshyari, M, LL Kamkar, and M Daneshyari [2010], "Epileptic EEG: a comprehensive study of nonlinear behavior," *Adv Exp Med Biol*, 680, pp. 677–683. (Cited on p. 34.)

Doyle, PW and BF Matta [1999], "Burst suppression or isoelectric encephalogram for cerebral protection: evidence from metabolic suppression studies," *Br J Anaesth*, 83, 4, pp. 580–584. (Cited on p. 78.)

Drover, DR, HJ Lemmens, ET Pierce, G Plourde, G Loyd, E Ornstein, LS Prichep, RJ Chabot, and L Gugino [2002], "Patient State Index: titration of delivery and recovery from propofol, alfentanil, and nitrous oxide anesthesia," *Anesthesiology*, 97, 1, pp. 82–89. (Cited on p. 76.)

Errando, CL, JC Sigl, M Robles, E Calabuig, J García, F Arocas, R Higueras, E Del Rosario, D López, CM Peiró, JL Soriano, S Chaves, F Gil, and R García-Aguado [2008], "Awareness with recall during general anaesthesia: a prospective observational evaluation of 4001 patients," *Br J Anaesth*, 101, 2, pp. 178–185. (Cited on p. 76.)

Esteller, R, G Vachtsevanos, J Echauz, and B Litt [2001], "A comparison of waveform fractal dimension algorithms," *IEEE Trans Biomed Eng*, 48, 2, pp. 177–183. (Cited on pp. 34, 35, 48.)

Ferenets, R, T Lipping, A Anier, V Jäntti, S Melto, and S Hovilehto [2006], "Comparison of entropy and complexity measures for the assessment of depth of sedation," *IEEE Trans Biomed Eng*, 53, 6, pp. 1067–1077. (Cited on p. 34.)

Ferenets, R, A Vanluchene, T Lipping, B Heyse, and MM Struys [2007], "Behavior of entropy/complexity measures of the electroencephalogram during propofol-induced sedation: dose-dependent effects of

remifentanil," *Anesthesiology*, 106, 4, pp. 696–706. (Cited on pp. 34, 76.)
Fraser, AM and HL Swinney [1986], "Independent coordinates for strange attractors from mutual information," *Phys Rev A*, 33, 2, pp. 1134–1140. (Cited on p. 19.)
Ghali, R, EG Palazzo, DI Rodriguez, M Zammit, DL Loudenback, RP DeMuth, MP Spencer, and LR Sauvage [1997], "Transcranial doppler intraoperative monitoring during carotid endarterectomy: experience with regional or general anesthesia, with and without shunting," *Ann Vasc Surg*, 11, 1, pp. 9–13. (Cited on p. 61.)
Grassberger, P and I Procaccia [1983], "Measuring the strangeness of strange attractors," *Physica D*, 9, 1-2, pp. 189–208. (Cited on p. 16.)
Grice, SJ, MW Spratling, A Karmiloff-Smith, H Halit, G Csibra, M de Haan, and MH Johnson [2001], "Disordered visual processing and oscillatory brain activity in autism and Williams syndrome," *Neuroreport*, 12, 12, pp. 2697–2700. (Cited on pp. 88, 98.)
Henderson, G, E Ifeachor, N Hudson, C Goh, N Outram, S Wimalaratna, C Del Percio, and F Vecchio [2006], "Development and assessment of methods for detecting dementia using the human electroencephalogram," *IEEE Trans Biomed Eng*, 53, 8, pp. 1557–1568. (Cited on p. 71.)
Hénon, M [1976], "A two-dimensional mapping with a strange attractor," *Commun Math Phys*, 50, 1, pp. 69–77. (Cited on p. 15.)
Henry, B, N Lovell, and F Camacho [2001], "Nonlinear dynamics time series analysis," in *Nonlinear biomedical signal processing*, vol. II, Metin Akay, New York. (Cited on p. 14.)
Higuchi, T [1988], "Approach to an irregular time series on the basis of the fractal theory," *Physica D*, 31, 2, pp. 277–283. (Cited on pp. 30, 33–35, 37, 53.)
– [1990], "Relationship between the fractal dimension and the power law index for a time series: A numerical investigation," *Physica D*, 46, pp. 254–264. (Cited on pp. 51, 55.)
Hobson, JA and EF Pace-Schott [2002], "The cognitive neuroscience of sleep: neuronal systems, consciousness and learning," *Nat Rev Neurosci*, 3, 9, pp. 679–693. (Cited on p. 88.)
Inouye, T, S Ukai, K Shinosaki, A Iyama, Y Matsumoto, and S Toi [1994], "Changes in the fractal dimension of alpha envelope from wakefulness to drowsiness in the human electroencephalogram," *Neurosci Lett*, 174, 1, pp. 105–108. (Cited on p. 34.)
Jasper, H [1958], "Report of the Committee on Methods of Clinical Examination in Electroencephalography: 1957," *Electroencephalogr Clin Neurophysiol*, 10, pp. 370–375. (Cited on p. 10.)
Jones, JG [1994], "Perception and memory during general anesthesia," *Br J Anaesth*, 73, 1, pp. 31–37. (Cited on p. 75.)
Jordan, D, G Schneider, A Hock, T Hensel, G Stockmanns, and EF Kochs [2006], "EEG parameters and their combination as indicators of depth of anaesthesia," *Biomed Tech Berlin*, 51, 2, pp. 89–94. (Cited on p. 76.)
Kalkman, CJ [2004], "Con: Routine shunting is not the optimal management of the patient undergoing carotid endarterectomy, but neither

is neuromonitoring," *J Cardiothorac Vasc Anesth*, 18, 3, pp. 381–383. (Cited on p. 61.)

Kantz, H and T Schreiber [2004], *Nonlinear time series analysis*, Second Edition, Cambridge University Press, New York, chap. 1-6. (Cited on p. 14.)

Katz, M [1988], "Fractals and the analysis of waveforms," *Comput Biol Med*, 18, 3, pp. 145–156. (Cited on pp. 30, 33–36.)

Kedem, B [1986], "Spectral analysis and discrimination by zero-crossings," in vol. 74, 11, pp. 1477–1493. (Cited on pp. 64, 80, 103.)

Kelley, SD [2010], *Monitoring consciousness using the Bispectral Index (BIS^{TM}) during anesthesia: a pocket guide for clinicians*. (Cited on p. 76.)

Kennel, MB, R Brown, and HD Abarbanel [1992], "Determining embedding dimension for phase-space reconstruction using a geometrical construction," *Phys Rev A*, 45, 6, pp. 3403–3411. (Cited on p. 18.)

Klimesch, W [1999], "EEG alpha and theta oscillations reflect cognitive and memory performance: a review and analysis," *Brain Research Review*, 29, 2-3, pp. 169–195.

Klockars, J, A Hiller, S Münte, MJ van Gils, and T Taivainen [2011], "Spectral Entropy as a Measure of Hypnosis and Hypnotic Drug Effect of Total Intravenous Anesthesia in Children during Slow Induction and Maintenance," *Anesthesiology*. (Cited on p. 76.)

Kreuer, S, A Biedler, R Larsen, S Altmann, and W Wilhelm [2003], "Narcotrend monitoring allows faster emergence and a reduction of drug consumption in propofol-remifentanil anesthesia," *Anesthesiology*, 99, 1, pp. 34–41. (Cited on p. 76.)

Kulisek, R, Z Hrncir, M Hrdlicka, L Faladova, K Sterbova, P Krsek, E Vymlatilova, M Palus, A Zumrová, and V Komárek [2008], "Nonlinear analysis of the sleep EEG in children with pervasive developmental disorder," *Neuro Endocrinol Lett*, 29, 4, pp. 512–517. (Cited on p. 88.)

Laman, DM, CS van der Reijden, GH Wieneke, H van Duijn, and AC van Huffelen [2012], "EEG evidence for shunt requirement during carotid endarterectomy: optimal EEG derivations with respect to frequency bands and anesthetic regimen," *J Clin Neurophysiol*, 18, 4, pp. 353–363. (Cited on pp. 63, 71.)

Li, D, X Li, S Hagihira, and JW Sleigh [2011], "The effect of isoflurane anesthesia on the electroencephalogram assessed by harmonic wavelet bicoherence-based indices," *J Neural Eng*, 8, 5. (Cited on p. 76.)

Liang, Z, D Li, G Ouyang, Y Wang, LJ Voss, JW Sleigh, and X Li [2011], "Clin Neurophysiol," *Multiscale rescaled range analysis of EEG recordings in sevoflurane anesthesia*. (Cited on p. 76.)

Lin, DC, A Sharif, and HC Kwan [2006], "Scaling and organization of electroencephalographic background activity and alpha rhythm in healthy young adults," *Biol Cybern*, 95, 5, pp. 401–411. (Cited on p. 71.)

Lorenz, EN [1963], "Deterministic nonperiodic flow," *J Atmos Sci*, 20, 2, pp. 130–141. (Cited on p. 15.)

Malow, BA [2004], "Sleep disorders, epilepsy, and autism," *Ment Retard Dev Disabil Res Rev*, 10, 2, pp. 122–125. (Cited on p. 88.)
Mandelbrot, BB [1982], *The fractal geometry of nature*, Freeman, New York. (Cited on pp. 30, 33–35.)
– [1985], "Self-affine fractals and fractal dimension," *Phys Scr*, 32, 4, pp. 257–260. (Cited on p. 33.)
Mandelbrot, BB and JW Van Ness [1968], "Fractional Brownian motions: Fractional noises and applications," *SIAM Rev*, 10, 4, pp. 422–437. (Cited on pp. 25, 53.)
Maquet, P [2001], "The role of sleep in learning and memory," *Science*, 294, 5544, pp. 1048–1052. (Cited on p. 88.)
Maragos, P and FK Sun [1983], "Measuring the fractal dimension of signals: morphological covers and iterative optimization," *IEEE Trans Signal Proc*, 41, 1, pp. 108–121. (Cited on p. 30.)
McFarland, HR, JA Jr Pinkerton, and D Frye [1988], "Continuous electroencephalographic monitoring during carotid endarterectomy," *J Cardiovasc Surg*, 29, 1, pp. 12–18. (Cited on p. 61.)
Mengotti, P, S D'Agostini, R Terlevic, C De Colle, E Biasizzo, D Londero, A Ferro, G Rambaldelli, M Balestrieri, S Zanini, F Fabbro, M Molteni, and P Brambilla [2011], "Altered white matter integrity and development in children with autism: a combined voxel-based morphometry and diffusion imaging study," *Brain Res Bull*, 84, 2, pp. 189–195. (Cited on p. 87.)
Miller, A, JW Sleigh, J Barnard, and DA Steyn-Ross [2004], "Does bispectral analysis of the electroencephalogram add anything but complexity?" *Br J Anaesth*, 92, 1, pp. 8–13. (Cited on p. 76.)
Miller, RD [2005], *Miller's anesthesia*, 6th ed., Elsevier Churchill Livingstone, Philadelphia. (Cited on p. 76.)
Minicucci, F, M Cursi, C Fornara, C Rizzo, R Chiesa, A Tirelli, G Fanelli, MV Meraviglia, L Giacomotti, and G Comi [2000], "Computer-assisted EEG monitoring during carotid endarterectomy," *J Clin Neurophysiol*, 17, 1, pp. 101–107. (Cited on pp. 62, 65, 71.)
Mizuno, T, T Takahashi, RY Cho, M Kikuchi, T Murata, K Takahashi, and Y Wada [2010], "Assessment of EEG dynamical complexity in Alzheimer's disease using multiscale entropy," *Clin Neurophysiol*, 121, 9, pp. 1438–1446. (Cited on p. 34.)
Moore, WS, JM Yee, and AD Hall [1973], "Collateral cerebral blood pressure - An index of tolerance to temporary carotid occlusion," *AMA Arch Surg*, 106, 4, pp. 520–523. (Cited on p. 61.)
Morimoto, Y, S Hagihira, Y Koizumi, K Ishida, M Matsumoto, and T Sakabe [2004], "The relationship between bispectral index and electroencephalographic parameters during isoflurane anesthesia," *Anesth Analg*, 98, 5, pp. 1336–1340. (Cited on p. 76.)
Osterman, JE, J Hopper, WJ Heran, TM Keane, and BA van der Kolk [2001], "Awareness under anesthesia and the development of posttraumatic stress disorder," *Gen Hosp Psychiatry*, 23, 4, pp. 198–204. (Cited on p. 75.)

Packard, NH, JP Crutchfield, JD Farmer, and RS Shaw [1980], "Geometry from a time series," *Phys Rev Lett*, 45, 9, pp. 712–716. (Cited on p. 18.)

Paramanathan, P and R Uthayakumar [2008], "Application of fractal theory in analysis of human electroencephalographic signals," *Comput Biol Med*, 38, 3, pp. 372–378. (Cited on pp. 30, 34, 35, 48.)

Peitgen, HO and D Saupe [1988], *The science of fractal images*, Springer-Verlag, New York. (Cited on p. 21.)

Penn, AI and MH Loew [1997], "Estimating fractal dimension with fractal interpolation function models," *IEEE Trans Med Imaging*, 16, 6, pp. 930–937. (Cited on p. 55.)

Penn, HE [2006], "Neurobiological correlates of autism: a review of recent research," *Child Neuropsychol*, 12, 1, pp. 57–59. (Cited on p. 87.)

Petrosian, A [1995], "Kolmogorov complexity of finite sequences and recognition of different preictal EEG patterns," *Proc IEEE Symp Computer-Based Medical Syst*. (Cited on pp. 30, 34.)

Philip, RC, MR Dauvermann, HC Whalley, K Baynham, SM Lawrie, and AC Stanfield [2012], "A systematic review and meta-analysis of the fMRI investigation of autism spectrum disorders," *Neurosci Biobehav Rev*, 36, 2, pp. 901–942. (Cited on p. 87.)

Phothisonothai, M and M Nakagawa [2009], "A classification method of different motor imagery tasks based on fractal features for brain-machine interface," *J Integr Neurosci*, 8, 1, pp. 95–122. (Cited on pp. 34, 52.)

Pinkerton, JA Jr [2002], "EEG as a criterion for shunt need in carotid endarterectomy," *Ann Vasc Surg*, 16, 6, pp. 756–761. (Cited on p. 61.)

Plestis, KA, P Loubser, EM Mizrahi, G Kantis, ZD Jiang, and JF Howell [1997], "Continuous electroencephalographic monitoring and selective shunting reduces neurologic morbidity rates in carotid endarterectomy," *J Vasc Surg*, 25, 4, pp. 620–628. (Cited on p. 61.)

Polychronaki, GE, PY Ktonas, S Gatzonis, A Siatouni, PA Asvestas, H Tsekou, D Sakas, and KS Nikita [2010], "Comparison of fractal dimension estimation algorithms for epileptic seizure onset detection," *J Neural Eng*, 4, p. 046007. (Cited on p. 34.)

Pop-Jordanova, N, T Zorcec, A Demerdzieva, and Z Gucev [2010], "QEEG characteristics and spectrum weighted frequency for children diagnosed as autistic spectrum disorder," *Nonlinear Biomed Phys*, 4, 1. (Cited on pp. 88, 98.)

Pritchard, WS [1992], "The brain in fractal time: 1/f-like power spectrum scaling of the human electroencephalogram," *Intern J Neuroscience*, 66, pp. 119–129. (Cited on pp. 25, 29, 30, 52.)

Raghavendra, BS and DN Dutt [2009], "A note on fractal dimensions of biomedical waveforms," *Comput Biol Med*, 39, 11, pp. 1006–1012. (Cited on pp. 34, 38, 39, 48.)

Raghavendra, BS, DN Dutt, HN Halahalli, and JP John [2009], "Complexity analysis of EEG in patients with schizophrenia using fractal dimension," *Physiol Meas*, 30, 8, pp. 795–808. (Cited on p. 34.)

Rampil, IJ [1998], "A primer for EEG signal processing in anesthesia," *Anesthesiology*, 89, 4, pp. 981–1001. (Cited on p. 80.)

Ramsay, MA, TM Savege, BR Simpson, and R Goodwin [2012], "Controlled sedation with alphaxalone-alphadolone," *Br Med J*, 2, 5920, pp. 656–659. (Cited on p. 76.)
Rankine, L, N Stevenson, M Mesbah, and B Boashash [2007], "A nonstationary model of newborn EEG," *IEEE Trans Biomed Eng*, 54, 1, pp. 19–28. (Cited on pp. 34, 52.)
Rapin, I [1997], "Autism," *N Engl J Med*, 337, 2, pp. 97–104. (Cited on p. 87.)
Rippon, G, J Brock, C Brown, and J Boucher [2007], "Disordered connectivity in the autistic brain: challenges for the "new psychophysiology"," *Int J Psychopshysiol*, 63, 2, pp. 164–172. (Cited on p. 87.)
Salvian, AJ, DC Taylor, YN Hsiang, HD Hildebrand, HK Litherland, MF Humer, PA Teal, and DB MacDonald [2012], "Selective shunt with EEG monitoring is safer than routine shunting for carotid endarterectomy," *Cardiovasc Surg*, 5, 5, pp. 481–485. (Cited on pp. 61, 71, 73.)
Sanei, S and J Chambers [2007], *EEG signal processing*, Wiley, Chichester, England, chap. 1. (Cited on p. 7.)
Sauer, T, J Yorke, and M Casdagli [1994], "Embedology," *J Stat Phys*, 65, 3-4, pp. 579–616. (Cited on p. 18.)
Schneider, G, S Schöniger, and E Kochs [2004], "Does bispectral analysis add anything but complexity? BIS sub-components may be superior to BIS for detection of awareness," *Br J Anaesth*, 93, 4, pp. 596–597. (Cited on p. 76.)
Schreiber, T [1997], "Detecting and analyzing nonstationarity in a time series using nonlinear cross predictions," *Phys Rev Lett*, 78, 5, pp. 843–846. (Cited on pp. 40, 53.)
Schweiger, H, HD Kamp, and M Dinkel [1991], "Somatosensory-evoked potentials during carotid artery surgery: experience in 400 operations," *Surgery*, 109, 5, pp. 602–609. (Cited on p. 61.)
Schwender, D, H Kunze-Kronawitter, P Dietrich, S Klasing, H Forst, and C Madler [1998], "Conscious awareness during general anaesthesia: patientsí perceptions, emotions, cognition and reactions," *Br J Anaesth*, 80, 2, pp. 133–139. (Cited on p. 75.)
Sevcik, C [2006], "On fractal dimension of waveforms," *Chaos Soliton Fract*, 28, pp. 579–580. (Cited on p. 30.)
Shah, DM, RC 3rd Darling, BB Chang, DE Bock, PS Paty, and RP Leather [1994], "Carotid endarterectomy in awake patients: its safety, acceptability, and outcome," *J Vasc Surg*, 19, 6, pp. 1015–1019. (Cited on p. 61.)
Sleigh, JW, DA Steyn-Ross, ML Steyn-Ross, ML Williams, and P Smith [2001], "Comparison of changes in electroencephalographic measures during induction of general anaesthesia: influence of the gamma frequency band and electromyogram signal," *Br J Anaesth*, 86, 1, pp. 50–58. (Cited on pp. 78, 84.)
Takagi, T [1903], "A simple example of a continuous function without derivative," *Proc Phys Math Japan*, 1, pp. 176–177. (Cited on p. 39.)

Takens, F [1981], "Detecting strange attractors in turbulence," in *Dynamical systems and turbulence*, ed. by DA Rand and LS Young, Berlin. (Cited on p. 18.)

Tuchman, R, M Alessandri, and M Cuccaro [2010], "Autism spectrum disorders and epilepsy: moving towards a comprehensive approach to treatment," *Brain Dev*, 32, 9, pp. 19–30. (Cited on p. 88.)

Van Putten, MJ [2006], "Extended BSI for continuous EEG monitoring in carotid endarterectomy," *Clin Neurophysiol*, 117, 12, pp. 2661–2666. (Cited on pp. 62, 64–66, 70, 72.)

Van Putten, MJ, JM Peters, SM Mulder, JA de Haas, CM Bruijninckx, and DL Tavy [2004], "A brain symmetry index (BSI) for online EEG monitoring in carotid endarterectomy," *Clin Neurosphysiol*, 115, 5, pp. 1189–1194. (Cited on pp. 62, 64, 70, 72.)

Viertiö-Oja, H, V Maja, M Särkelä, P Talja, N Tenkanen, H Tolvanen-Laakso, M Paloheimo, A Vakkuri, A Yli-Hankala, and P Meriläinen [2004], "Description of the Entropy^{TM} algorithm as applied in the Datex-Ohmeda S/5^{TM} Entropy Module," *Acta Anaesthesiol Scand*, 48, 2, pp. 154–161. (Cited on p. 76.)

Visser, GH, GH Wieneke, and AC van Huffelen [1999], "Carotid endarterectomy monitoring: patterns of spectral EEG changes due to carotid artery clamping," *Clin Neurophysiol*, 110, 2, pp. 286–294. (Cited on pp. 61, 65, 73.)

Visser, GH, GH Wieneke, AC Van Huffelen, JW De Vries, and PF Bakker [2001], "The development of spectral EEG changes during short periods of circulatory arrest," *J Clin Neurophysiol*, 18, 2, pp. 169–177. (Cited on p. 62.)

Von Koch, H [1904], "Sur une courbe continue sans tangente, obtenue par une construction géométrique élémentaire," *Arkiv mat astron fys*, 1, pp. 681–704. (Cited on p. 22.)

Wilson, TW, DC Rojas, ML Reite, PD Teale, and SJ Rogers [2007], "Children and adolescents with autism exhibit reduced MEG steady-state gamma responses," *Biol Psychiatry*, 62, 3, pp. 192–197. (Cited on p. 87.)

LIST OF PUBLICATIONS

This thesis is based on the following original publications:

1. Accardo, A, M Cusenza and F Monti [2009], "Linear and non-linear parameterization of EEG during monitoring of carotid endarterectomy," *Comput Biol Med*, 39, 6, pp. 512-518.

2. Cusenza, M and A Accardo [2010], "Estimation of EEG fractal dimension: sensitivity to sampling frequency and time window length," *Atti del Secondo Congresso Nazionale di Bioingegneria (GNB 2010)*, pp. 463-464.

3. Cusenza, M and A Accardo [2010], "Self-affinity in brain activity: relationship between fractal dimension and power-law beta exponent of EEG in sleeping newborns," *ESBME Proc*.

4. Cusenza, M and A Accardo [2012], "Sensitivity to sampling frequency and time window length in the estimation of EEG fractal dimension," submitted to *Biological Cybernetics*, manuscript number BICY-D-12-00026.

5. Cusenza, M, A Accardo and A Orsini [2012], "EEG fractal dimension combined with burst suppression ratio as a measure of depth of anesthesia," accepted for *2012 World Congress on Medical Physics and Biomedical Engineering (WC 2012)*, paper ID A11011.

6. Cusenza, M, A Accardo, S Zanini and P Brambilla [2012], "Characterization of awake and sleep EEG in autistic children," submitted to *Terzo Congresso Nazionale di Bioingegneria (GNB 2012)*.

Supplementary publications related to the fractal analysis of the EEG but not included in this thesis:

7. Cusenza, M, A Accardo, F Monti and P Bramanti [2010], "Linear and non-linear effects of gradient artifact filtering methods in simultaneous EEG-fMRI," *Biomed Sci Instrum*, 46, pp. 374-379.

Other publications related to the fractal analysis of the heart rate variability, not included in this thesis:

8. Cusenza, M, A Accardo, G D'Addio and G Corbi [2010], "Relationship between fractal dimension and power-law exponent of heart rate variability in normal and heart failure subjects," *Computers in Cardiology Proc*, 37, pp. 935-938.

9. Cusenza, M, A Accardo and G D'Addio [2011], "Day-time and night-time HRV ultradian rhythms in normal and pathological subjects," *IFMBE Proc*, 37, pp. 450-453.

10. Accardo, A, M Cusenza, A De Felice and G D'Addio [2012], "Ultradian rhytms during day and night in normal and COPD subjects," submitted to *XXIV European Medical Informatics Conference (MIE 2012)*.

INDEX